THE UNIVERSITY OF MICHIGAN
COLLEGE OF ENGINEERING
Department of Electrical Engineering
Space Physics Research Laboratory

Scientific Report No. GS-1

ELECTROSTATIC PROBE MEASUREMENTS OF THE IONOSPHERE

Prepared on behalf of the project by:
R. L. Boggess

UMRI Projects 2816-1, 2521, 03484

rch reported in this document has been sponsored by the Ballistics Research Laboratory, Aberdeen Proving Ground, Contract No. DA-20-018-509-ORD-103, Project No. DA-5B03-06-011 ORD(TB3-0538), and the Geophysics Research Directorate of the Air Force Cambridge Research Center, Air Research and Development Command, under Contract No. AF 19(604)-1843, Project No. 7643. (Report printed under Contract No. AF 19(604)-6124)

November 1959

ERRATA

"Null potential" should be "wall potential" throughout.

Page 11: $A_c = \pi r^2$ [after Eq. (7)].

12: Fig. 3: "J_p" should be "i_p".

15: "lower limit $u = u_1$" should be "lower limit $u = 0$" [after Eq. (22)].

16: "$(V/V_o) > 1$" should be "$(V/V_o) > 0$" [after Eq. (27)].

17: "$(V/V_o) < 1$" should be "$(V/V_o) < 0$" [after Eq. (28)].

34: Add to the right-hand side of the equations for "Cylinder," in "2. General Approximate" and "3. Asymptotic Orbital-Motion-Limited": " $x \frac{2}{\sqrt{\pi}}$."

118: "I. DELAYED DATA" should be "I. ABM 10.200 DELAYED DATA."

TABLE OF CONTENTS

TABLE OF CONTENTS (Concluded)

PREFACE

This report is concerned with an electrostatic ionosphere probe experiment, whose objectives include the measurement of various properties of the earth's ionosphere. The report presents (a) a history of the work, (b) a theoretical development in part like that presented in an earlier report, (c) an application of the theoretical development to a practical case, (d) a discussion of the design of a particular probe and its instrumentation, (e) a description of the immediate results of a launching, (f) a discussion of the data reduction procedure, (g) the data obtained from the flight and (h) a brief description of the results and data from an additional but preceding launching of a similar probe.

This report was prepared by R. L. Boggess,* who was responsible for the theoretical development and prediction, the detailed design of the external electrical characteristics of the probe, the general aspects of the probe internal instrumentation (with L. H. Brace), and data reduction.**

L. H. Brace was responsible for the internal instrumentation development and operation.

Many other individuals contributed in large measure to the development construction, preparation, and flight of the experiment. In particular, G. Carignan (BRL) was responsible for assembly and operation of the telemetry ground station as well as for various aspects of the preflight preparations. The undersigned had general responsibility for system design, final preparations, and launching.

N. W. Spencer
Project Director
Professor of
Electrical Engineering

*Now at IBM, Lexington, Kentucky.

**The considerable portions of this research contributed by R. L. Boggess, and the preparation of this report constituted a portion of the requirements for the Doctor of Philosophy degree which he has since received.

ABSTRACT

A rocket-borne adaptation of a Langmuir probe was used to measure the properties of the E-layer of the ionosphere. The design was considered an exploratory experiment which would provide a basis for future ionospheric probes. Therefore equal importance was placed on establishing the reasonableness of the theoretical treatment and determining ionospheric parameters.

Earlier attempts to use a rocket-borne probe were usually hampered by design concessions made for other experiments, considered primary, on the same rocket, and as a result, such probes generally yielded ambiguous results. The probe described here was completely separated from the carrier vehicle and therefore no design compromises of this kind were necessary.

In anticipation of the use of spherical electrodes, the general probe theory is reviewed emphasizing a spherical geometry. Additional spherical approximate current-voltage relations are derived and the criteria for using two special solutions, a sheath-area-limited or an orbital-motion-limited solution, are determined. Since a fixed reference potential is not available in the ionosphere, a multiple electrode system must be used. Several designs are considered, and one particular bipolar design, two 6-in. spheres separated by a 10-in.-long, 2-1/4-in.-diam cylinder, was chosen. In this particular design the spheres were split and the outer hemispheres acted as information electrodes. The inner hemispheres acted as guard electrodes. The equal-area two-electrode probe causes the least disturbance of the plasma being measured.

Equally important in the design were certain additional considerations such as the overlap of the sheaths, gas contamination, telemetering rf disturbing the plasma, and the photoelectric effect.

Important accomplishments of the experiment were:

(1) The first measurements of electron temperatures in the altitude range between 112 km to 177 km. A typical value was 1980°K at 153 km.
(2) The measurement of ion number density between 112 km and 177 km. A typical value was 2.4×10^{11} positive ions per cubic meter at 153 km.
(3) The rf (227.5 Mc) was determined to have a negligible effect by providing a delayed data channel such that data taken with and without the transmitter operating could be compared.
(4) The successful ejection of the probe in working order from a rocket moving at a high velocity.

The electron temperature and temperature gradient were both found to be greater than generally expected. The results demonstrate the usefulness of the probe for the explorations of an ionized atmosphere.

LIST OF TABLES

LIST OF FIGURES

LIST OF FIGURES (Continued)

LIST OF FIGURES (Continued)

LIST OF FIGURES (Continued)

LIST OF FIGURES (Concluded)

LIST OF SYMBOLS

A	area
A_c	cross-sectional area
A_{eff}	effective area
J_e	random electron current density
J_p	random positive-ion current density
J_n	random negative-ion current density
J	current density
N_e	number density of electrons
N_p	number density of positive ions
N_n	number density of negative ions
N_g	number density of gas molecules
V_o	voltage equivalent of temperature of the undisturbed plasma*
v_o	most probable velocity of the undisturbed plasma*
T_e	electron temperature
T_p	positive-ion temperature
T_n	negative-ion temperature
T_g	gas temperature
i_e	electron electrode current
i_p	positive-ion electrode current
i_n	negative-ion electrode current
i_t	total electrode current
I_n	normalized current
a	sheath radius

*$1/2\ mv_o^2 = kT_o = eV_o$

r	collector radius
s	sheath thickness, $a-r = s$
e	unit charge 1.602×10^{-19} coulombs
k	Boltzmann's gas constant 1.3803×10^{-23} joules/°K
m_e	mass of an electron 9.11×10^{-31} kilograms
m_p	mass of a positive ion
m_n	mass of a negative ion
m_g	mass of a gas molecule
V	voltage between the sheath edge and an electrode
δV	voltage between two electrodes of a bipolar probe
r_i	radius of influence
r_e	effective radius
P	constant $[(8\sqrt{\pi}\,\epsilon_o k)/9e^2]\,(T/Nr^2)$
α^*	transcendental function of (a/r) for sphere
β^*	transcendental function of (a/r) for cylinder
ϵ_o	dielectric constant of free space 8.854×10^{-12} farads/meter

*See W. G. Dow, Fundamentals of Engineering Electronics, John Wiley and Son, New York, 1952.

I. INTRODUCTION

For the past twelve years the Department of Electrical Engineering of The University of Michigan has been engaged in measuring various properties of the upper atmosphere through the use of several sounding rockets.* Four of these rockets have carried as a secondary experiment an elementary adaptation of the Langmuir probe for study of the ionosphere. The information obtained from the probe experiment on these flights indicated that this should become a useful upper-atmosphere measuring device. The design, however, was seriously compromised in each case by the primary experiment carried by the rocket and by the unknown surface condition of the rocket. A re-study of the practical aspects of the problems encountered indicates that advances in rocket instrumentation techniques and vehicles now make designs feasible which would have been considered impractical previously. For example, the complete ejection of the instrumentation can now be done with confidence. In addition, advances in circuit components allow remarkable reduction in instrumentation size, thereby easing the ejection problem and allowing greater

*The earlier work in conjunction with V-2 rockets was supported by Air Materiel Command, Air Force Cambridge Research Laboratories (AFCRL), Contract No. AF 19(122)-55. Probe study was resumed with the support of the Geophysics Research Directorate, Air Force Cambridge Research Center (AFCRC), Contract No. AF 19(604)-1843. This latter contract supports the present probe investigations jointly with Ballistic Research Laboratory, Aberdeen Proving Ground, Contract No. DA-20-018-509-ORD-103, Project No. DA 5B03-06-011 ORD (TB 3-0538).

freedom in choice of geometry and size. This, in turn, reduces the problems encountered in the transition from theory to practice.

The experience gained from the previous firings, combined with a review of basic probe theory and its extension in some areas, has led to the design of a specific probe instrumentation. One was carried aloft by a Nike-Cajun rocket October 20, 1958, followed by a second on an Aerobee-300, November 30, 1958. The Nike-Cajun experiment proved the soundness of the ejection mechanism and obtained sufficient ionosphere data to indicate that the instrumentation design was basically correct. The Aerobee-300 obtained ionosphere data from 88.5 km to 186 km. The electron temperatures measured were higher than the model-atmosphere temperatures selected for design purposes. The higher temperatures measured were not surprising, however, since the model atmosphere is an estimate of the kinetic gas temperature rather than electron temperature. In general the success of the Aerobee-300 flight, although limited by technical difficulties, demonstrates the applicability of the probe technique to measurements in an ionized atmosphere.

II. HISTORICAL OUTLINE

In 1901, when Marconi proved that radio waves could be received across the Atlantic Ocean, he thereby demonstrated that the earth was not, as had been previously thought, surrounded by free space. In the following year, the existence of an ionized region was independently postulated by Heaviside and Kennelly. This hypothesis was confirmed experimentally in 1925 by Appleton and Barnett, who measured arrival angles of waves transmitted from a distant transmitter. It was demonstrated that the waves came from an elevated angle and thus were "sky" waves. By 1926, the "radar" technique of short vertical pulse soundings had been devised by Bret and Tuve, and thus man's study of the ionosphere was initiated.

As study of the ionosphere has progressed through the years, many refinements in sounding equipment have been made. With each refinement it has become possible to learn more of the complex nature of the ionosphere, thereby drawing attention to the need for a more direct type of measurement (preferably point-by-point), capable of determining fine detail rather than grosser aspects.

It became possible to conduct direct measurements when V-2 rockets were available shortly after World War II. It was quite natural that probe techniques, used in the study of gaseous discharge tubes, should be considered in connection with measuring properties of the ionosphere.

It was at this time that a probe experiment was included in the instrumentation being prepared for V-2 flights in connection with a contract between The University of Michigan and the Air Materiel Command of the U. S. Air Force. (A quite different method, based on the relative delay of two rf signals, was also carried out on early rocket flights by The University of Michigan and AFCRC, and a still different method based on the propagation of two CW signals harmonically related was used by the Naval Research Laboratory.[1-4])

Probes were placed on three successful V-2 flights in 1946 and 1947. The results of these flights were reported in detail in several articles and reports.[5-8] Unfortunately, since the location and shape of the probes were dictated to a great extent by the other instruments being flown, they were awkward in design. This resulted in a great deal of uncertainty in the data because

(a) the probes did not approximate any ideal geometry;

(b) the sheaths of the electrodes overlapped; and

(c) the ion energy distribution seen by the probe was disturbed in an unknown manner when the rocket velocity was high.

But results, however ambiguous, did indicate that the experiment could become a valuable tool for measuring properties of the ionosphere.

At this time, however, interest was greater in carrying out studies of the lower rather than the upper regions of the upper atmosphere and support for the probe experiment was considerably delayed. Consequently, no further investigations were carried out for several years.

The University of Michigan remained interested in the probe experiment and, following the development of the Aerobee-Hi rocket, which is capable of lifting an instrument load well into the ionosphere, study was resumed.* This involved a review of the earlier work in the light of then current knowledge of the ionosphere and additional theoretical considerations.

Following this study, additional support allowed the development and launching of an elementary probe as a secondary experiment on a rocket instrumented primarily to measure pressure, temperature, and density (separate contract with AFCRC). This experiment utilized a sphere (extended from the rocket) as one electrode and the main rocket body as a second electrode. But partially due to failure of the spherical electrode to become extended adequately, the experiment suffered from many of the problems noted previously. Thus the ideas previously held, that the probe geometry must be carefully controlled, and that ejection of the probe instrument is essential to permit a nearly ideal experiment, were largely confirmed.

In the laboratory, thin cylindrical electrodes or small planar surfaces are usually preferred for their geometrical convenience. In the ionosphere, however, a sphere has several advantages due to its symmetry. It was therefore desirable to review the basic probe theory as presented by I. Langmuir and H. Mott Smith[9] and L. Tonks and I. Langmuir[10] by deriving the plasma-to-electrode volt-ampere relations for

*Sponsored by the Geophysics Research Directorate of the Air Force Cambridge Research Center, Contract No. AF 19(604)-1843.

a spherical rather than a cylindrical geometry. In addition, it was necessary to determine certain simplified expressions and the criteria for their use. The following two sections are thus devoted primarily to development of theoretical current voltage relations of a spherical electrode.

III. THEORETICAL DEVELOPMENT

When a small exploring probe is placed in an ionized gas, it is surrounded by a space-charge region which is commonly referred to as the sheath. The probe may be either a conductor or a nonconductor, but for the purposes of this study it is considered to be a conductor and can be called an electrode. If the electrode is allowed to assume a potential that is determined only by the properties of the plasma, it must assume a potential with respect to the plasma such that the net current to the electrode is zero. In general, this potential, which is referred to as the null potential, will be negative with respect to the plasma.

If the potential of the electrode is changed in some manner from this null potential, a current will result. The current will be determined by the voltage across the sheath, the velocity of the ions and electrons arriving at its edge, and its dimensions. The current, however, is nearly independent of the potential distribution within the sheath, whose potential distributions and thickness depends upon space-charge considerations. Neither the potential difference between the plasma and the electrode nor the initial velocities of the positive ions play an important role in this latter regard.

For the purpose of mathematical convenience, it is desirable to define several boundaries surrounding the electrode (Fig. 1). These are:

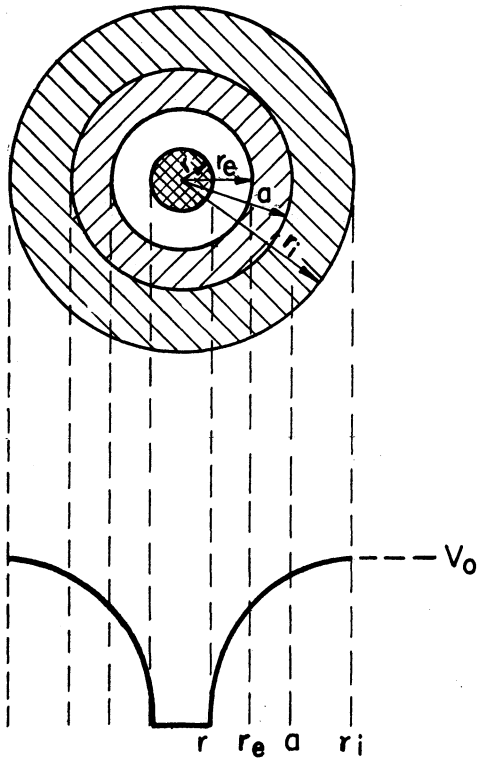

Fig. 1. Potential distribution and boundaries of regions surrounding an electrode.

(a) electrode radius r,

(b) sheath boundary a,

(c) sphere of influence of radius r_i, and

(d) effective sphere radius r_e.

The region between r and a, the sheath, has a positive-ion space charge and will be referred to as a positive-ion sheath. In general, the region is considered to have a negligible number of electrons.

The sheath thickness can be measured accurately by optical means in the laboratory when the probe technique is used for gas-discharge tube studies. Other plasma parameters, such as gas temperature, composition, etc., are also measurable in a laboratory application, and thus certain aspects of the theory can be checked.

The region of influence (bounded by r_i) is that region of the plasma altered by the existence of the electrode. In the more elementary theoretical approach, it is assumed to correspond to the sheath, but may be defined as a region larger than the sheath. In this instance, Boltzmann's relations are assumed to apply in the region not considered sheath.

A spherical electrode collects more positive ions by virtue of its negative charge than an uncharged sphere of equal size. A larger sphere, uncharged, may be defined such that the random current collected is equal to that collected by the smaller charged sphere. This hypothetical sphere is referred to herein as having an effective radius r_e.

The region between r_i and a is a transition region from the undisturbed plasma to the sheath. The voltage across this region is usually small[11] and can be neglected. A sketch of a potential distribution in which the transition region is exaggerated is also shown in Fig. 1.

A. ELEMENTARY SOLUTION

Consider now a negatively charged spherical electrode and its "spherical region of influence" of radius r_i lying in a region containing positive ions. When the radius of influence is large compared with the electrode radius, and the velocity of the ions is appreciable at the boundary of the region of influence, orbital motion of the ions must be considered in determining the current to the electrode. Referring to Fig. 2, AB predicts the path of an uninfluenced ion and AC depicts the path of an orbiting ion. It is assumed that no collisions occur. One can calculate the behavior of an ion in the "sphere of influence" using the law of conservation of angular momentum and the law of conservation of energy.

The kinetic energy gained by the ion in passing from a point on r_i to the point m is given by

$$1/2\ mv^2 = e(V_m - V_o) \quad , \qquad (1)$$

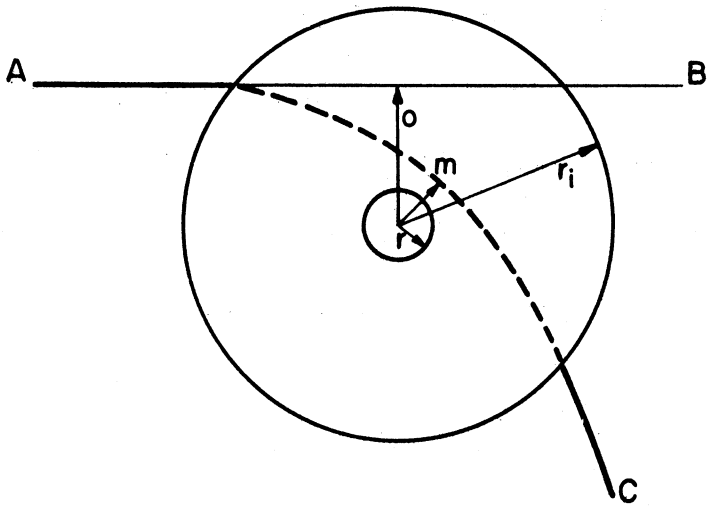

Fig. 2. Positive-ion trajectory about a negative spherical electrode.

where V_o is the potential at point o (undisturbed plasma) and V_m is the potential at point m. The conservation of angular momentum demands that

$$mr_o v_o = mr_m v_m \quad , \tag{2}$$

where r_o is the distance to point o, v_o is the uninfluenced velocity, r_m is the distance to point m, and v_m is the velocity at point m. By manipulation of Eqs. (1) and (2) and letting $V = V_m - V_o$, it can be shown that

$$r_o = r_m \sqrt{1 + V/V_o} \quad . \tag{3}$$

If the value of $r_m \leq r$, the ion will strike the probe or just graze it and, for the purposes of this study, will be considered collected. In this case, r_m is effectively r, and r_o can be interpreted as r_e, the effective radius, allowing Eq. (3) to be written as

$$r_e = r \sqrt{1 + V/V_o} \quad . \tag{4}$$

Equation (4) may be used to determine, for example, the current to a sphere in a region where all the ions have high equal velocities and the same direction with respect to the electrode. This situation may in effect be encountered in rocket applications when the electrode velocity is very high with respect to the ion velocity. When the electrode velocity is sufficiently great, the actual velocity distribution of the ions is unimportant.

The ion current density may be then written

$$J_p = eN_p v_p \quad , \tag{5}$$

where J_p is the positive-ion current density, e a unit charge, N_p is the number density of the ions, and v_p is the common ion velocity. The current, i_p, to the electrode then will equal the current density times its effective cross-sectional area:

$$i_p = J_p \pi r_e^2 \quad . \tag{6}$$

Substituting Eq. (4) into Eq. (6) gives

$$i_p = J_p A_c \, (1 + V/V_o) \quad , \tag{7}$$

where $A_c = \pi r^2$. The corresponding expression for a unit length of a cylinder whose axis lies perpendicular to the direction of the ions is

$$i_p = J_p A_c \sqrt{1 + V/V_o} \quad , \tag{8}$$

where A_c is the projected area of the cylinder, $2\pi rl$. Figure 3 is a sketch of the variation of i_p vs. V for (1) a sphere, (2) a cylinder, and (3) a plane.

If all ions have the same velocity but are random in direction, then the entire surface of the electrode is effective. In this case the

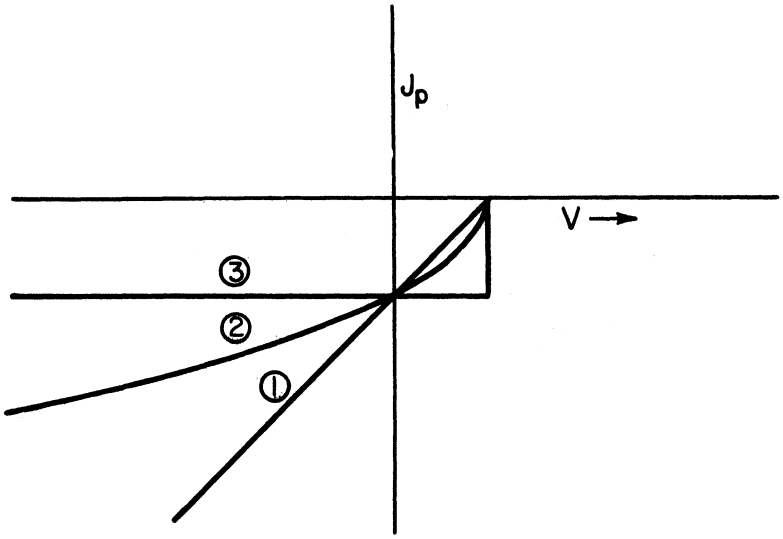

Fig. 3. Electrode volt-ampere characteristics for unidirectional energy distribution.

total area rather than the cross-sectional area of the electrode applies. Again in the case of high ion velocities Eqs. (9) and (10) are obtained corresponding to Eqs. (7) and (8), respectively.

$$i_p = J_p A \left(1 + V/V_o\right) \tag{9}$$

$$i_p = J_p A \sqrt{1 + V/V_o} \tag{10}$$

Figure 3 also represents this situation since only the scale is different.

B. GENERAL SOLUTION

The above elementary solution does not consider the effect of the space-charge region (sheath) or the energy-distribution function of the particles. A more general solution is necessary.

As noted previously, if a spherical electrode is immersed in a uniformly ionized region, it will be surrounded by a concentric spherical

positive-ion sheath of radius a. The region of influence is assumed to correspond to the sheath edge (r_i = a), that is, the potential at the sheath edge is assumed to be equal to the potential of the undisturbed plasma.

Consider the outer edge of the sheath in terms of a right-hand Cartesian coordinate system with u the radially directed velocity component and tangent velocity components v and w. The velocity u is considered positive when directed toward the center of the sphere (see Fig. 4).

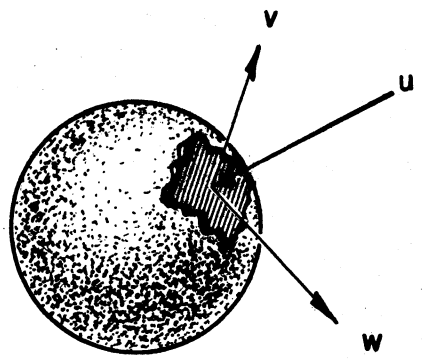

Fig. 4. Velocity-space coordinate system at sheath edge.

If the number of ions N_p at the sheath edge in an incremental volume, $d\tau$, has a velocity distribution

$$f(u,v,w)dudvdw \ , \qquad (11)$$

then

$$N_p f(u,v,w)dudvdwd\tau \qquad (12)$$

is the number of ions that can be expected to have velocities lying in the ranges u to u + du, v to v + dv, and w to w + dw. The number of ions that can be expected to cross the spherical sheath boundary per unit time of the ions within the velocity limits given is

$$4\pi a^2 \, N_p uf(u,v,w)dudvdw \ . \qquad (13)$$

This assumes uniform ionization and velocity distribution throughout the r _ ı of influence.

The total current crossing the boundary is then obtained by multiplying Eq. (13) by the ionic charge (e) and integrating between the proper

limits. Thus

$$i_p = 4\pi a^2 N_p e \int_{o,u_1}^{\infty} \int_{-v_1}^{+v_1} \int_{-w}^{+w} uf(u,v,w)dwdvdu \quad . \qquad (14)$$

The lower limit u_1 applies for a retarding potential on the probe, and the lower limit zero applies for an accelerating potential.

If a Maxwellian distribution is assumed, it may be expressed in Cartesian coordinates as

$$f(u,v,w) = \left(\frac{m}{2\pi kT}\right)^{3/2} \exp\left[-\frac{m}{2kT}(u^2+v^2+w^2)\right] \quad , \qquad (15)$$

where k is Boltzmann's constant and T is the absolute temperature in °K. In the above and the following equations, temperature subscripts have

tted, for the reason that the appropriate temperature (positive

ative ion, or electron) is implied.

is convenient to transform Eq. (15) using

$$u = u \ , \quad v = p \sin\theta \ , \quad w = p \cos\theta \ ,$$

is the velocity component normal to the sheath, p is the corre-

tangential component and θ is the angle between p and an arbi-

ference. Thus the Maxwellian distribution may be written

$$f(u,p) = 2\pi \left(\frac{m}{2\pi kT}\right)^{3/2} \exp\left[-\frac{m}{2kT}(u^2+p^2)\right] \quad . \qquad (16)$$

Equation (14) may be written in terms of the new variables, and upon using Eq. (16) to express the distribution function, the following results:

$$i_p = 4\pi a^2 N_p e \int_{u_1}^{\infty} \int_{o}^{p_1} 2\pi up \left(\frac{m}{2\pi kT}\right)^{3/2} \exp\left[-\frac{m}{2kT}(u^2+p^2)\right] dpdu \quad . \qquad (17)$$

The limits u_1 and p_1 are dependent upon the orbital motion of the ions within the sheath. Thus they are determined by the laws of angular momentum and conservation of energy. The resulting expressions are

$$u_1^2 = -2\frac{e}{m_p}V \tag{18}$$

and

$$p_1^2 = \frac{r^2}{a^2-r^2}\left(u^2 + 2\frac{e}{m_p}V\right) . \tag{19}$$

Using Eqs. (18) and (19) as limits in solving Eq. (17), the following is obtained:

$$i_p = 4\pi a^2 \sqrt{\frac{kT}{2\pi m_p}} N_p e \left\{1 - \frac{a^2-r^2}{a^2}\exp\left[-\frac{eV}{kT}\left(\frac{r^2}{a^2-r^2}\right)\right]\right\} . \tag{20}$$

If V_o represents the voltage equivalent of temperature,

$$\frac{eV}{kT} = \frac{V}{V_o} . \tag{21}$$

Substituting Eq. (21) in Eq. (20) and rearranging gives

$$i_p = A N_p e \sqrt{\frac{kT}{2\pi m_p}}\left\{\left(\frac{a}{r}\right)^2 - \left(\frac{a^2-r^2}{r^2}\right)\exp\left[-\left(\frac{V}{V_o}\right)\left(\frac{r^2}{a^2-r^2}\right)\right]\right\} . \tag{22}$$

Equation (22) is the current to the electrode, when the potential is accelerating [lower limit $u = u_1$ in Eq. (14)]. A is equal to $4\pi r^2$.

In the case of a retarding potential [lower limit $u = 0$ in Eq. (14)],

$$i_p = A N_p e \sqrt{\frac{kT}{2\pi m_p}} \exp\left(\frac{V}{V_o}\right) . \tag{23}$$

The total current entering the sheath (not all ions are collected) may be calculated by integrating Eq. (17) over all velocities. Thus

$$J_p = N_p e \int_o^\infty \int_o^\infty up\, f(u,p)dudp \qquad (24)$$

becomes, for the Maxwellian distribution,

$$J_p = N_p e \sqrt{\frac{kT}{2\pi m_p}} \quad . \qquad (25)$$

This is the random ion current crossing a unit area of the sheath. It represents an isotropic current density in a region where the velocity is everywhere Maxwellian. This is actually not the case at the sheath edge since in general more ions enter the sheath than leave it. In an extreme case all the ions enter the sheath and none leaves it, as will be demonstrated later in the case of sheath-area-limited current. Even in the latter case, the energy distribution is Maxwellian if the sheath is thin with respect to the ion mean free path. It is convenient to normalize Eqs. (22) and (23), letting

$$I_{np} = \frac{i_p}{AJ_p} \quad . \qquad (26)$$

This is a normalized current and is the ratio of the current to the electrode in the presence of a sheath, to the current in the absence of a sheath. Using Eqs. (25) and (26), Eq. (22) becomes

$$I_{np} = \left(\frac{a}{r}\right)^2 - \left(\frac{a^2-r^2}{r^2}\right) \exp\left[-\left(\frac{V}{V_o}\right)\left(\frac{r^2}{a^2-r^2}\right)\right] \qquad (27)$$

for accelerating potential, that is

$$(V/V_o) > 1 \quad ,$$

and Eq. (23) becomes

$$I_{np} = \exp (V/V_o) \qquad (28)$$

for a retarding potential, that is

$$(V/V_o) < 1 \quad .$$

In the latter case, the current is independent of the sheath dimensions, and its logarithm is a linear function of the collector potential. This permits the determination of the temperature of the charge carriers independent of many ionospheric parameters.

In the case of an accelerating potential, the current :
on the sheath radius and thus requires another independent
make possible the calculation of current. An approximate r
this type can be determined from relationships describing s
limited flow in a spherical system in which the entering io
initial velocities; this relationship is

$$i = \frac{4\sqrt{2}}{9} \pi \epsilon_o \sqrt{\frac{e}{m}} \frac{V^{3/2}}{(-\alpha^2)} \quad ,$$

where $(-\alpha^2)$ is a transcendental function of (a/r) that has
in Fig. 5, and ϵ_o is the dielectric constant of the free spa
normalized according to Eqs. (25) and (26),

$$I_{np} = \frac{P}{(-\alpha^2)} \left(\frac{V}{V_o}\right)^{3/2} \quad ,$$

where

$$P = \frac{8\sqrt{\pi}\, \epsilon_o k}{9e^2} \frac{T}{Nr^2} = 7.51 \times 10^3 \frac{T}{Nr^2} \quad . \qquad (31)$$

Equations (27) and (30) form, with $f(a/r) = (-\alpha^2)$, a transcendental system of equations which in general permit only numerical or graphical

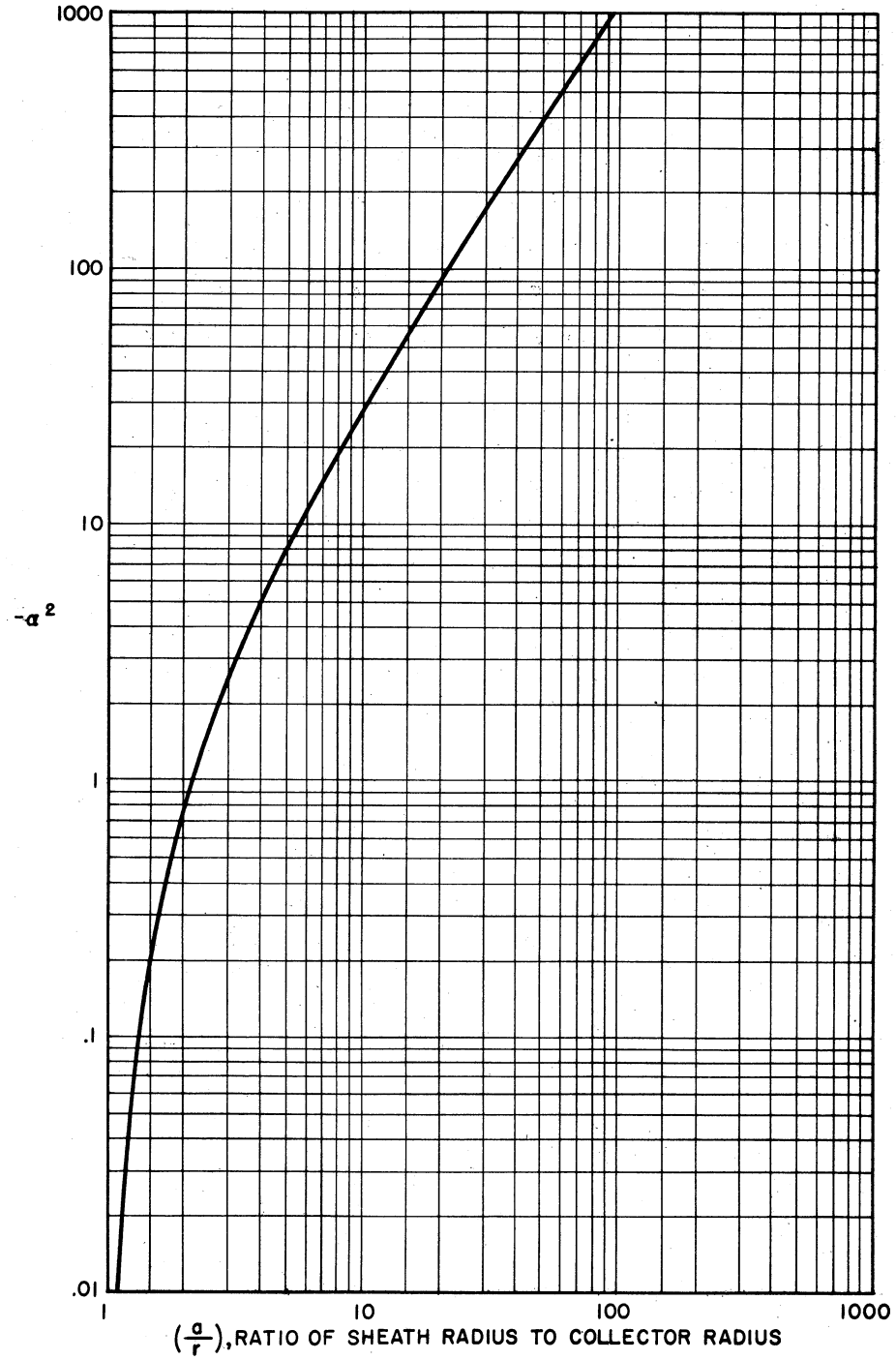

Fig. 5. $(-\alpha^2)$ vs. (a/r), ratio of sheath radius to collector radius.

solutions. If Eq. (27) is plotted on log-log coordinates as a family of curves with (a/r) as the parameter (Fig. 6), then a particular solution of Eq. (31) would appear as a straight line with a slope of 3/2 in the same coordinates. Thus the intersection of a solution of Eq. (30) (straight line) with a solution of Eq. (27) (curve) for a particular (a/r) is a simultaneous solution of the two equations. A curve through a series of such intersections for a given temperature, number density, and electrode size is the volt-ampere characteristic of the electrode. In making calculations, Figs. 7-13, which are enlarged sections of Fig. 6, were used.

Depending on the temperature, number density, and the electrode size, the current to an electrode may be determined by (a) the motion of the ions in the sheath, (b) the size of the sheath, or (c) by a combination of both. The various modes of operation are referred to as (a) orbital-motion-limited, (b) sheath-area-limited, or (c) intermediate. The intersections of the straight line with the curves which represent each of the above are designated in Fig. 6 by a, b, c.

In the case of an orbital-motion-limited solution (high ion temperature, or low number density, or small electrode radius), the ions arriving at the sheath have relatively high velocities, and their collection by the electrode is determined by the law of conservation of angular momentum and the law of conservation of energy. In this case the space charge in the sheath is relatively unimportant, and Eq. (29) does not apply.

In the case of a sheath-area-limited solution (low temperature, or high number density, or large collector radius), the ions arriving at the

sheath have relatively low velocities and all are collected. In this case Eq. (29) does apply with reasonable accuracy. To correct for the initial velocity of Maxwellian distribution, one might replace $V^{3/2}$ with $(1 + 0.0247\sqrt{T/V})V^{3/2}$, which is the correction for parallel plane electrodes;* but this would assume that the effect of the initial velocities of the ions is small, and thus it can only be applied when the probe is sheath-area-limited or nearly sheath-area-limited. As the orbital motion of the ion becomes important, this modification can no longer be applied. In the present study, no other modification was necessary since it was anticipated that the electrodes selected would be either orbital-motion-limited or sheath-area-limited.

C. APPROXIMATIONS OF THE GENERAL SOLUTION

Often an approximate solution is required in a preliminary study of a particular electrode design. Thus one of three appropriate simpler relations may be used. Two of these are asymptotic solutions of Eq. (27), while the third approximates the numerical solution of Eq. (27) and Eq. (30) in the form of one of the asymptotic solutions. The spherical approximate solutions presented herein correspond to the cylindrical approximate solutions previously presented by Hok et al.[5]

The first asymptotic solution applies in the case of either low ion density, or small collector radius, or high temperature. In this case, the sheath is thick $(a/r) \to \infty$. Thus the numerical solutions are asymptotic

*This use of the planar modification has been suggested in the literature; see, e.g., I. Langmuir and K. T. Compton, Rev. Mod. Phys., 3, 191 (1931).

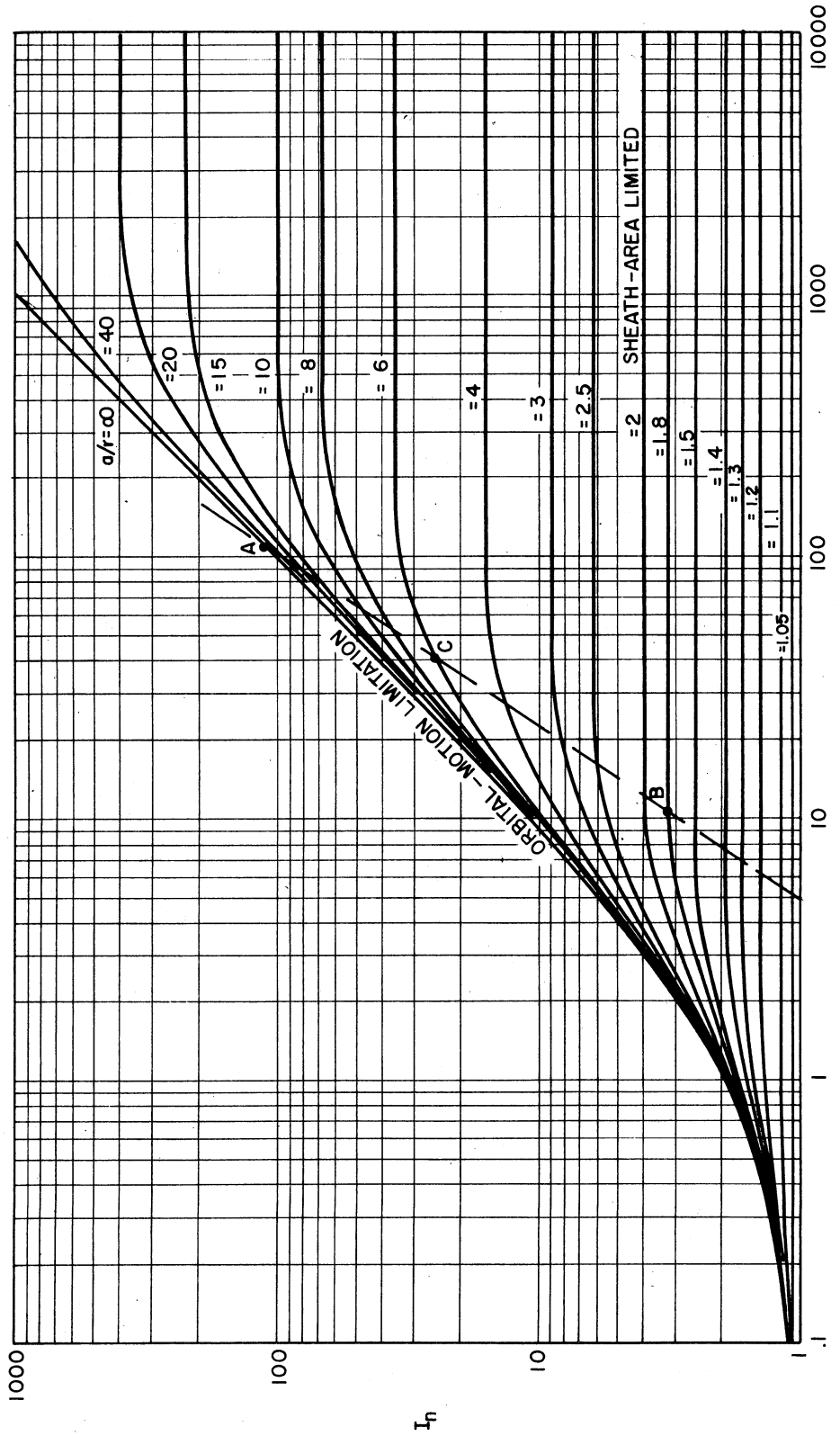

Fig. 6. Normalized current for a spherical electrode. $1 < I_n < 1000$; $0.1 < V/V_o < 10{,}000$.

$$I_n = \left(\frac{a}{r}\right)^2 - \left(\frac{a^2-r^2}{r^2}\right) \exp - \left(\frac{V}{V_o}\right)\left(\frac{r^2}{a^2-r^2}\right)$$

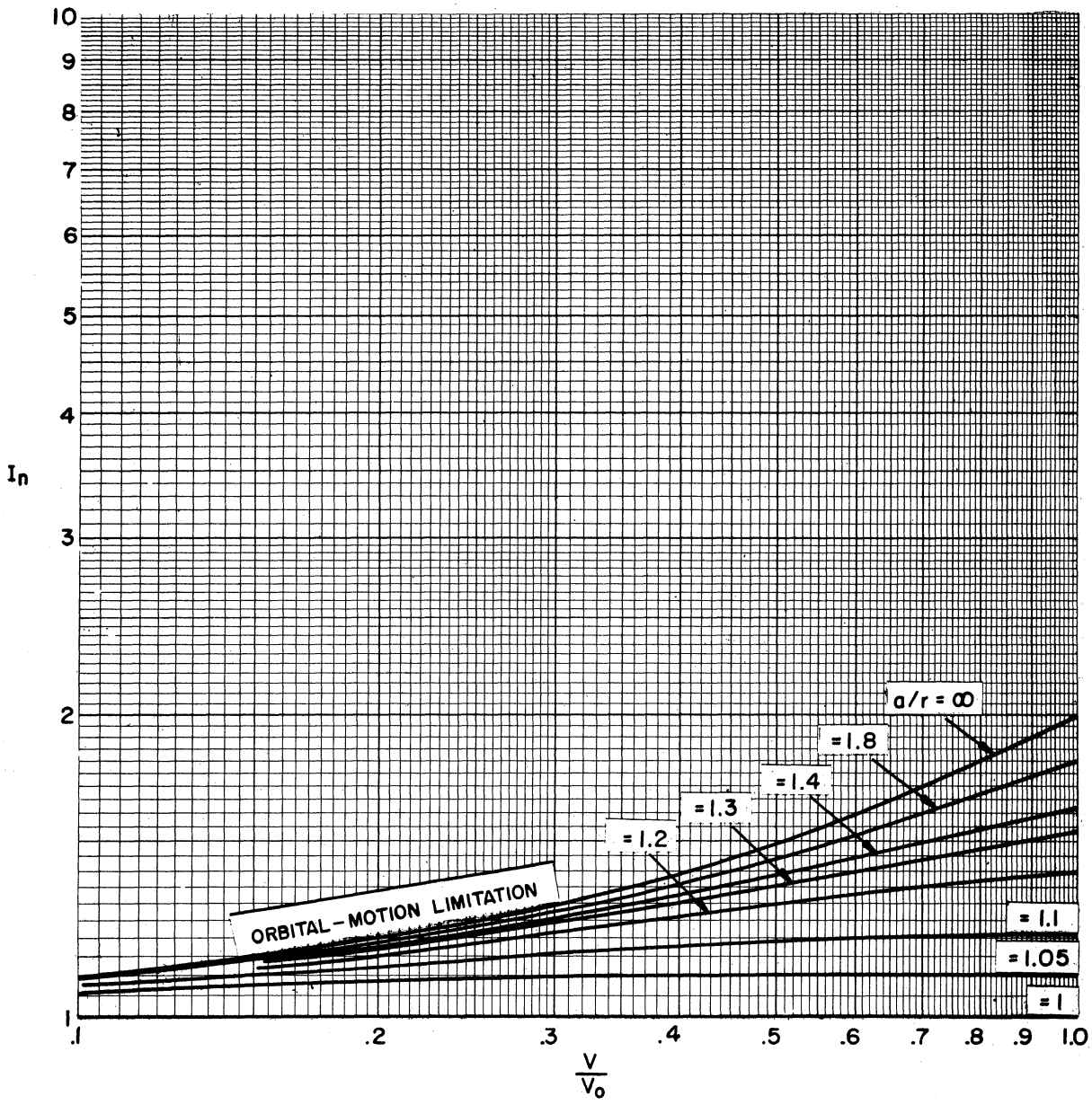

Fig. 7. Normalized current for a spherical electrode. $1 < I_n < 10$; $0.1 < V/V_o < 1$.

$$I_n = \left(\frac{a}{r}\right)^2 - \left(\frac{a^2-r^2}{r^2}\right) \exp - \left(\frac{V}{V_o}\right)\left(\frac{r^2}{a^2-r^2}\right)$$

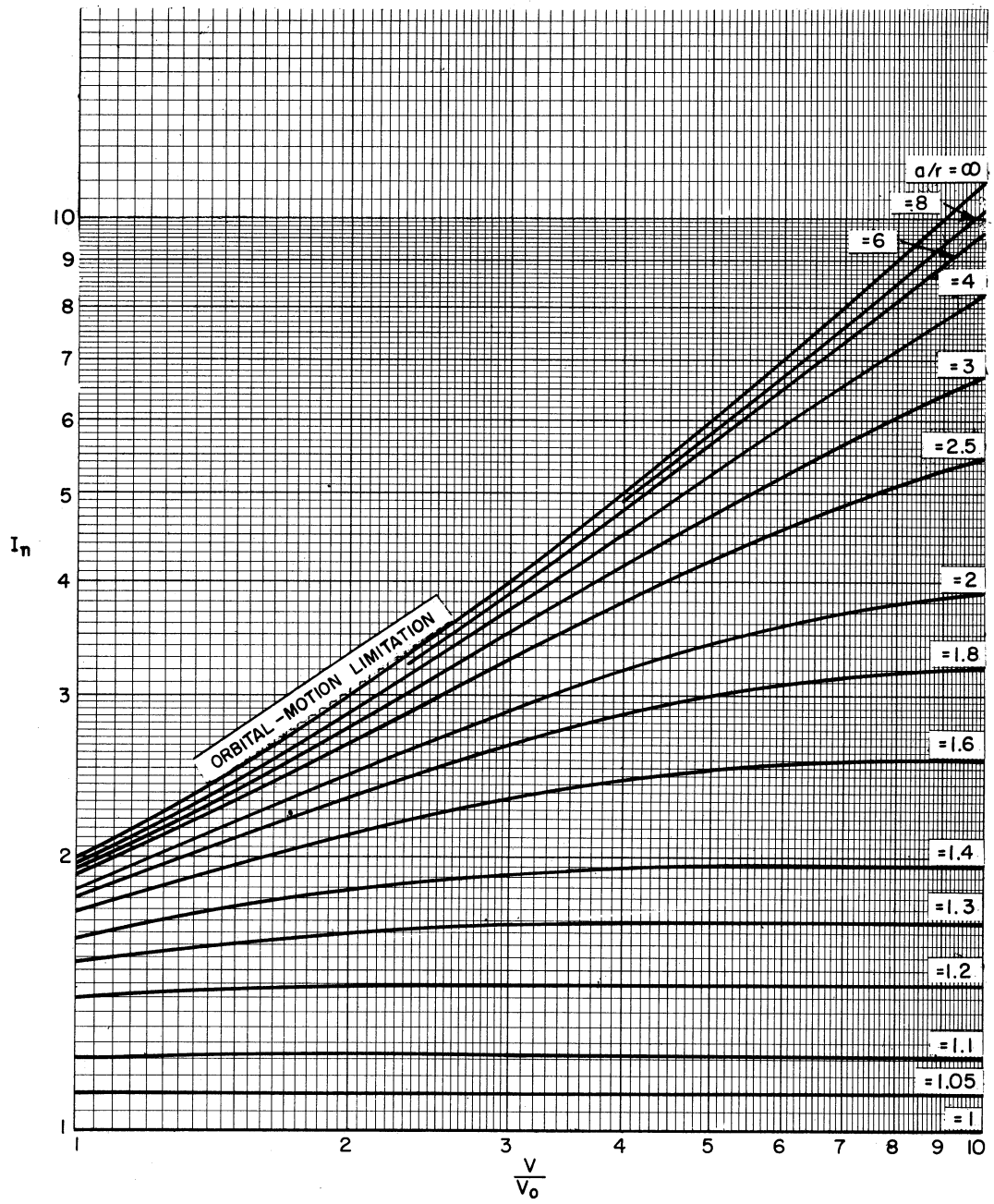

Fig. 8. Normalized current for a spherical electrode. $1 < I_n < 10$; $1 < V/V_o < 10$.

$$I_n = \left(\frac{a}{r}\right)^2 - \left(\frac{a^2-r^2}{r^2}\right) \exp - \left(\frac{V}{V_o}\right)\left(\frac{r^2}{a^2-r^2}\right)$$

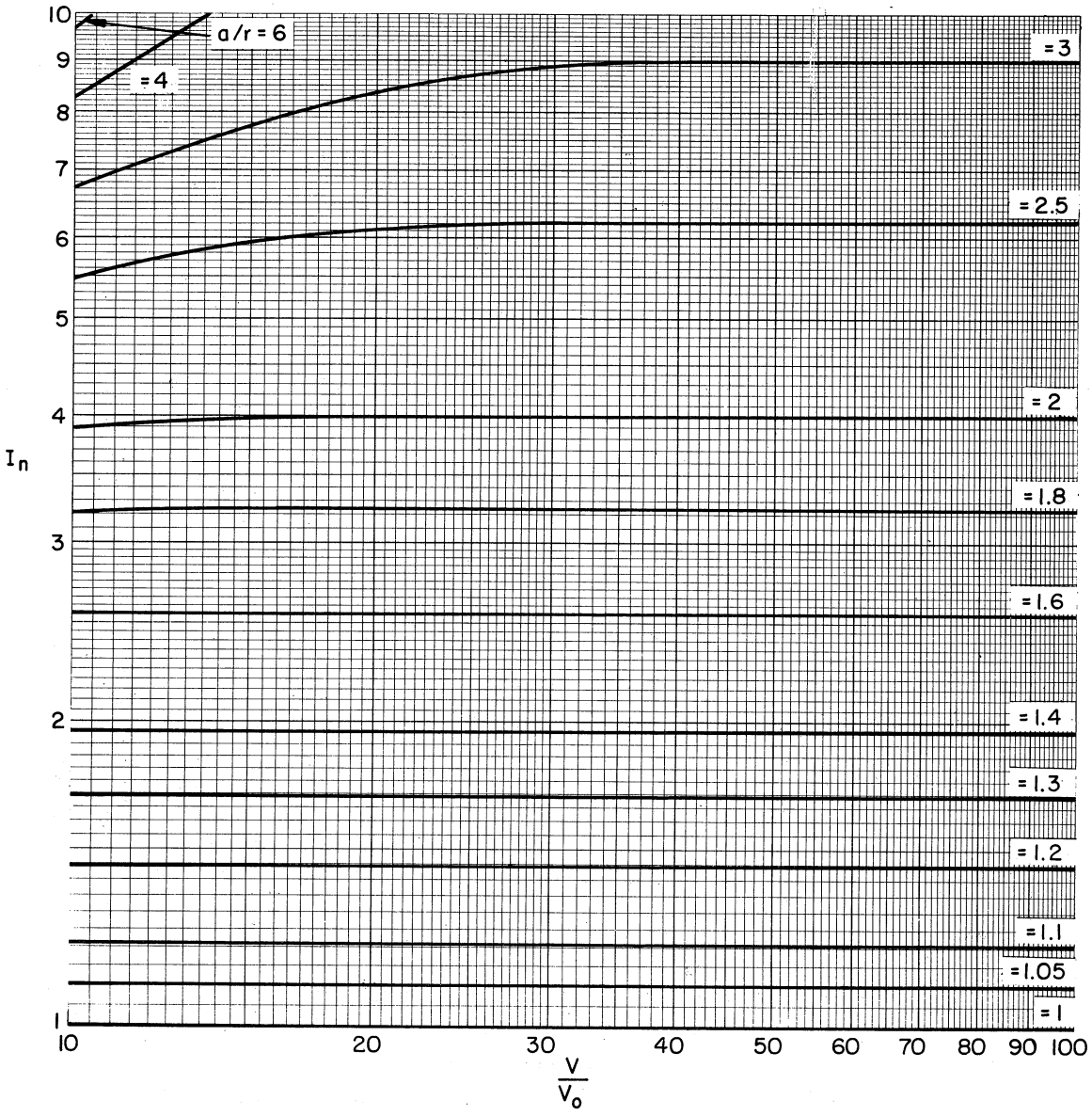

Fig. 9. Normalized current for a spherical electrode. $1 < I_n < 10$; $10 < V/V_o < 10^2$.

$$I_n = \left(\frac{a}{r}\right)^2 - \left(\frac{a^2-r^2}{r^2}\right) \exp - \left(\frac{V}{V_o}\right)\left(\frac{r^2}{a^2-r^2}\right)$$

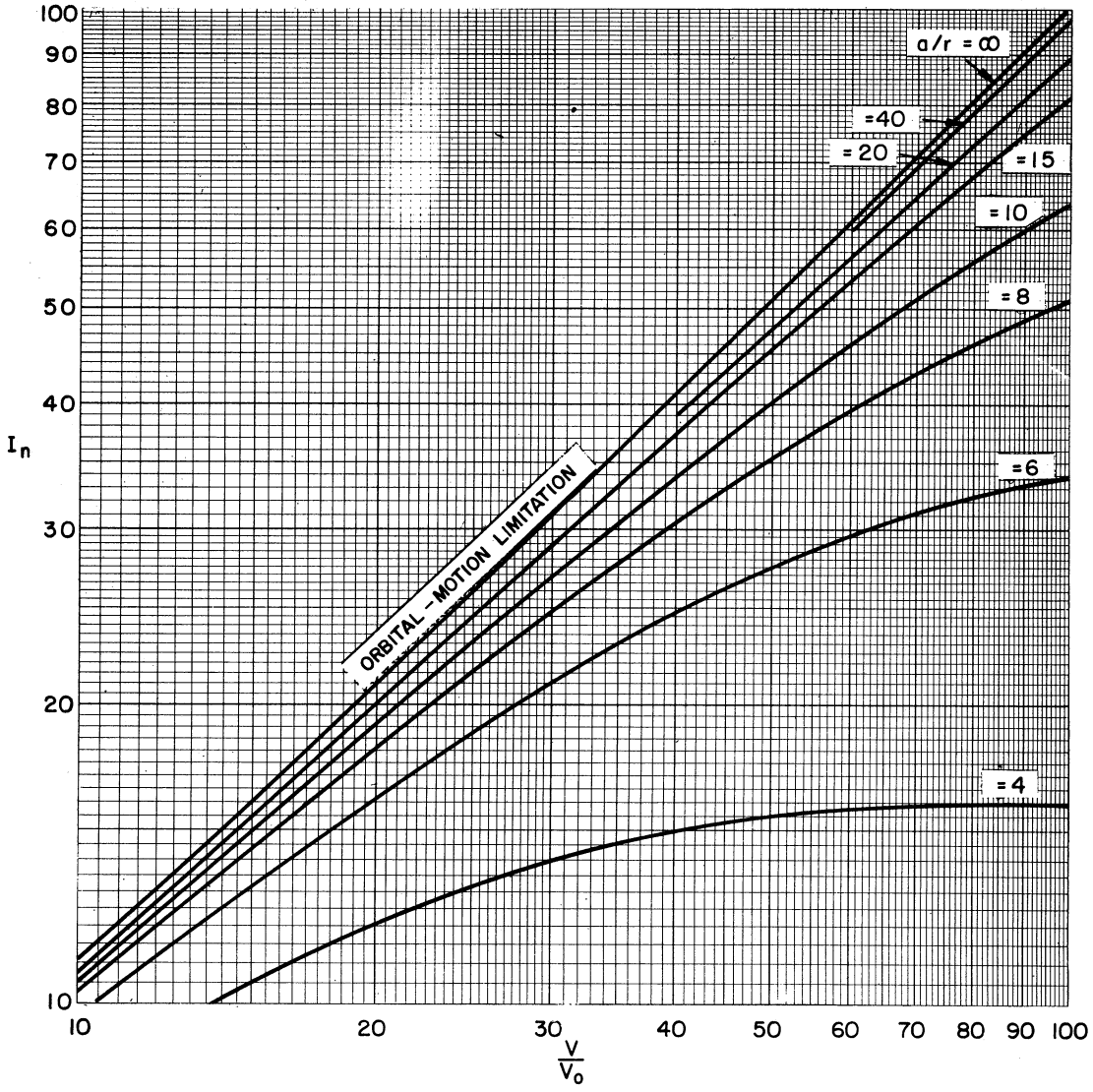

Fig. 10. Normalized current for a spherical electrode. $10 < I_n < 10^2$; $10 < V/V_o < 10^2$.

$$I_n = \left(\frac{a}{r}\right)^2 - \left(\frac{a^2-r^2}{r^2}\right) \exp - \left(\frac{V}{V_o}\right)\left(\frac{r^2}{a^2-r^2}\right)$$

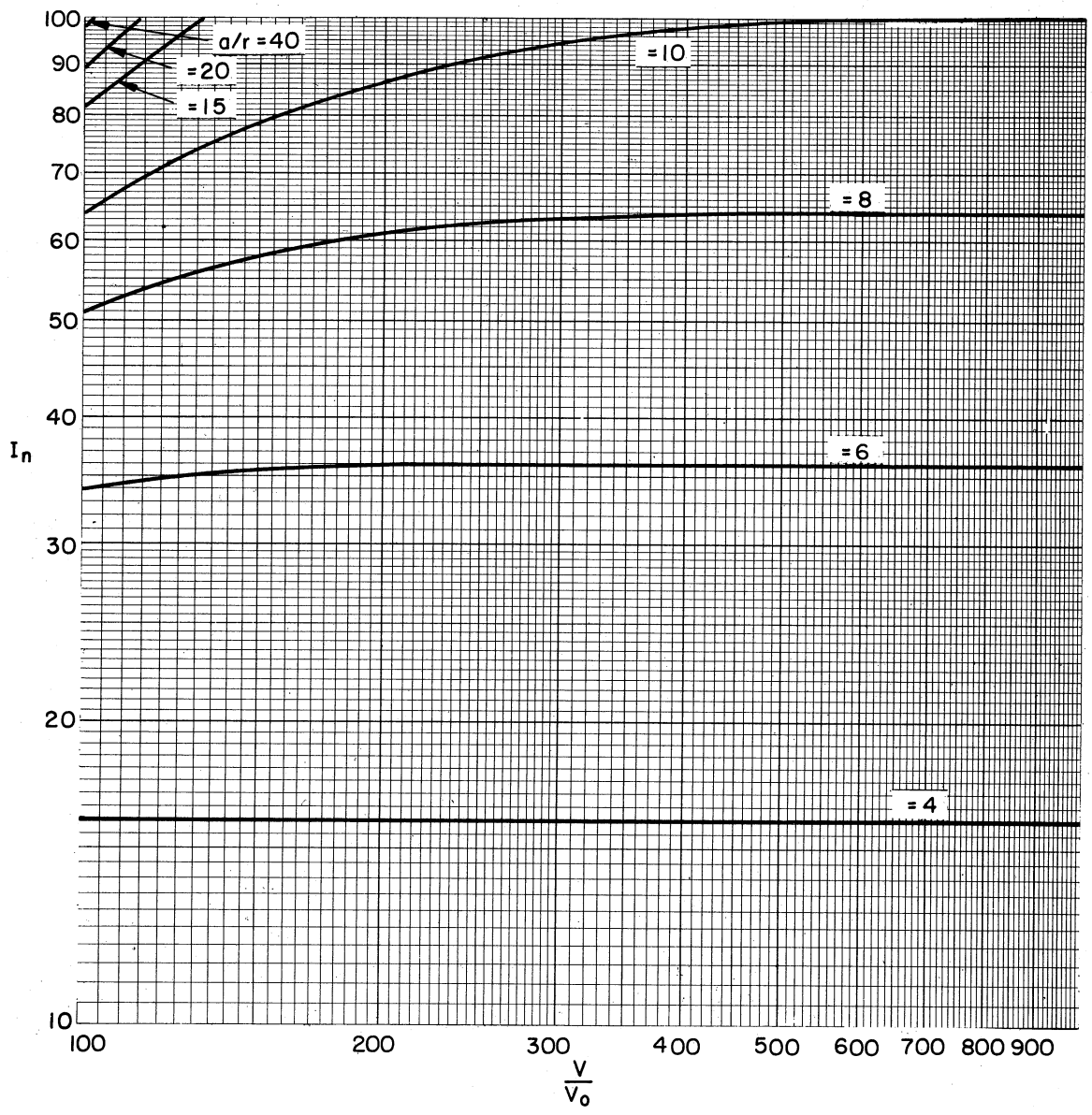

Fig. 11. Normalized current for a spherical electrode. $10 < I_n < 10^2$; $10^2 < V/V_o < 10^3$.

$$I_n = \left(\frac{a}{r}\right)^2 - \left(\frac{a^2-r^2}{r^2}\right) \exp - \left(\frac{V}{V_o}\right)\left(\frac{r^2}{a^2-r^2}\right)$$

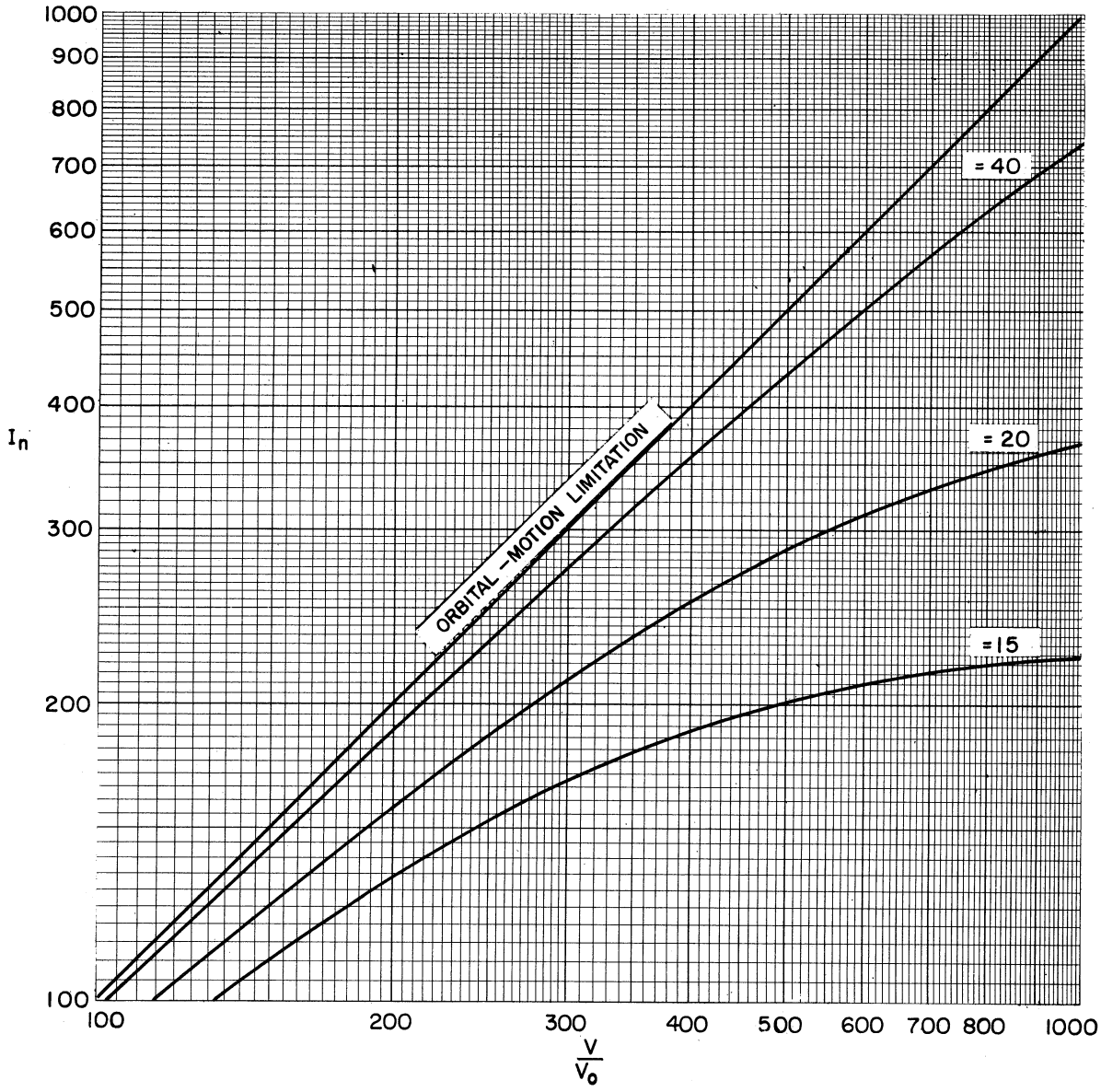

Fig. 12. Normalized current for a spherical electrode. $10^2 < I_n < 10^3$; $10^2 < V/V_o < 10^3$.

$$I_n = \left(\frac{a}{r}\right)^2 - \left(\frac{a^2-r^2}{r^2}\right) \exp - \left(\frac{V}{V_o}\right)\left(\frac{r^2}{a^2-r^2}\right)$$

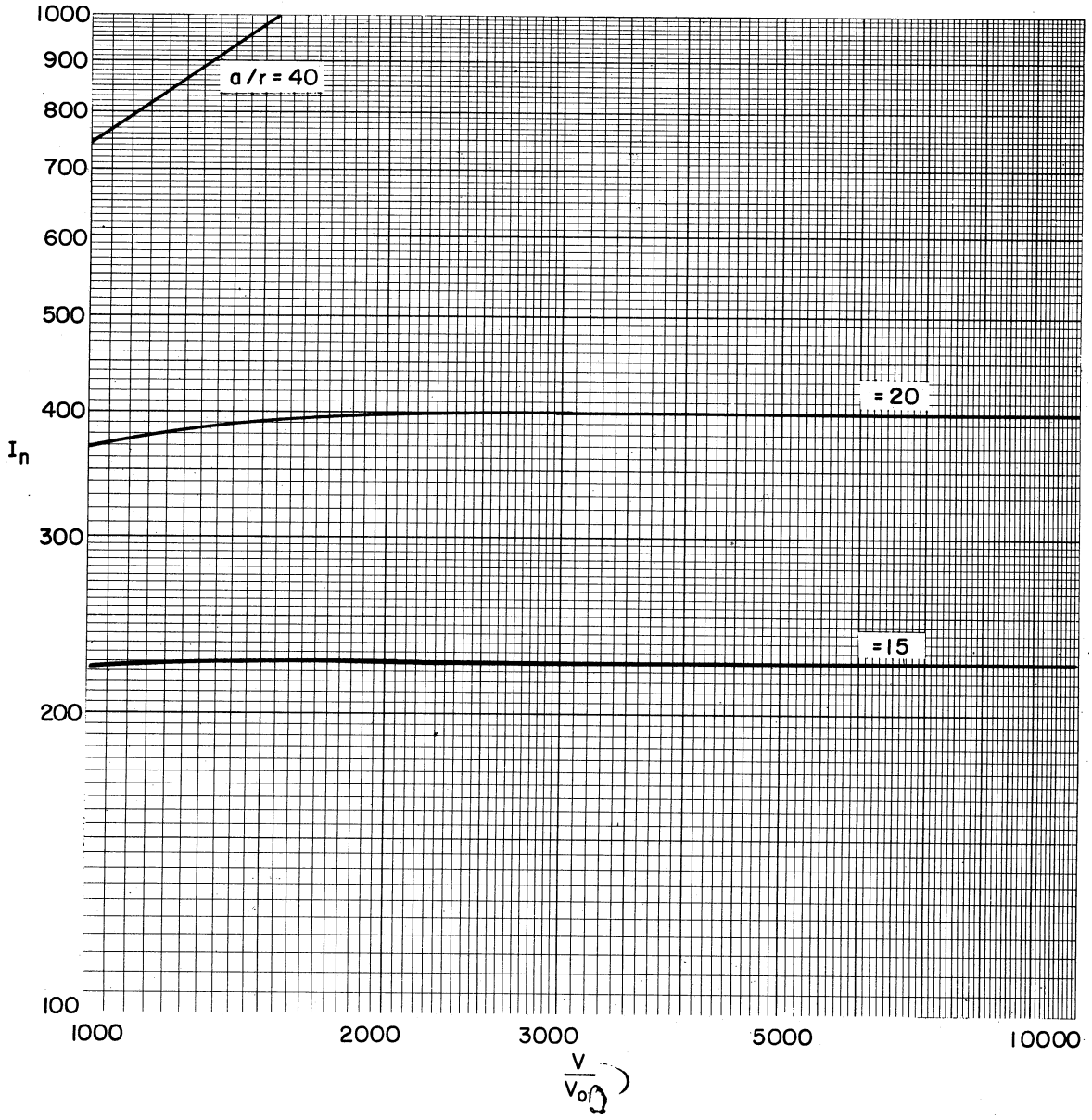

Fig. 13. Normalized current for a spherical electrode. $10^2 < I_n < 10^3$; $10^3 < V/V_o < 10^4$.

$$I_n = \left(\frac{a}{r}\right)^2 - \left(\frac{a^2-r^2}{r^2}\right) \exp - \left(\frac{V}{V_o}\right)\left(\frac{r^2}{a^2-r^2}\right)$$

to the $(a/r) = \infty$ curve in Fig. 6. This is determined mathematically by expanding Eq. (27) as a power series and allowing (a/r) to approach infinity. The result is

$$I_{np} = (1 + V/V_o) \qquad (32)$$

for

$$(V/V_o) > 2 \quad .$$

This is called the orbital-motion-limited solution since the current is dependent on the motion of the ions within the sheath. It is interesting to note that this is the normalized form of Eq. (9) which was obtained in the case of an equal velocity randomly directed energy distribution.

The second asymptotic solution applies in the case of either low ion temperature, or high ion density, or large collector radius. In this case, the sheath is thin $(a/r \to 1)$ and Eq. (27) reduces to

$$I = (a/r)^2 \quad . \qquad (33)$$

All ions arriving at the sheath are collected and the current is dependent only on the sheath area. Thus this is termed the sheath-area-limited current.

Equations (32) and (33) are very useful, but occasionally it is necessary to consider an intermediate case, neither sheath-area-limited nor orbital-motion-limited. It is thus desirable to obtain an approximate solution for this intermediate case.

When Eqs. (27) and (30) are combined with the relation between $-\alpha^2$ and (a/r), a family of curves may be generated with P [see Eq. (31)] as the parameter. Figure 14 compares the solutions of a spherical electrode,

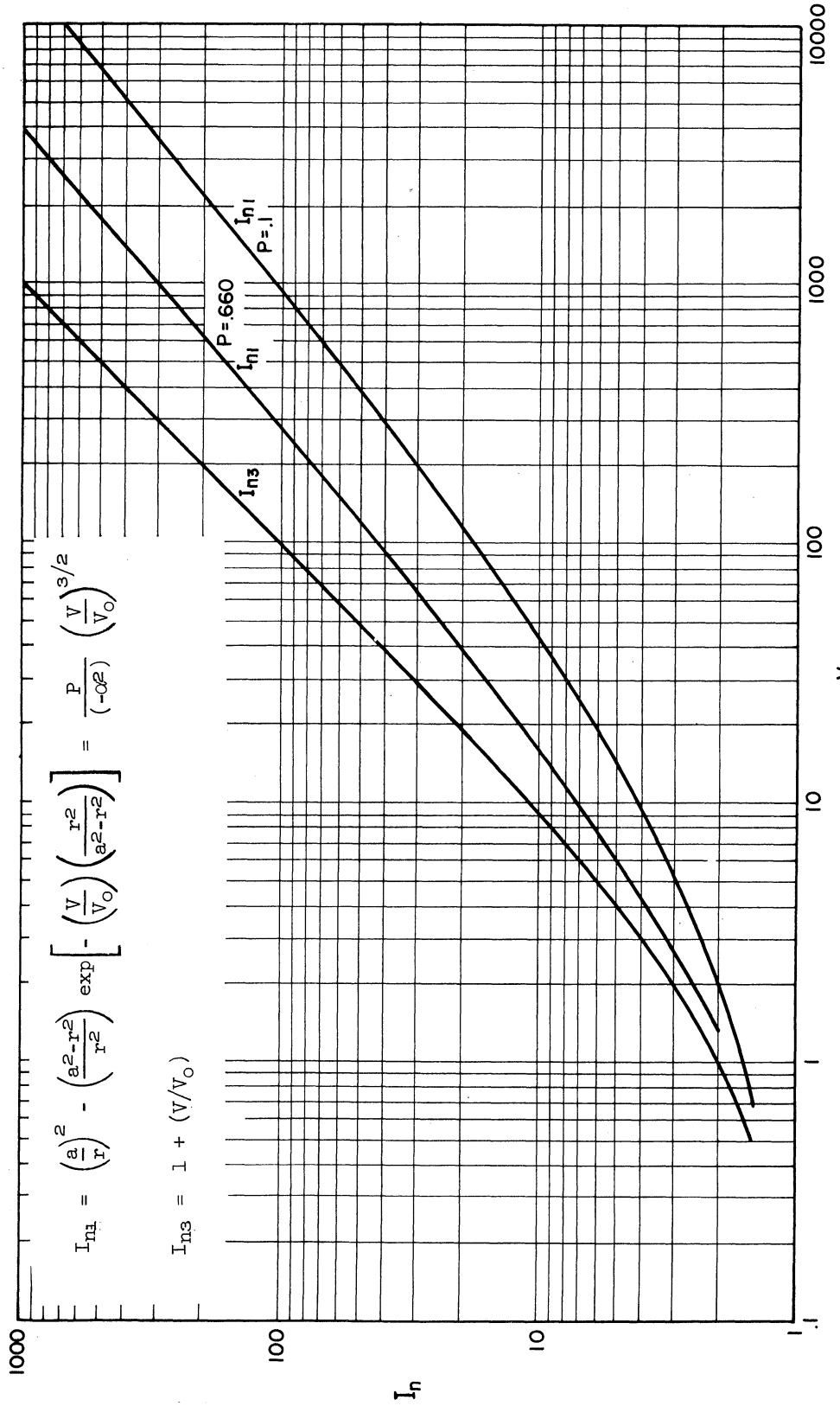

Fig. 14. Numerical solutions (I_{n1}) and orbital-motion-limited solution (I_{n3}).

when P = 0.666 and P = 0.1, with the orbital-motion-limited solution. It is seen that the curves have approximately the same curvature but are displaced horizontally by an amount depending on P. Thus an approximation can be expressed by

$$I_n = 1 + \mu(V/V_o) \quad , \tag{34}$$

where the correction factor $\mu \leq 1$. If the probe is sheath-area-limited μ is approximately $1.5\ P^{2/3}$, where $P = 7.51 \times 10^3\ T/Nr^2$. If the probe is orbital-motion-limited, μ is equal to 1. In intermediate cases the values of μ are obtained by equating the right side of Eq. (34) to a numerically determined solution and solving for μ. The value of μ in the intermediate region is given in Fig. 15 as a function of T/Nr^2.

In the graphical presentation of μ vs. T/Nr^2, Fig. 15, the criteria for the sheath-area-limited and orbital-motion-limited cases become clear. Thus the electrode is sheath-area-limited if

$$T/Nr^2 \leq 5 \times 10^{-6} \quad . \tag{35}$$

It is orbital-motion-limited if

$$T/Nr^2 \geq 10^{-3} \quad . \tag{36}$$

In summation, while the general solution results in transcendental equations requiring either machine or graphical solution, there are several approximating equations which afford reasonable accuracy. Four methods of calculating the current to an electrode which has an accelerating potential for the particles, with respect to the plasma, are as follows.

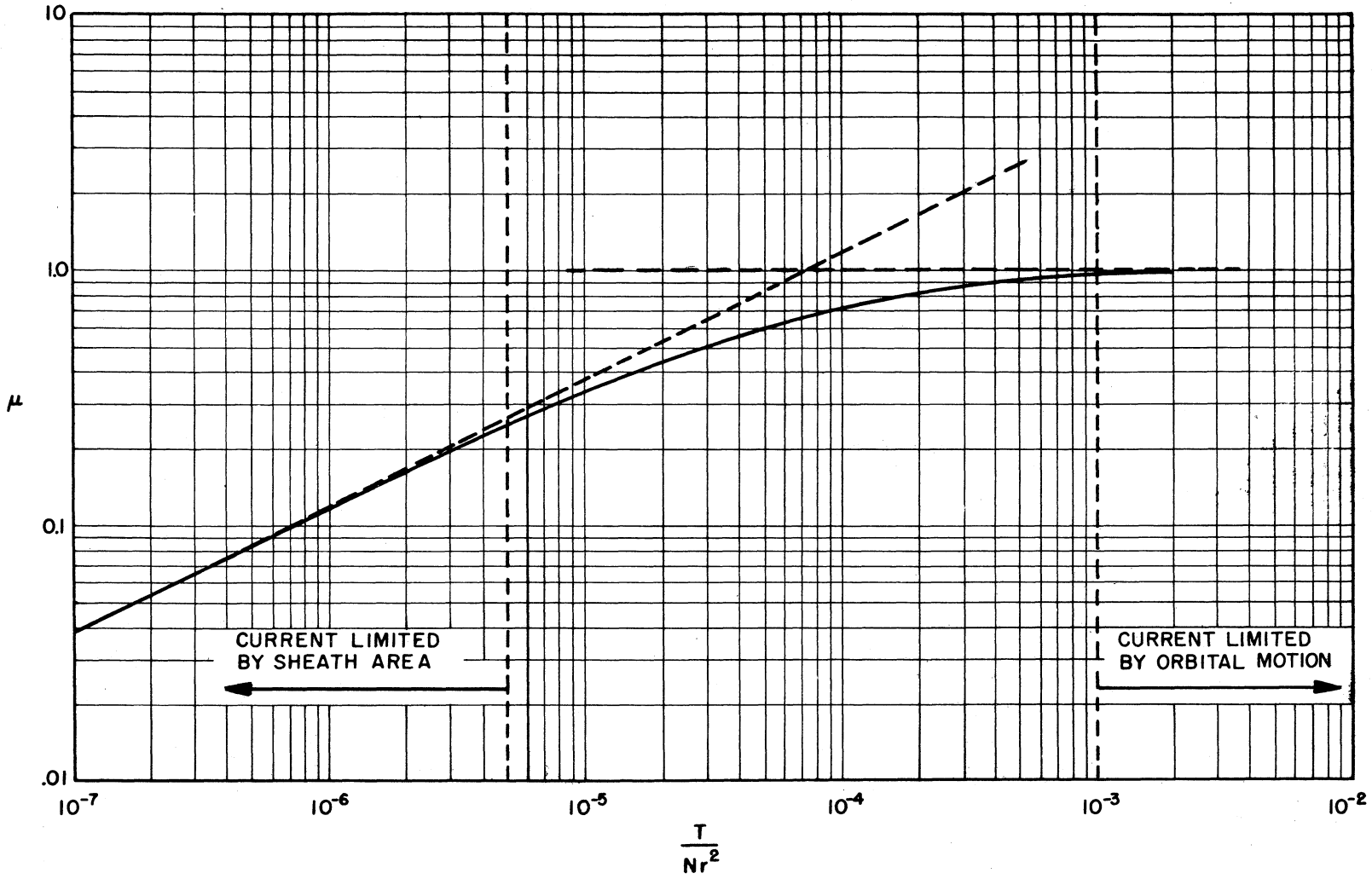

Fig. 15. Numerical values of μ for spherical electrode.

1. General.—The numerical solution, which is the simultaneous solution of Eqs. (27) and (30) with the relations of a/r and $-\alpha^2$, either by machine or graphical means.

2. General.—An approximate solution which adapts the orbital-motion limited solution, Eq. (32), for use in intermediate or sheath-area-limited cases.

3. Asymptotic.—The orbital-motion-limited solution, Eq. (32), when it applies.

4. Asymptotic.—The sheath-area-limited solution, Eq. (33), when it applies.

The various equations, both general and approximate, for sphere and cylinder and plane are tabulated in Table I. The choice between using the general equations or an approximate solution depends on the accuracy required. The appropriate choice of approximate solution may be based on consideration of the factor T/Nr^2, presented in Fig. 15 and appearing in Eqs. (35) and (36).

To aid in the choice of the most appropriate solution for a particular application, the numerical solution is compared in Fig. 16 with the approximate solution, and in Fig. 17, with the sheath-area-limited solution for 3 values of P. The values of (V/V_o) generally encountered in a practical application lie between 2 and 20.

TABLE I

PLASMA-IMMERSED-ELECTRODE CURRENTS

	Sphere	Cylinder	Plane
Retarding Potential, $V/V_o > 0$			
1. General Numerical	$I_n = \left(\frac{a}{r}\right)^2 - \left(\frac{a^2-r^2}{r^2}\right) \exp - \left(\frac{V}{V_o}\right)\left(\frac{r^2}{a^2-r^2}\right)$	$I_n = \frac{a}{r} \operatorname{erf}\left[\frac{r^2(V/V_o)}{a^2-r^2}\right]^{1/2} + \left\{1 - \operatorname{erf}\left[\frac{a^2(V/V_o)}{a^2-r^2}\right]^{1/2}\right\} \exp\left(\frac{V}{V_o}\right)$	$I_n = 1$
	$I_n = \frac{P}{-\alpha^2}\left(\frac{V}{V_o}\right)^{3/2}$	$I_n = \frac{P}{-\beta^2}\left(\frac{V}{V_o}\right)^{3/2}$	$I_n = \frac{8\sqrt{\pi}\,\epsilon_o\,kT}{9\,N\,e^2\beta^2}\left(\frac{V}{V_o}\right)^{3/2}$
	where $P = \frac{8\sqrt{\pi}\,\epsilon_o\,kT}{9\,N\,e^2r^2}$	$P = \frac{8\sqrt{\pi}\,\epsilon_o\,kT}{9\,N\,e^2r^2}$; $\operatorname{erf} X = \frac{2}{\sqrt{\pi}}\int_o^X e^{-y^2}\,dy$	
2. General Approximate	$I_n = 1 + \mu_s\left(\frac{V}{V_o}\right)$	$I_n = \sqrt{1 + \mu_c(V/V_o)}$	$I_n = 1$
3. Asymptotic Orbital-Motion-Limited	$I_n = 1 + \left(\frac{V}{V_o}\right)$	$I_n = \sqrt{1 + (V/V_o)}$	$I_n = 1$
4. Asymptotic Sheath-Area-Limited	$I_n = \left(\frac{a}{r}\right)^2$	$I_n = \frac{a}{r}$	$I_n = 1$
Retarding Potential, $V/V_o < 0$			
	$I_n = \exp\left(\frac{V}{V_o}\right)$	$I_n = \exp\left(\frac{V}{V_o}\right)$	$I_n = \exp\left(\frac{V}{V_o}\right)$

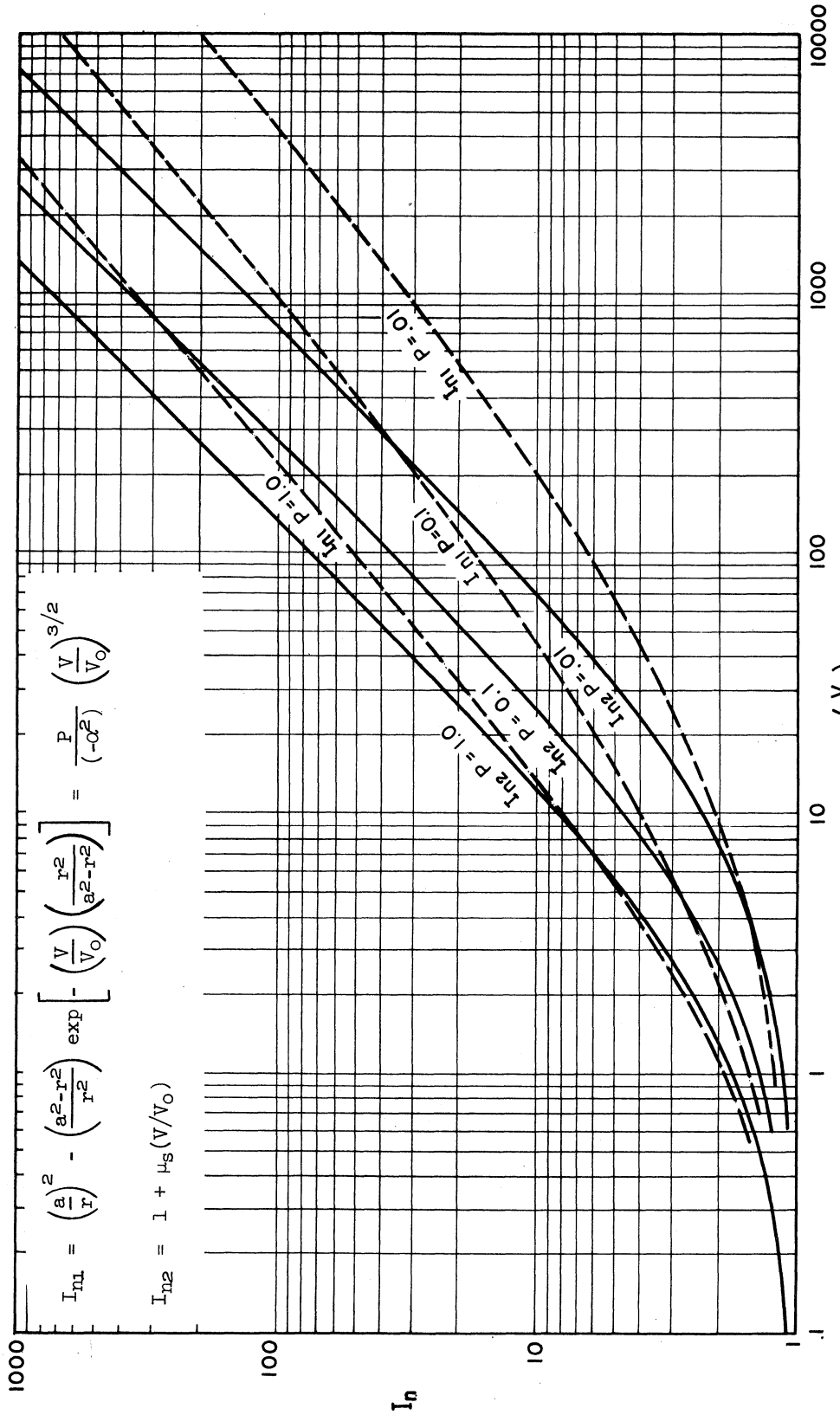

Fig. 16. Numerical (I_{n1}) and approximate (I_{n2}) solutions shown for comparison.

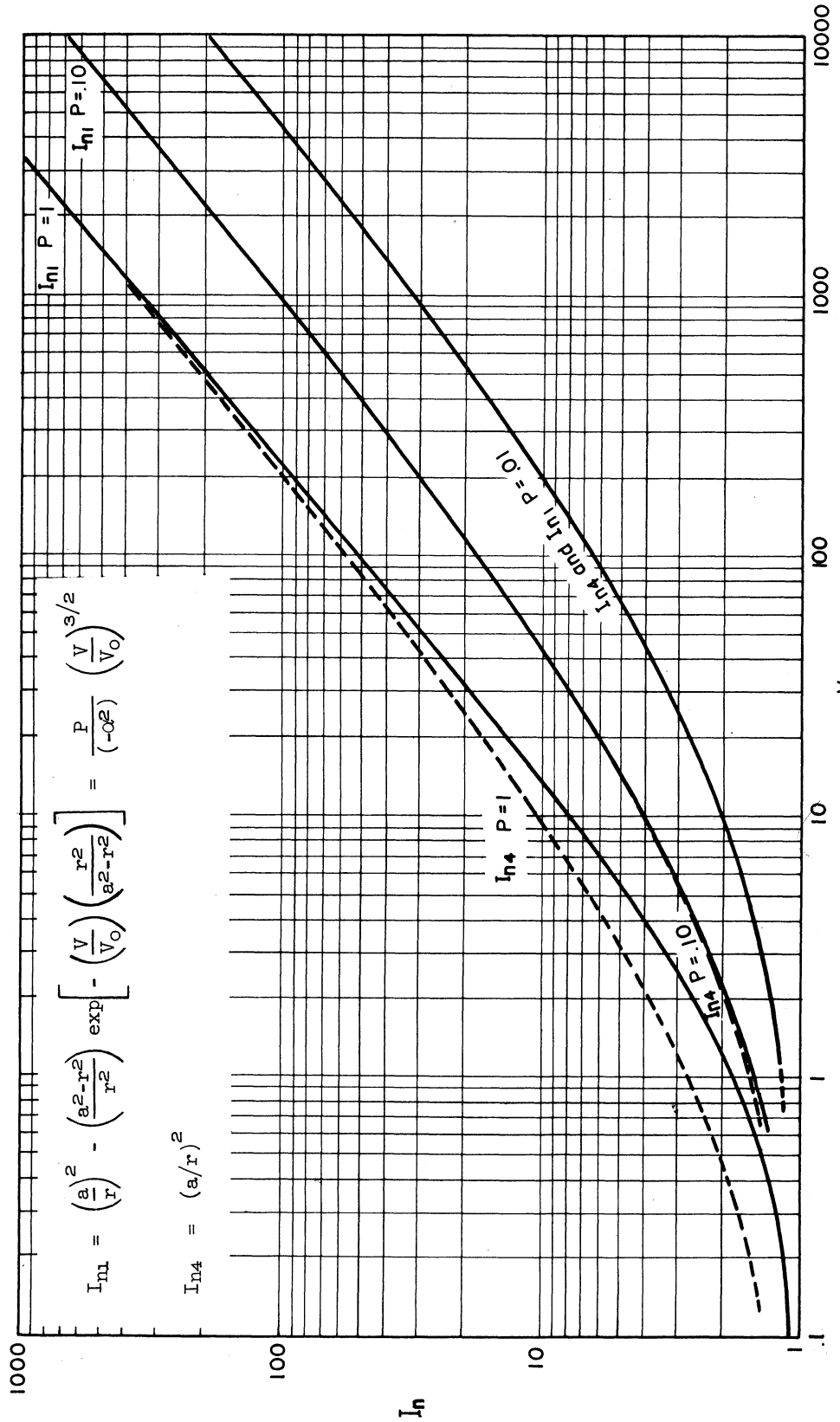

Fig. 17. Numerical (I_{n1}) and sheath-area-limited (I_{n4}) solutions shown for comparison.

IV. APPLICATION OF THEORETICAL DEVELOPMENT TO HYPOTHETICAL PROBES

A. SINGLE-ELECTRODE PROBE

The net current to an electrode in a plasma is composed of positive ions, negative ions, and electrons. Thus to obtain the net current it is necessary to add algebraically the individual currents calculated by Eq. (28) in combination with any one of Eqs. (27), (32), or (33).

The current to a single spherical electrode in a plasma containing only positive ions and electrons is shown in Fig. 18.

Curve (1) is a sketch of electron current to the probe. Curve (2) shows orbital-motion-limited ion current; Eq. (32) applies in this case. Curve (3) is the algebraic sum of curves (1) and (2); thus it is the net current to an individual electrode as a function of its sheath voltage.

Experimentally, curve (3) (Fig. 18) is obtained by measuring the current resulting from applying a linearly changing voltage between the plasma-immersed electrode and a fixed reference. If this voltage reference is the cathode, as it usually is in laboratory applications, the applied voltage will be zero at some point to the left of V_w. The voltage between the reference voltage and the current axis of Fig. 18 is then called the plasma voltage, V_p.

B. BIPOLAR PROBE OF EQUAL-AREA ELECTRODES

In the design of an ionosphere probe, no fixed reference is available. Even the entire carrier vehicle, in general, cannot be assumed

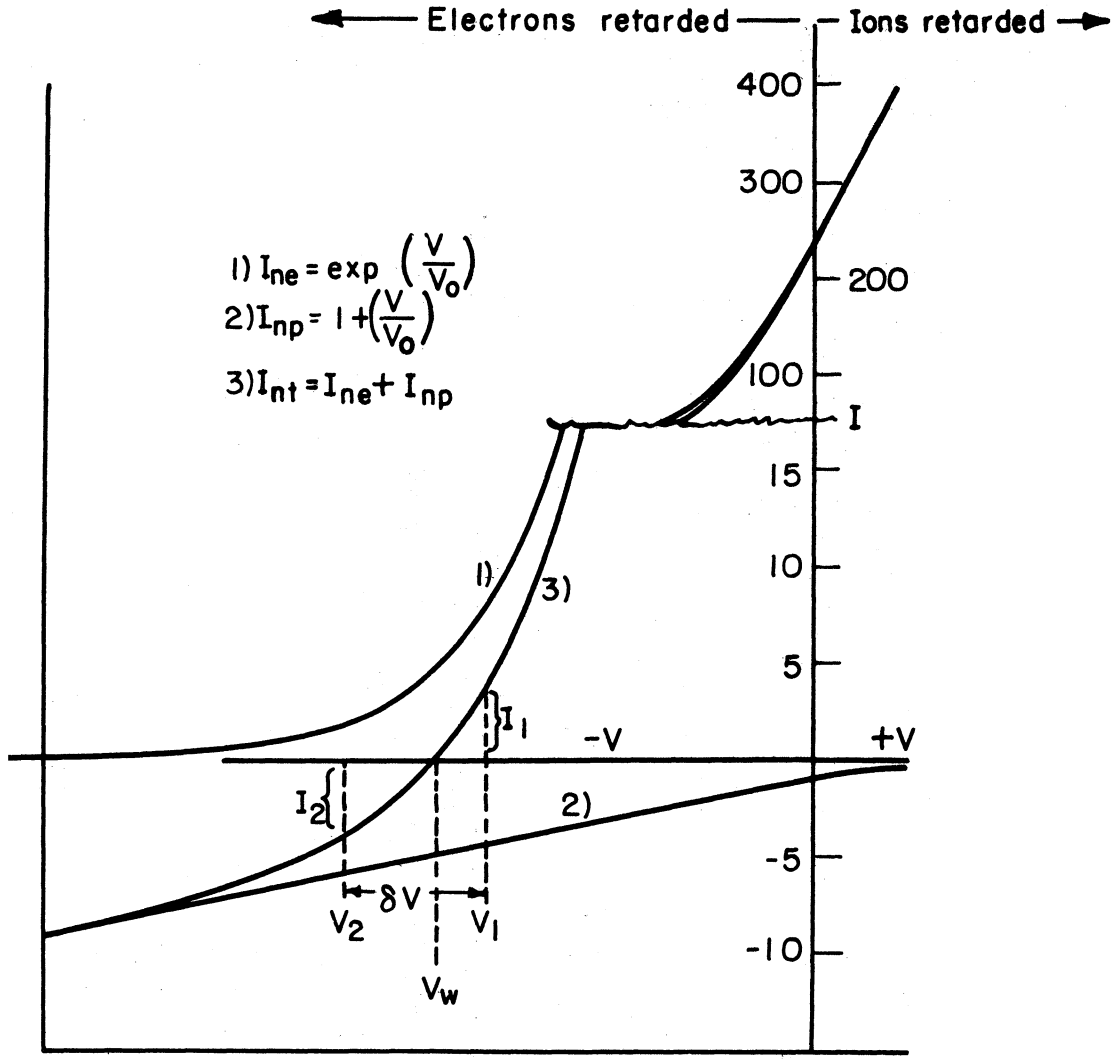

Fig. 18. Single spherical electrode volt-ampere characteristics.

provide a fixed reference. Thus, one must consider a two-electrode tem, referred to herein as a bipolar probe, and must then recognize that net current to the system from the plasma is zero except for transient effects.

Bipolar probes have been used to advantage in gas-discharge-tube studies as well as in the previously mentioned rocket instrumentations. In the former, they have proven to yield certain data with less disturbance of the plasma than a single-electrode probe.[12,13]

If two identical unconnected conducting spherical electrodes are immersed in a plasma, they will assume voltages with respect to the plasma such that the current to each is zero. This condition is depicted in Fig. 19, which shows a sketch of the voltage distribution along a line passing through the center of the spheres. Here each sphere is considered completely isolated in the plasma, no attempt being made to show the alterations of the voltage distribution due to a connecting lead (to be added) or the presence of the second sphere.

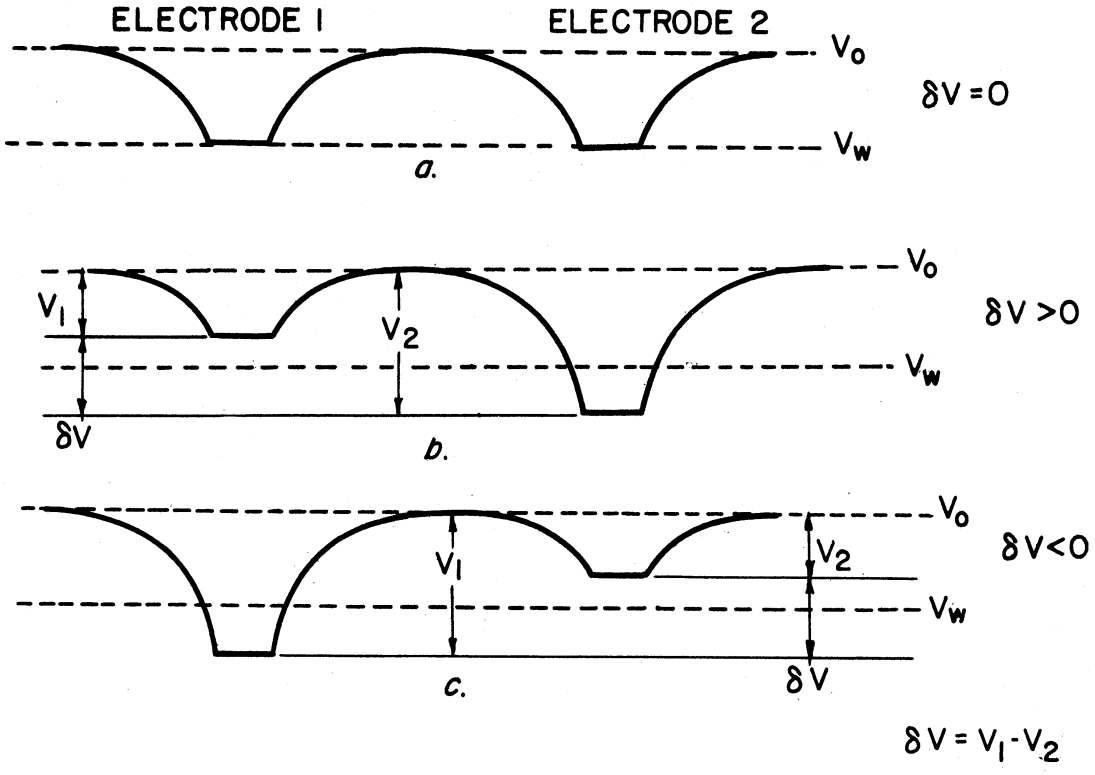

Fig. 19. Potential diagram of a bipolar probe.

In practice, the two probes are connected by a voltage source which provides a linearly changing voltage as

$$\delta V = V_1 - V_2 \tag{37}$$

where V_1 is the voltage between electrode 1 and the plasma, and V_2 is the voltage between electrode 2 and the plasma. It is seen that, when δV is positive, probe 1 rises above V_w (null potential) and draws an electron current. Simultaneously probe 2 will fall below V_w and draw an equal positive-ion current (see also Fig. 18). Only δV can be varied; V_1 and V_2 are determined by the properties of space to meet the requirement of zero net current.

In predicting the characteristics of a bipolar probe, it is convenient to plot the current to the individual electrodes as shown in Fig. 20. Thus the volt-ampere characteristic of the particular probe pair can be determined by reading the voltage between the two curves for specific current values.

A typical curve so obtained is shown in Fig. 21. The letters on the curve indicate approximate boundaries of regions of particular interest. In the AB and EF regions, the electrode having a net electron flow ($V > V_w$) requires a relatively small change in potential for a large change in current; therefore the shape of the curve in this interval may be assumed to be determined entirely by the volt-ampere characteristics of the other electrode which is drawing a net positive-ion current. In the BC and DE regions the departure of the curve from the nearly straight line sections, AB and EF, is due to a change of the electron current to the electrode drawing a net positive-ion current.

In the CD region, both electrodes are approaching the null potential. Thus the change in current to one is almost identical to the inverse of

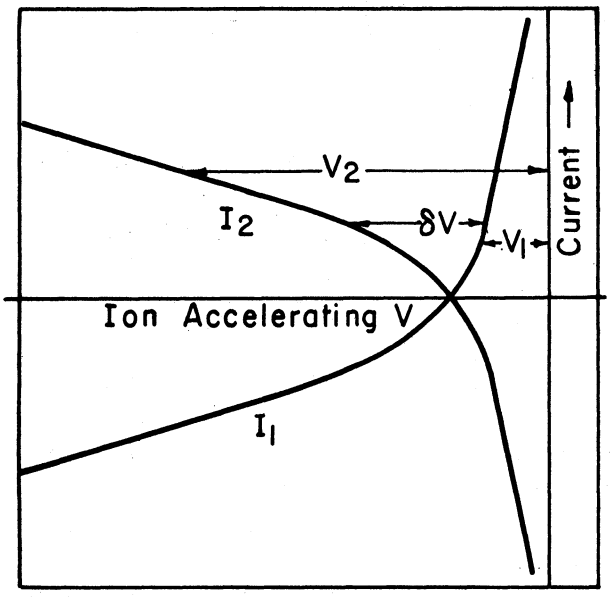

Fig. 20. Single spherical electrode volt-ampere characteristics.

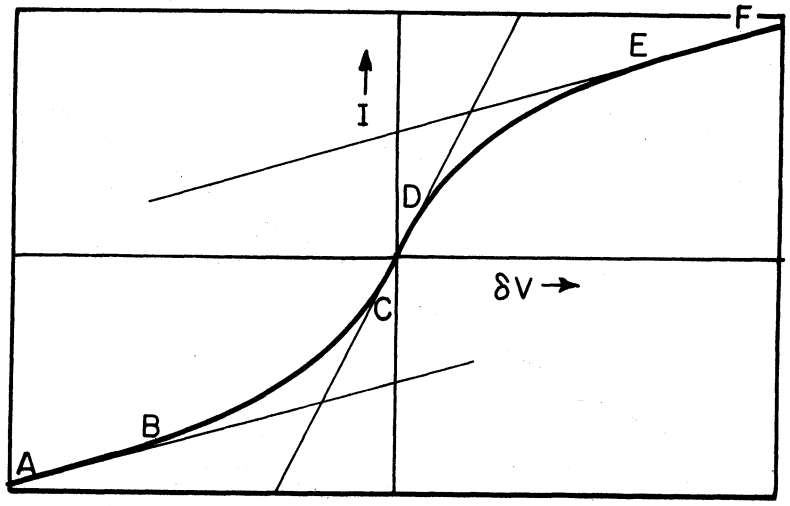

Fig. 21. Volt-ampere characteristic of a bipolar-equal-area probe.

the change to the other, resulting in a near-linear characteristic in this region. The origin is the point of inflection of the symmetrical curves and is also the maximum slope of the bipolar volt-ampere characteristic. Given an experimental curve, the electron current can be determined by extending the AB portion of the curve to determine the difference in current between this extended curve and the curve in the BC region. This is a good approximation of the electron current drawn by probe 1. The electron current so determined is, for practical purposes, represented by Eq. (23). Since this equation is an exponential function of V/V_o alone, it is seen that a plot of $\log_e i_e$ vs. voltage results in a straight line whole slope is the reciprocal of the voltage equivalent (V_T) of the electron temperature (Fig. 22).

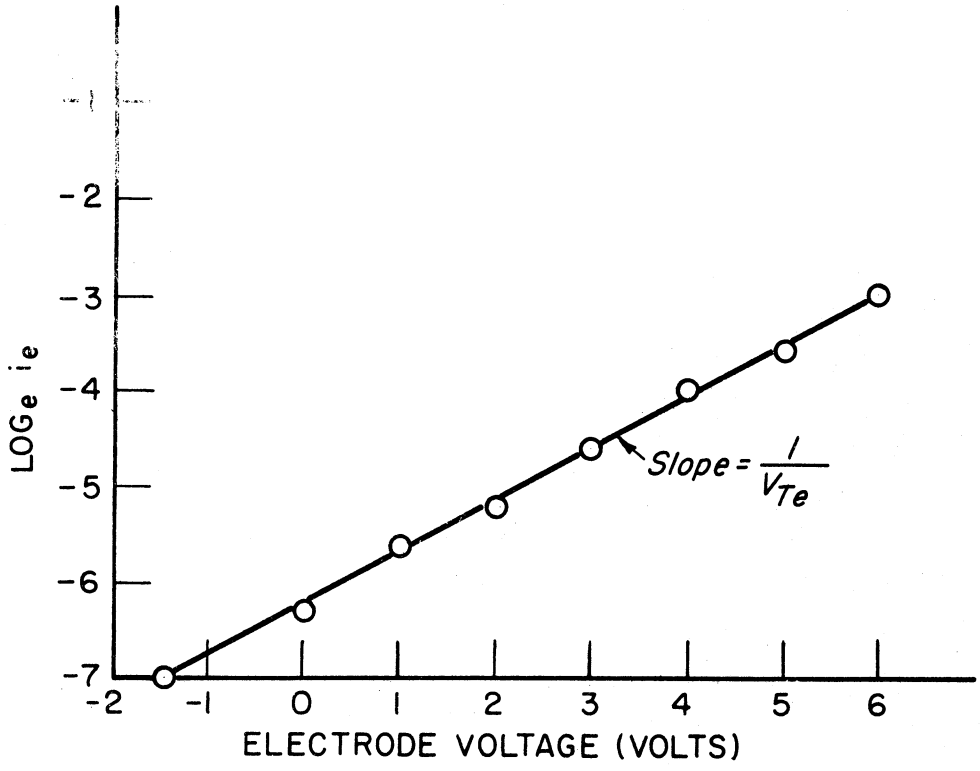

Fig. 22. $\text{Log}_e i_e$ vs. V, log electron current vs. electrode difference voltage.

The ion density may be obtained from such an experimental curve by utilizing the electron temperature as determined above and the AB or EF region of the characteristic curve as outlined in Section VIII J. A discussion of data reduction and its interpretation is also included in Section VIII.

C. BIPOLAR PROBE OF UNEQUAL-AREA ELECTRODES

If the two electrodes of a bipolar probe are unequal in area, or if they have different geometries, the volt-ampere characteristic will not be symmetrical. If they have the same geometry but are unequal in area, and if the ion current to each electrode is limited in the same manner, the current between the electrodes, signal current, is approximately zero when δV is zero. This condition is illustrated in Fig. 23 for two orbital-motion-limited electrodes where $A_1/A_2 = 1/2$. (A_1 is the area of the number 1 electrode and A_2 is the area of the number 2 electrode.)

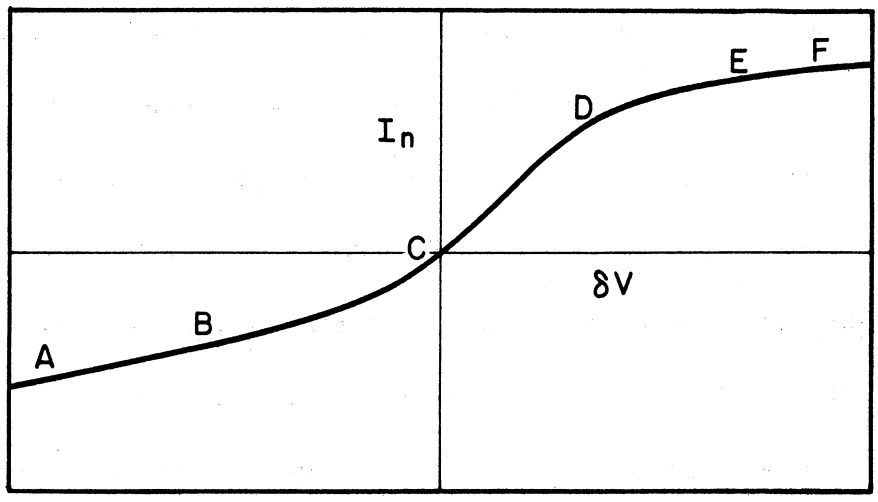

Fig. 23. Volt-ampere characteristics of unequal-area-bipolar probe.

The higher current for a given V/V_o occurs when the larger electrode is drawing predominantly positive-ion current, the smaller one drawing a net electron current. Unequal electrode systems sample a larger percentage of the electrons, thereby permitting electron energy distribution to be determined over a wider range of energies. This objective, however, requires greater area ratios than the 2-to-1 of the preceding example.

If the area ratio were great enough, the bipolar probe current would be limited by the electron flow to the smaller electrode rather than by the ion current to the larger. This would allow an independent measurement of ion temperature and electron density as well as energy distribution. However, more must be known about the physical processes taking place in the surrounding regions before the data from the electron-limited characteristic could be interpreted with confidence.

If the shapes of the electrodes are not alike, or if an area difference results in current-limiting conditions differing for two similar geometry electrodes, the characteristic will not be symmetrical, nor will zero δV result in zero signal current. The δV resulting in zero signal current is a function of the area ratio, number density ratio, square root of temperature ratio, and square root of ion and electron mass ratio, and the geometry of the electrodes. For example, take two electrodes with an area ratio of 54 in a region of atomic oxygen ions, square root of mass ratio 171, and ion and electron temperatures and number densities equal. The smaller electrode is an "orbital-motion-limited" cylinder, and the larger electrode is a "sheath-area-limited" sphere. In Fig. 24 the single-

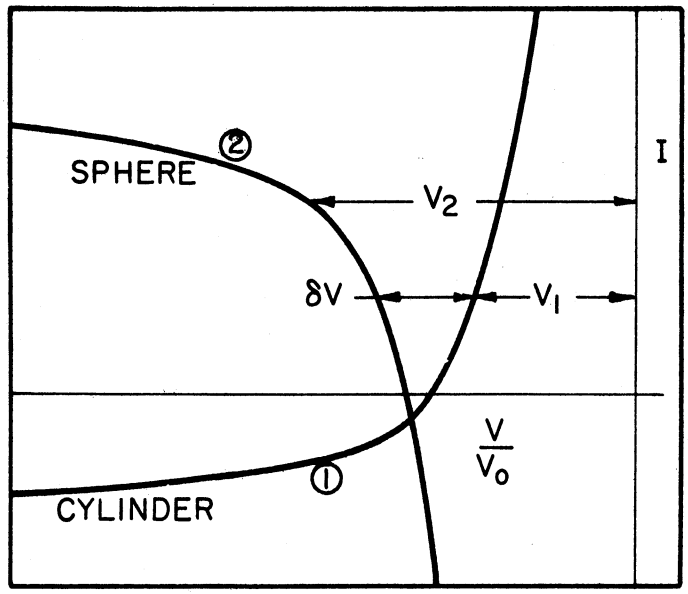

Fig. 24. Sphere and cylinder single-electrode volt-ampere characteristics.

electrode characteristic of the cylinder is shown as curve (1) and the single-electrode characteristic of the sphere is curve (2). The bipolar characteristic obtained from Fig. 24 is shown in Fig. 25. The AB region of this curve exhibits the ion current characteristic of the cylinder, and the EF region shows the ion current characteristic of the sphere. The difference between BC and AB extended is the electron current to the

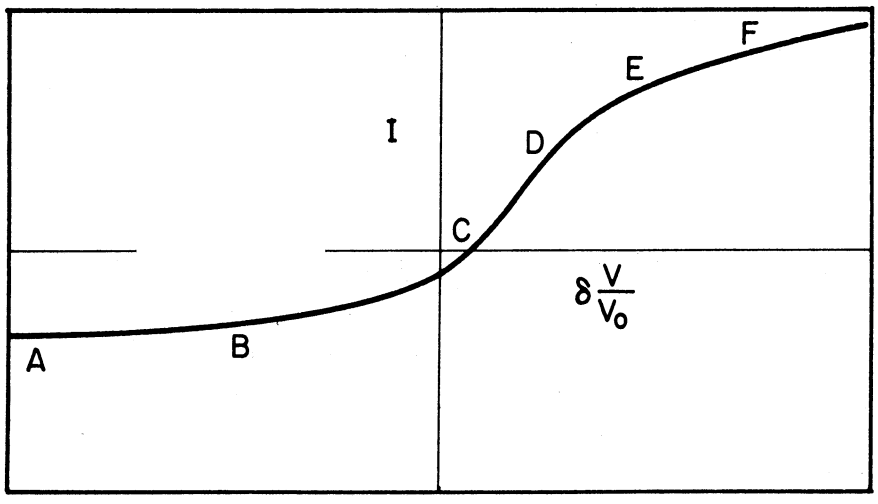

Fig. 25. Sphere-cylinder bipolar probe characteristic.

cylinder, and the difference between DF and EF extended is the electron current to the sphere. The CD region is still a nearly linear section corresponding to the minimum impedance to space seen by the probe, but is no longer at the origin.

D. BIPOLAR APPROXIMATION OF A SINGLE ELECTRODE

If the area ratio of the sphere and cylinder of the preceding example were still greater so that $A_1/A_2 \gg J_e/J_p$, the bipolar characteristic (Fig. 26) would be approximately that of a single cylindrical electrode. The sphere (the large electrode) acts as a fixed reference, deviating only slightly from its null potential (V_W in Fig. 26). The AB region again exhibits the positive-ion characteristics of the cylinder (the small electrode), but the EF region exhibits the characteristic of the electron-current saturation of cylinder rather than the ion-current saturation of the sphere as in the previous example. The difference between BC and AB extended is the electron current to the cylindrical electrode. In the DE

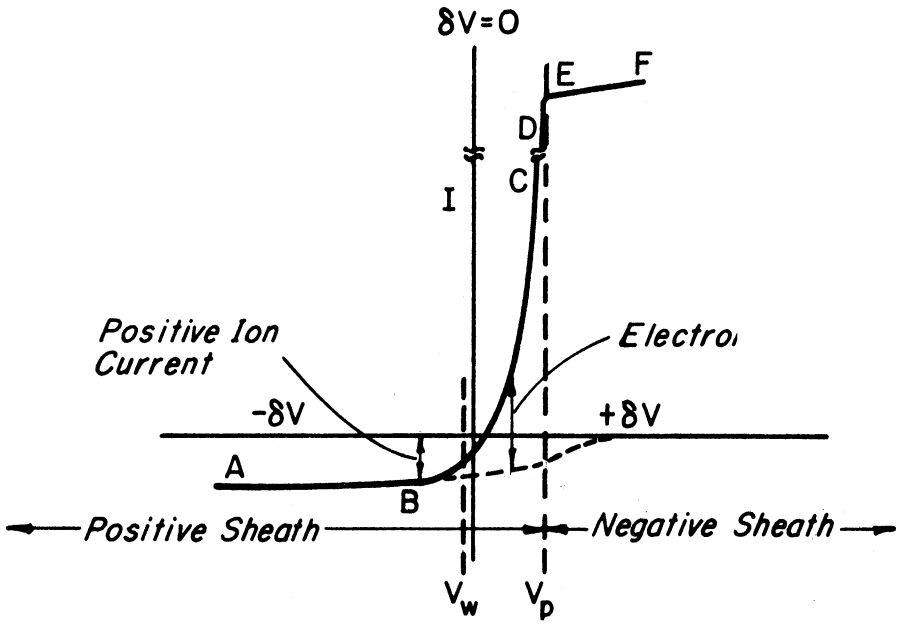

Fig. 26. Sphere-cylinder bipolar probe characteristic where $A_{sphere} \gg A_{cylinder}$.

region the electrode ion current is negligible and the electron current may be determined throughout the BF region.

A significant feature of this curve is the sharp break near E, which occurs when the potential of the small electrode is equal to the plasma potential (V_p). This permits the determination of the plasma potential. The wall potential of the sphere is assumed to correspond to $\delta V = 0$ and thus its potential with respect to the plasma is the value of δV which results in the sharp break. The across-the-sheath voltage of the cylinder in this case is zero. A change in δV from this value appears almost entirely as the cylinder sheath voltage.

For an electrode potential less than the plasma potential, the electrode current is determined by the rejection of the low-energy electrons, and thus the curve is a function of the electron-energy distribution. At the break no sheath exists and the current collected is the product of the random-electron-current density and electrode area. A higher potential results in the formation of a negative sheath of electrons and, when present, negative ions. The increase in current in the EF region is dependent on the same sheath relations as the increase of the ion-current in the AB region. (See the discussion of volt-ampere relations at the end of Section III.)

The probe of this example measures independently the electron temperature or energy distribution, electron density, ion density, ion temperature, and plasma potential. Since in theory it behaves as a single-electrode probe, the reader is referred to the several references on single-

electrode probes.[5,9,14,15]

The characteristic of many other possible electrode combinations may be visualized once familiarity is gained with typical single-electrode solutions. However, caution must be exercised in anticipating the results of a particular combination since the equations are functions of V, and the characteristic is a function of δV, which is not linearly related to V. Figure 27 illustrates three typical solutions for a spherical probe, and Fig. 28 illustrates the orbital-motion-limited solutions for three commonly used geometries.

In addition to the two-electrode systems discussed, multiple-electrode systems might prove more useful in satellite applications.[16] Screened electrodes also have been used to advantage when the instrumentation was not ejected.[17] Another technique which might be employed is the use of a radioactive material as a variable current source in lieu of a large-area second electrode. The δV would then become the measured quantity. The use of any type of charged particle emitter sufficiently isolated from the information electrode could replace the large-area electrode of the preceding example, and for practical considerations such charge-emitting systems might be more feasible.

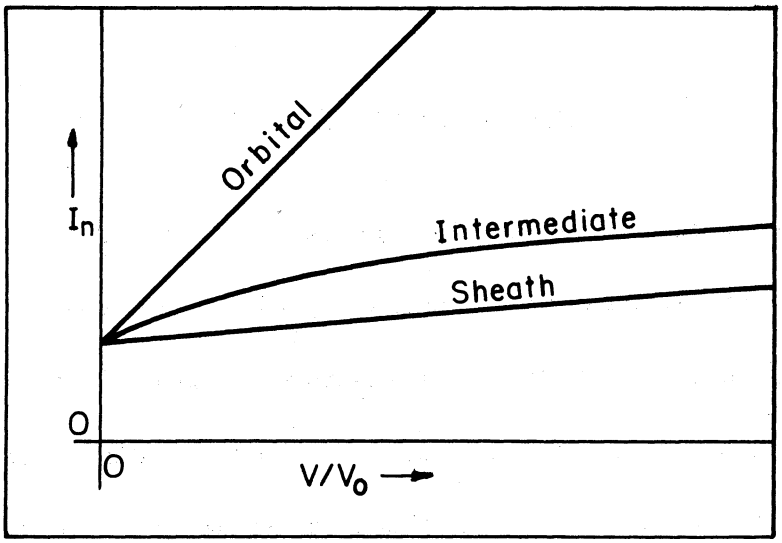

Fig. 27. Typical ion-current characteristics, spherical electrode.

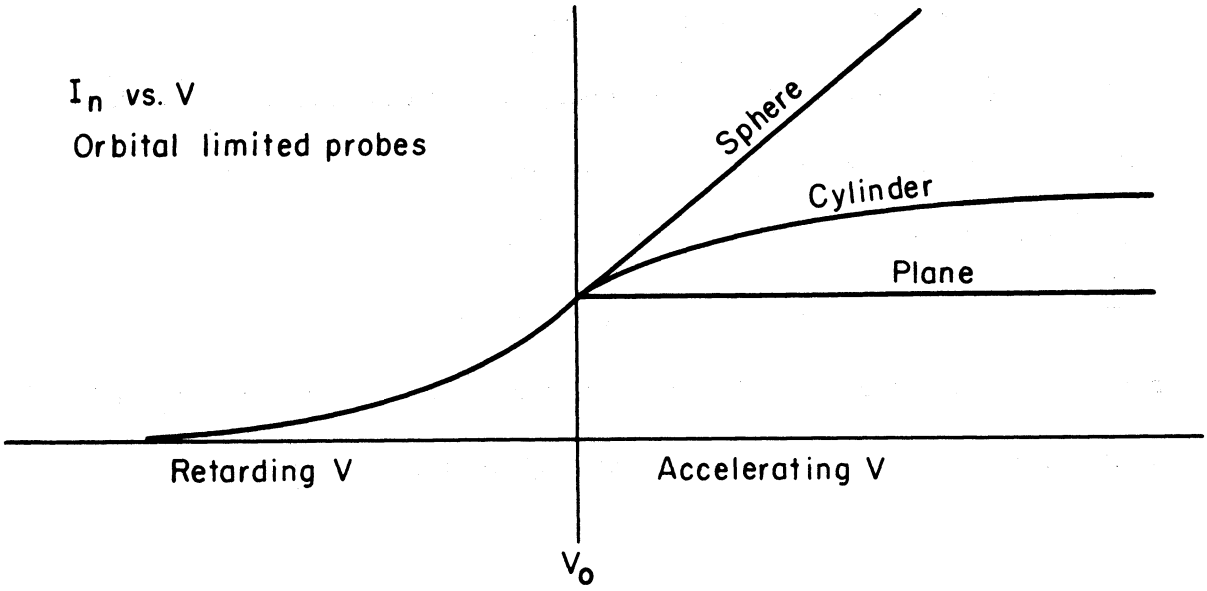

Fig. 28. Orbital-motion-limited electrode characteristics for sphere, cylinder, and plane.

V. BIPOLAR-PROBE DESIGN CONSIDERATIONS

In the preceding section the general concepts of multiple-electrode ionospheric probes have been discussed, and several possible bipolar-probe characteristics have been illustrated. Based on the principles outlined and on additional theoretical and practical design considerations to be discussed, one particular electrode system was chosen for an exploratory experiment. The objectives of this dumbbell configuration (Fig. 29) were (1) the experimental verification of the probe technique for measuring ionospheric parameters, (2) the determination of the magnitude of ionospheric disturbances resulting from the presence of the instrumentation, and (3) the measurement of ionospheric parameters. The order in which the objectives are listed signifies the need to tailor the experiment to establish the validity of the technique rather than to measure several ionospheric parameters. Once the technique is established, more specialized and more complicated probes are expected to be used with confidence, yielding a greater diversity of measurements.

A. THEORETICAL CONSIDERATIONS

It has been shown that the current to a conducting electrode immersed in an ionized region such as the ionosphere depends on several properties of the region, including (1) electron temperature, (2) electron density, (3) ion density, (4) ion temperature, and (5) the effective ion mass. If,

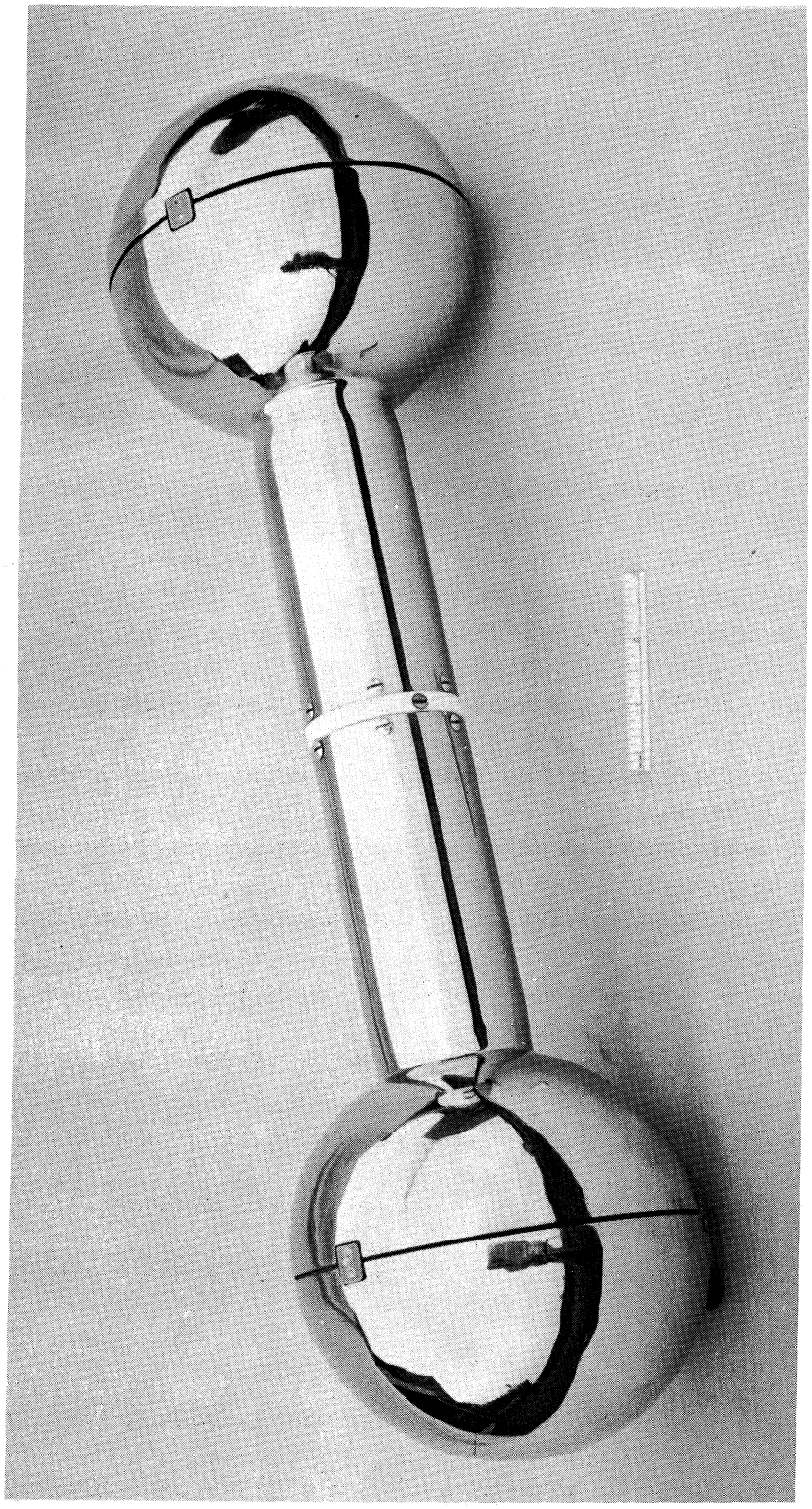

Fig. 29. Experimental model of double-sphere probe as employed for initial experiments.

in some manner, the potential of the electrode is varied, the resulting volt-ampere characteristic also depends on the geometry, and, if bipolar, the characteristic depends on the electrode area ratio. The interdependence of the various factors has been outlined so that the volt-ampere characteristic of a sphere, cylinder, or plane, or combination of these can be calculated.

The equations, however, are based on assumptions which are questionable in some cases because many of the ionospheric properties are not adequately known. The energy distribution is an example. A Maxwellian distribution has been assumed but some modified form, perhaps a "dual" system of high- and low-energy electrons exists. Such a "dual" distribution has been discovered in tube studies by Sloane and Emeleus.[18] Related to the distribution function is the nature of particle diffusion between the sheath and the undisturbed plasma, which generally has been assumed to be governed by the Boltzmann relation. This may not be an entirely suitable approximation, but significant use of the probe technique does not require full knowledge of the validity of these assumptions. For example, when a small fraction of the total available electrons is collected, the Boltzmann approximation is satisfactory. This was an important factor in the choice of equal-area electrodes which sample only a small fraction of the total electrons.

The assumption of temperature equilibrium is also questionable; however, it has been shown by Bohm et al.[19] that the ion-current region is more dependent on the electron temperature than ion temperature, thus

allowing this region to be interpreted in terms of electron temperature.

The assumption of charge neutrality is generally accepted, but the omission of negative ions in determining the volt-ampere characteristics might be questioned. However, the effect of an appreciable number of negative ions is small due to their low mobility. This is illustrated in Fig. 30, for three cases where the electrons comprise 100, 90, or 50% of the negative charge. Charge neutrality is assumed.

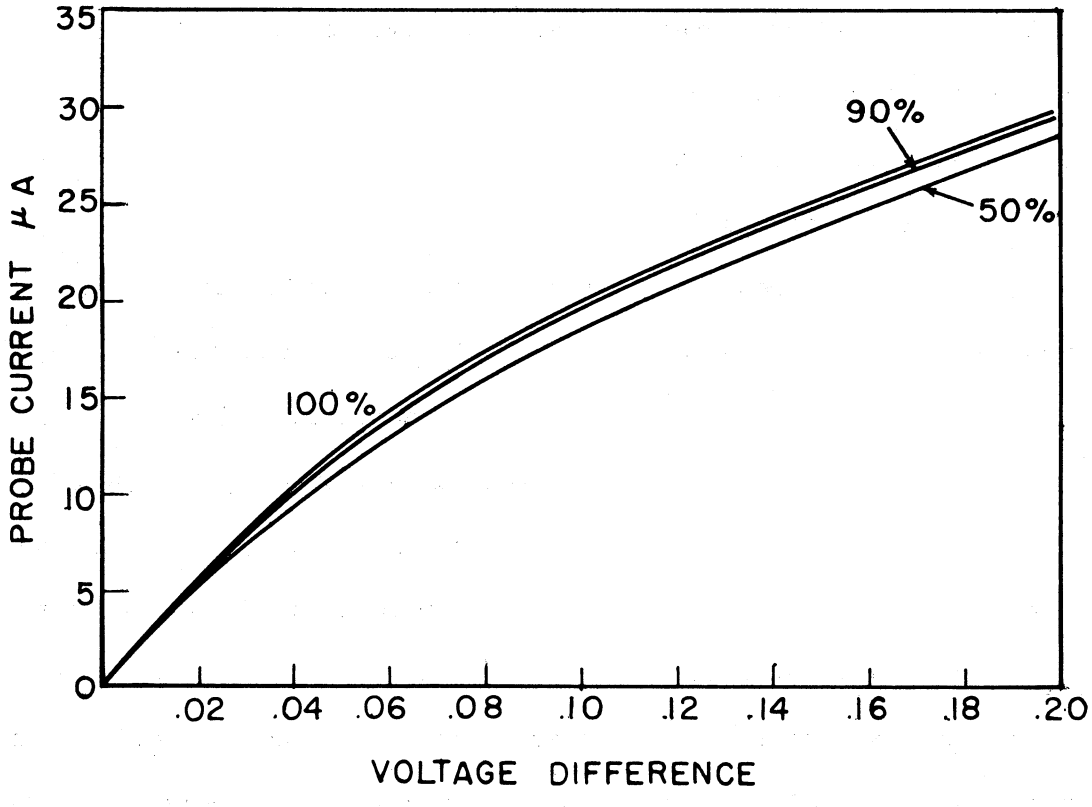

Fig. 30. Spherical electrode volt-ampere characteristic with the percentage of negative ions as a parameter.

B. DISTURBANCES

The presence of the instrumentation disturbs the ionosphere locally. This includes (1) contamination of the gas, (2) changes of the apparent plasma energy distribution due to the rf field of the data transmitter and

the relative velocity between the probe and the plasma, and (3) effects of interaction between two or more individual electrode sheaths.

The gas-contamination problem plus the aforementioned desire for an ideal geometry led to the decision to eject the entire probe instrumentation from the carrier vehicle. This ejected package was sealed to prevent the escape of gas, and the surface was cleaned previous to launching.

The disturbance of the ionospheric particle energy by the rf field of the transmitter was investigated by making measurements with and without the transmitter operating. The relative velocity effects between probe and ionosphere were minimized through symmetry and a minimum horizontal velocity component. The effect of overlapping sheaths was avoided through the use of guard electrodes.

Experimental results are also subject to errors due to thermoelectric, photoelectric, and contact potential effects. These have been minimized through consideration of materials and cleanliness. The magnitude of the photoelectric effect might be determined by launching at dawn or dusk so that the probe would make the transition from light to dark or dark to light in the ionosphere. However, the properties of the ionosphere are changing rapidly at this time of day, thus making the outcome of such an experiment ambiguous. Thus the experiment reported here did not include this study. (Another investigator's estimate of photoelectric emission is noted in the Appendix.)

C. PRACTICAL CONSIDERATIONS

An ionosphere probe must be considered as a two-or-more electrode system since, as previously mentioned, no fixed reference potential is

generally available. Orbital-motion-limited electrodes are desirable because of their mathematical simplicity, but they also result in low currents due to their small size. In addition, the electrode system must accommodate the necessary circuitry (current detectors, δV generators, telemetering, etc.); thus at least one of the electrodes will be too large to be orbital-motion-limited. It is desirable that the electrodes have a simple geometry (sphere, cylinder, or plane) and be of such size that the current may be expressed by one of the asymptotic forms. For this reason one of the electrodes will usually be chosen large enough to be sheath-area-limited. In this particular design, since the electrodes were identical, both were chosen sheath-area-limited.

After studying various electrode configurations, one simple design, two 6-in. spheres separated by a 2-1/4-in. cylinder approximately 10 in. long, was chosen. This design seemed most consistent with the objectives outlined above, the construction possibilities (vacuum tightness, antenna consideration, etc.), and the size (8-in. maximum) and weight (10-20 lb) launching capabilities of the available and anticipated rockets. The spherical geometry was chosen because of symmetry and the effectiveness of the guard electrodes. This geometry with equal-area electrodes is particularly suited for measuring electron temperature. In addition, measurements are obtained of the ion density and the minimum impedance to space as seen by the probe.

VI. PREDICTED PROBE VOLT-AMPERE CHARACTERISTICS

The adoption of nominal ionospheric parameters vs. altitude permits the prediction of volt-ampere characteristics for the bipolar-probe design chosen. Such calculations are necessary to determine the range of current to be measured and the appropriate voltage to be programmed between the electrodes.

A. IONOSPHERIC PARAMETERS

The available data include the estimates of gas kinetic temperature, the electron number density, and the positive-ion type. These three parameters are sufficient to calculate the desired volt-ampere characteristics if temperature equilibrium ($T_g = T_e = T_n = T_p$),* charge equilibrium ($N_e + N_n$) = N_p, and the absence of negative ions ($N_n = 0$) are postulated. Negative ions were shown to have negligible effect (Fig. 30).

The temperature (Fig. 31) was adopted from a proposed "Speculative Atmosphere" by Kallamun, Newell, and White[20] which was incorporated in The ARDC Model Atmosphere 1956[21] prepared by the Geophysics Research Directorate of AFCRC. The ARDC linearly segmented model appears in Fig. 31 as a dashed line. As can be seen, the two models are in close agreement. Thus, for the sake of consistency, the smooth curve was chosen for the calculations in this section since the other available parameters are

*This temperature equilibrium has been suggested in the literature; see, e.g., N. C. Gearson, Rep. Phys. Soc. Progr. Phy., 14, 316 (1951).

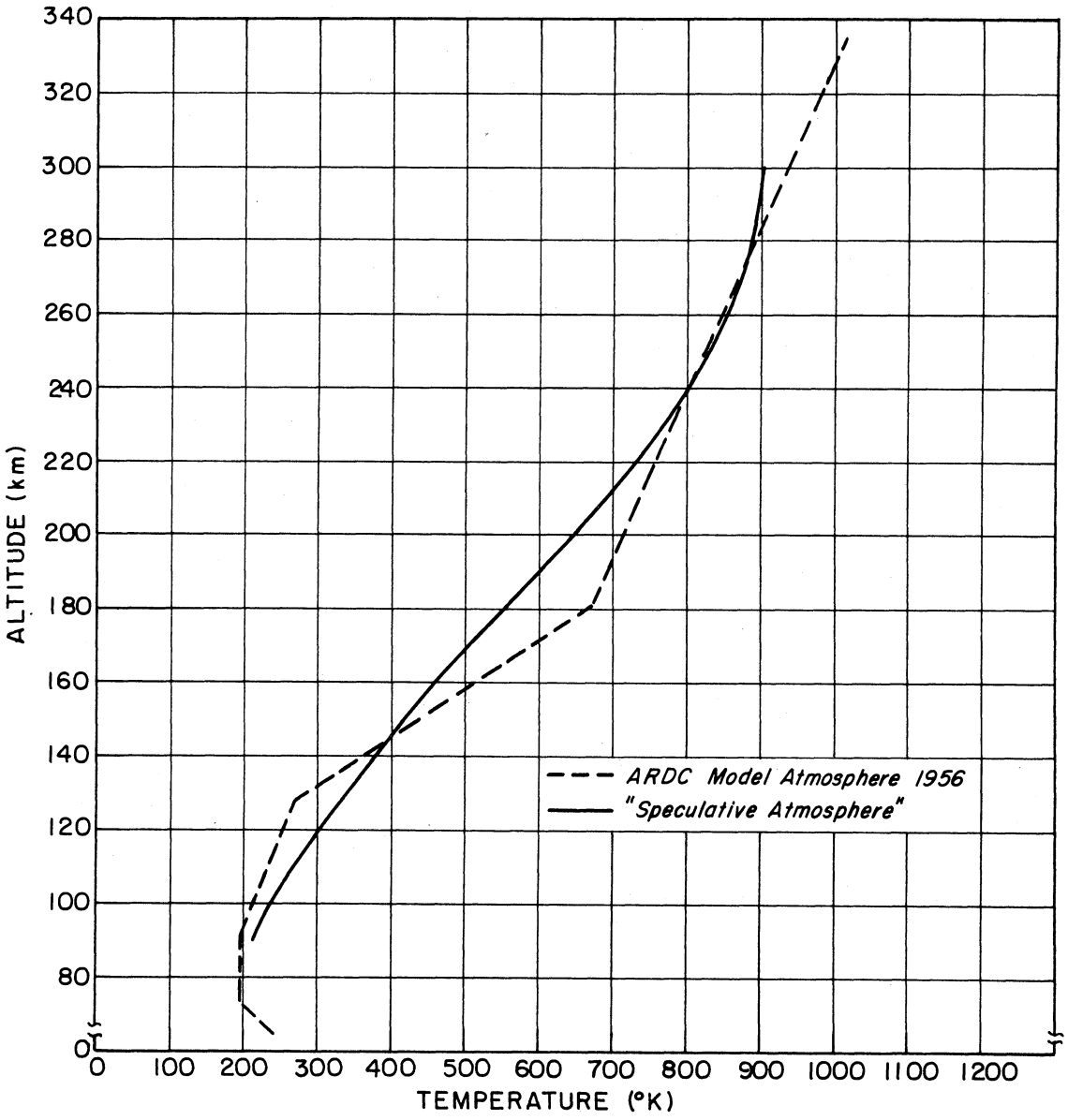

Fig. 31. Estimated kinetic gas temperature from 80 to 340 km.

smooth curves. This temperature model is based on assumptions of the degree of dissociation of O_2 and N_2 in the altitude range covered and assumes an isothermal exosphere beginning at 360 km. The model indicates lower temperatures and densities throughout the region than those deduced previously.

The electron density (Fig. 32) is a composite of data obtained by rocket-borne, CW radio-propagation experiments[1-4] previously mentioned in the introduction. The curve represents average data from several flights at White Sands Proving Ground, New Mexico, and includes seasonal variations.

The average ion mass (Fig. 33) is an interpretation of data obtained by C. Y. Johnson, E. B. Meadows, and J. C. Holmes.[22] Three Aerobee-Hi rockets instrumented with Bennett radiofrequency, ion-mass spectrometers were launched at Fort Churchill, Manitoba, Canada, in November, 1956, and February and March, 1958, the first two at night, the third during the day. Figure 33 is a composite of data from all three flights.

It must be emphasized at this point that these three parameters do not represent an actual, single ionosphere. They are averages of data taken at different locations including both seasonal and diurnal variations, with and without auroral and solar disturbances. No one model could ever hope to approach actual conditions except at a few points and then only by chance. The model chosen does serve its purpose adequately, which is the study of the ionospheric-probe theory and thereby the selection of appropriate instrumentation requirements.

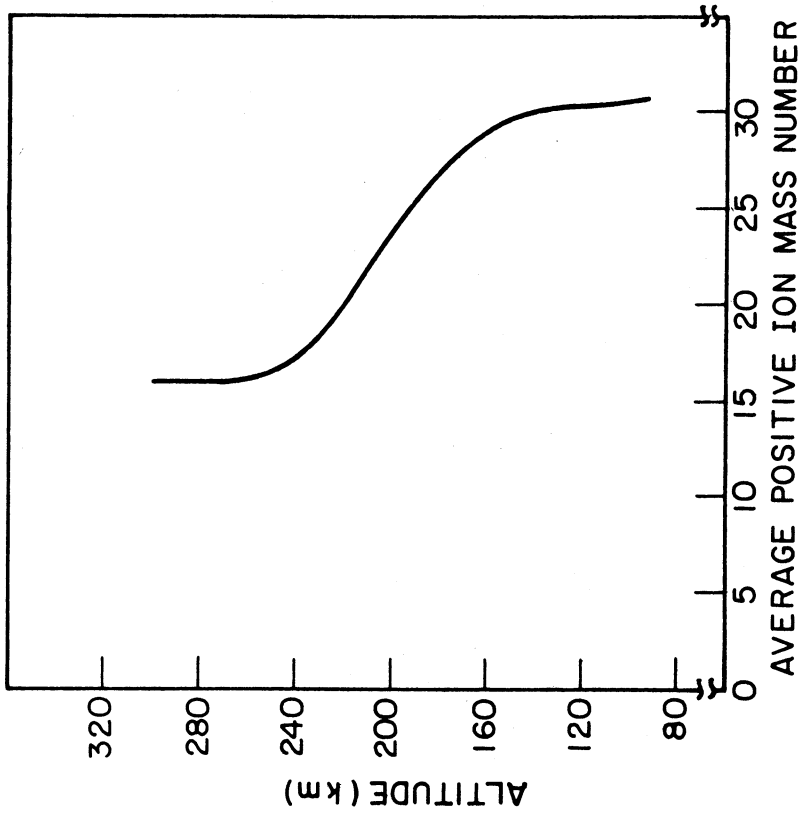

Fig. 33. Average positive ion mass from 80 to 290 km.

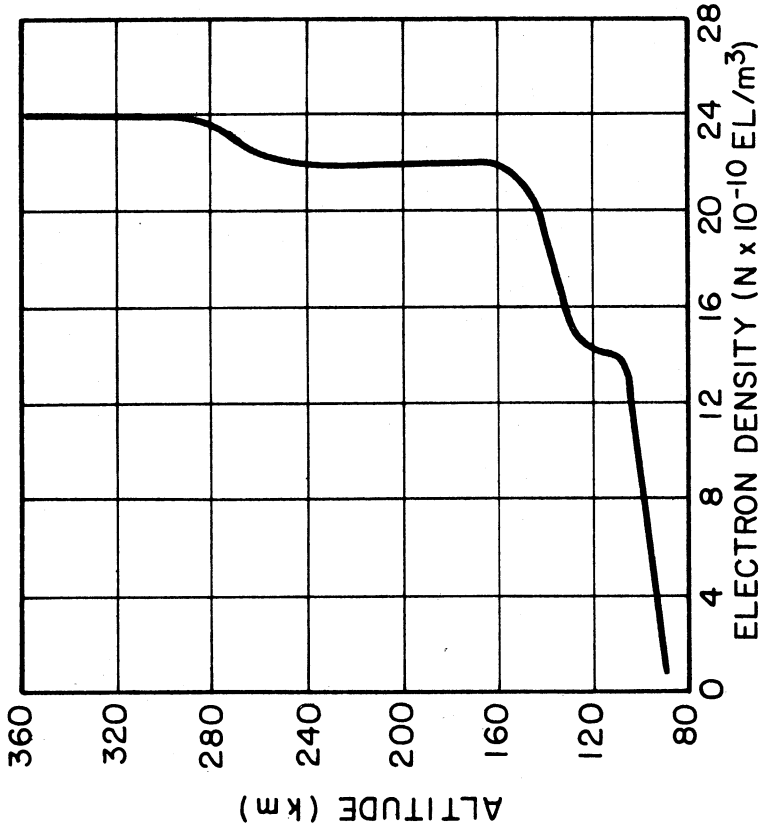

Fig. 32. Electron density from 80 to 360 km.

B. CURRENT LIMITING CRITERIA

Having selected a model, it is now desirable to predict the minimum radius which results in a sheath-area-limited current to a spherical electrode (Fig. 34), and the maximum radius which results in orbital-motion-limited current to a spherical electrode (Fig. 35). It is seen in Fig. 34 that the 3-in. radius chosen is sheath-area-limited throughout the altitude range presented. Note that if one desired to construct a bipolar probe of two spherical electrodes, one orbital-motion-limited, the other sheath-area-limited, the ratio of their radii would have to be at least 14.14 and their area ratio would be at least 200.

C. SHEATH THICKNESS

The sheath plays an important role in determining the probe characteristic; therefore it is desirable to calculate the sheath thickness to determine that (1) the individual information electrode sheaths are hemispherical and do not overlap, and (2) the sheath thickness is small compared to the gas mean-free-path, since it was assumed in the general theory that no collisions occurred within the sheath. Figure 36 illustrates the sheath thickness about a spherical electrode for the assumed 160-km parameters. This figure serves well for high electrode potentials at which time the probe difference voltage is approximately the potential difference between the ion-collecting electrode and the plasma. Figure 37 illustrates the sheath thickness about each of the electrodes as δV approaches zero. Note that both the ion- and electron-collecting electrodes have a positive-ion sheath. The sheath thickness is satisfactorily

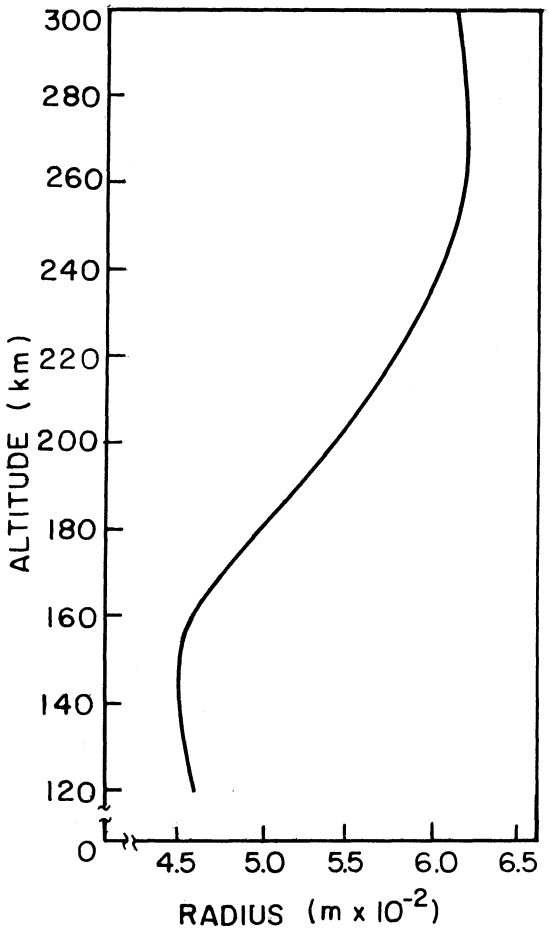

Fig. 34. Predicted minimum sheath-area-limited spherical electrode radius.

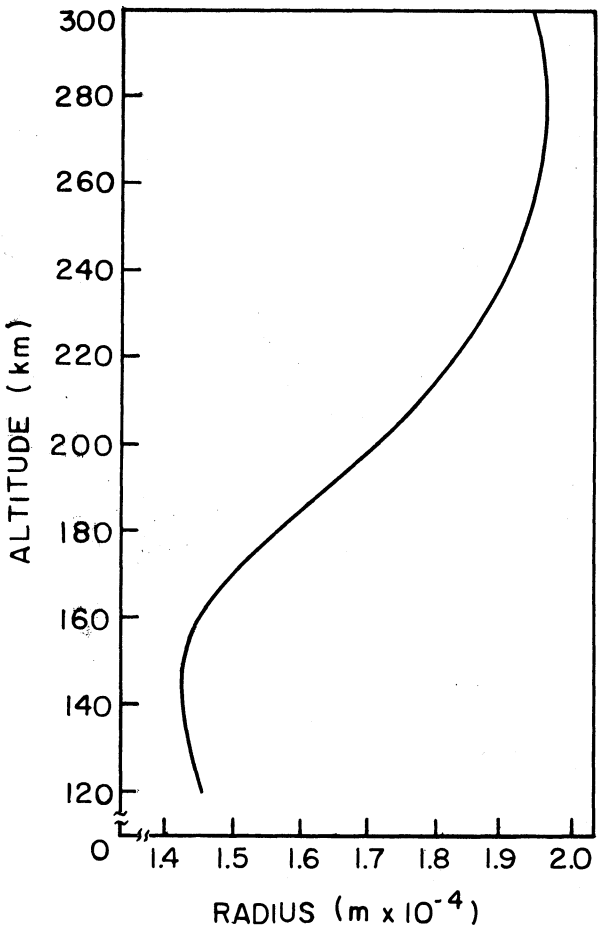

Fig. 35. Predicted maximum orbital-motion-limited spherical electrode

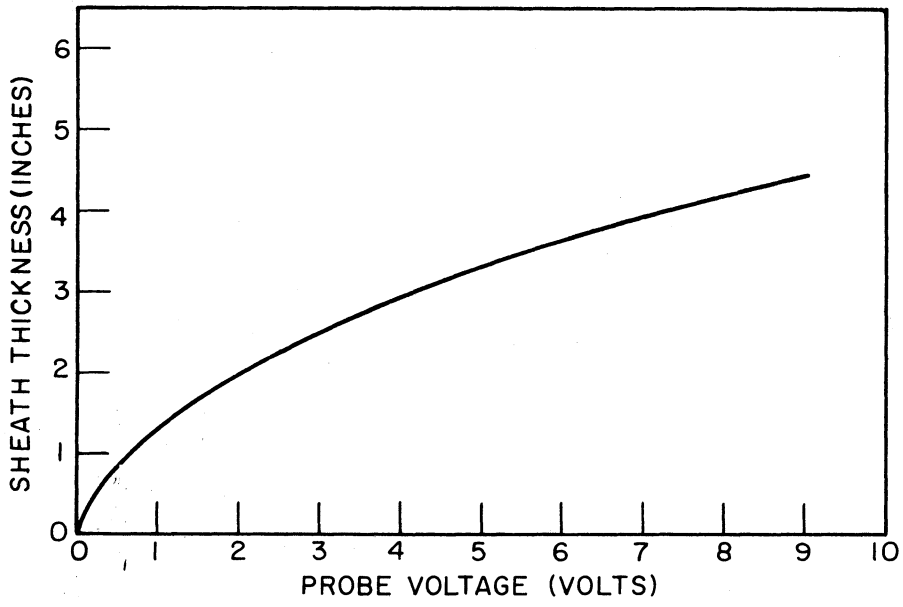

Fig. 36. Spherical sheath thickness at 160 km.

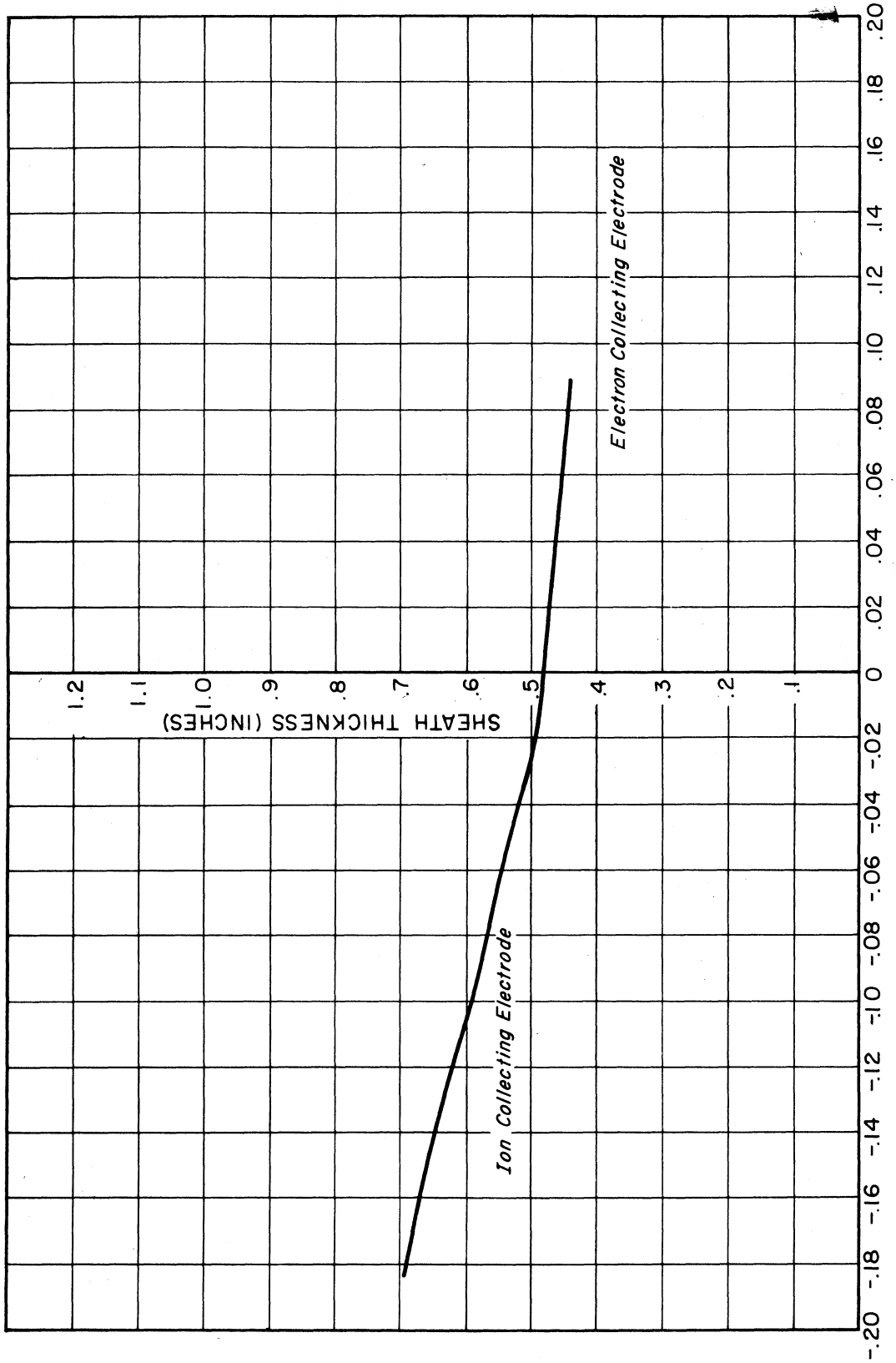

Fig. 37. Predicted sheath thickness vs. probe difference voltage when the electrodes are near null potentials at 160 km.

thin, since it is of the same order of magnitude as the electrode radius, and the gas-mean-free path at 160 km is approximately 7.9 meters (310 in.).

D. THEORETICAL PROBE CHARACTERISTICS

In developing the electrode-current equations, it was found expedient to write them in terms of a normalized current using the factor AJ [Eq. (26)], and a voltage ratio (V/V_o) where A is the electrode area, J is the appropriate (electron or ion) random-current density, V is the voltage between electrode and sheath, and V_o is the voltage equivalent of temperature at the sheath edge. Therefore the random-current density and voltage equivalent of temperature are directly applicable in determining the probe volt-ampere characteristics. Figure 38 illustrates the random-current density vs. altitude where the mass of the charged particle is treated as a parameter. The approximate random-ion-current-density variation with altitude is illustrated by the two curves in Fig. 38, using the daytime and nighttime average ion mass data mentioned previously. The altitude variation of V_o is illustrated in Fig. 39. Although this quantity is only a constant (k/e) times the temperature, its frequent use justifies Fig. 39.

The null potential is an additional parameter which is useful in visualizing the behavior of an electrode in the ionosphere. This potential is the potential assumed by an insulator in a plasma. It is independent of ion number density (charge equilibrium is assumed), but is dependent on the square root of the average-ion to electron-mass ratio, the electron temperature, ion temperature, and the electrode geometry. The predicted

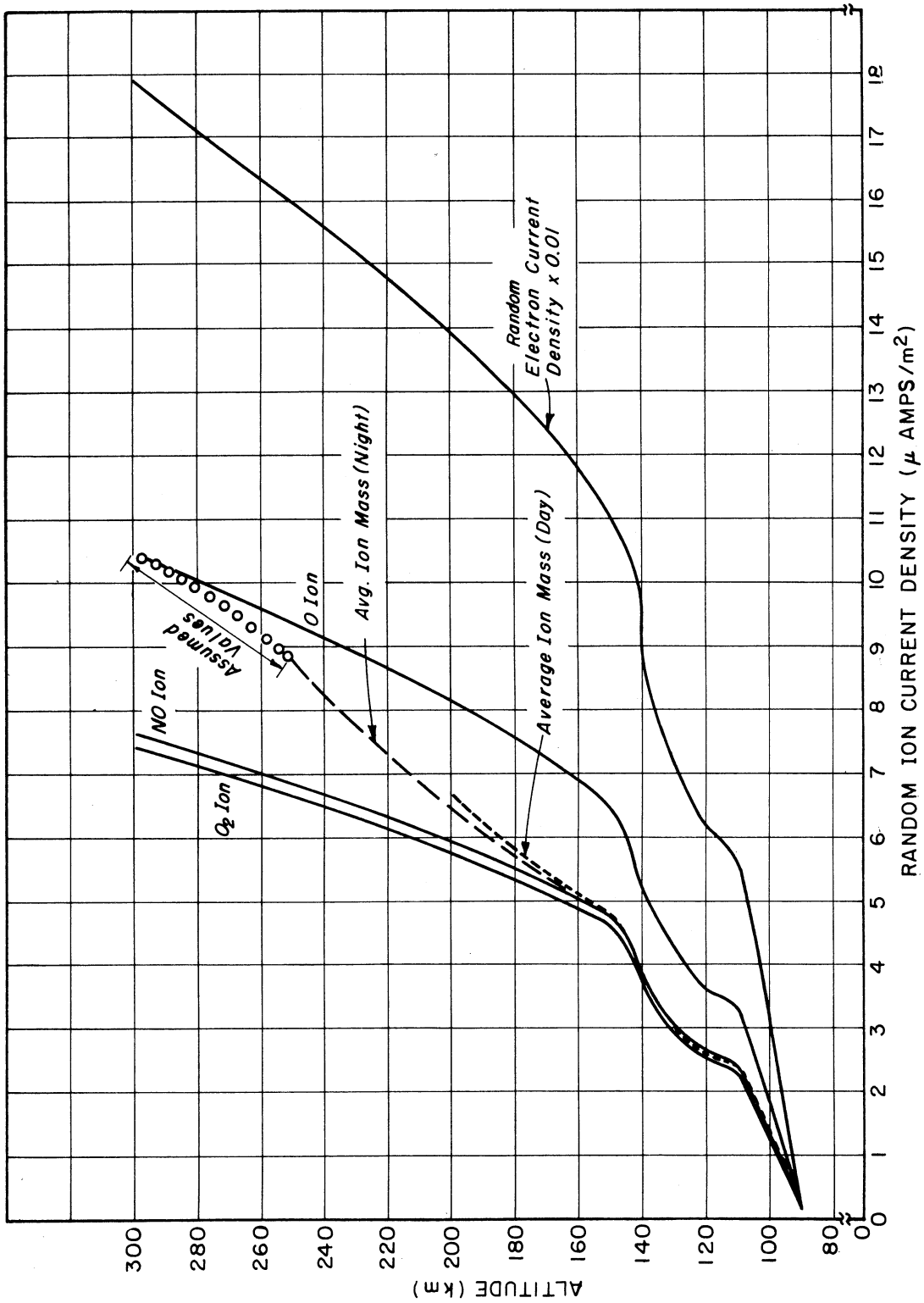

Fig. 38. Predicted random-current density vs. altitude.

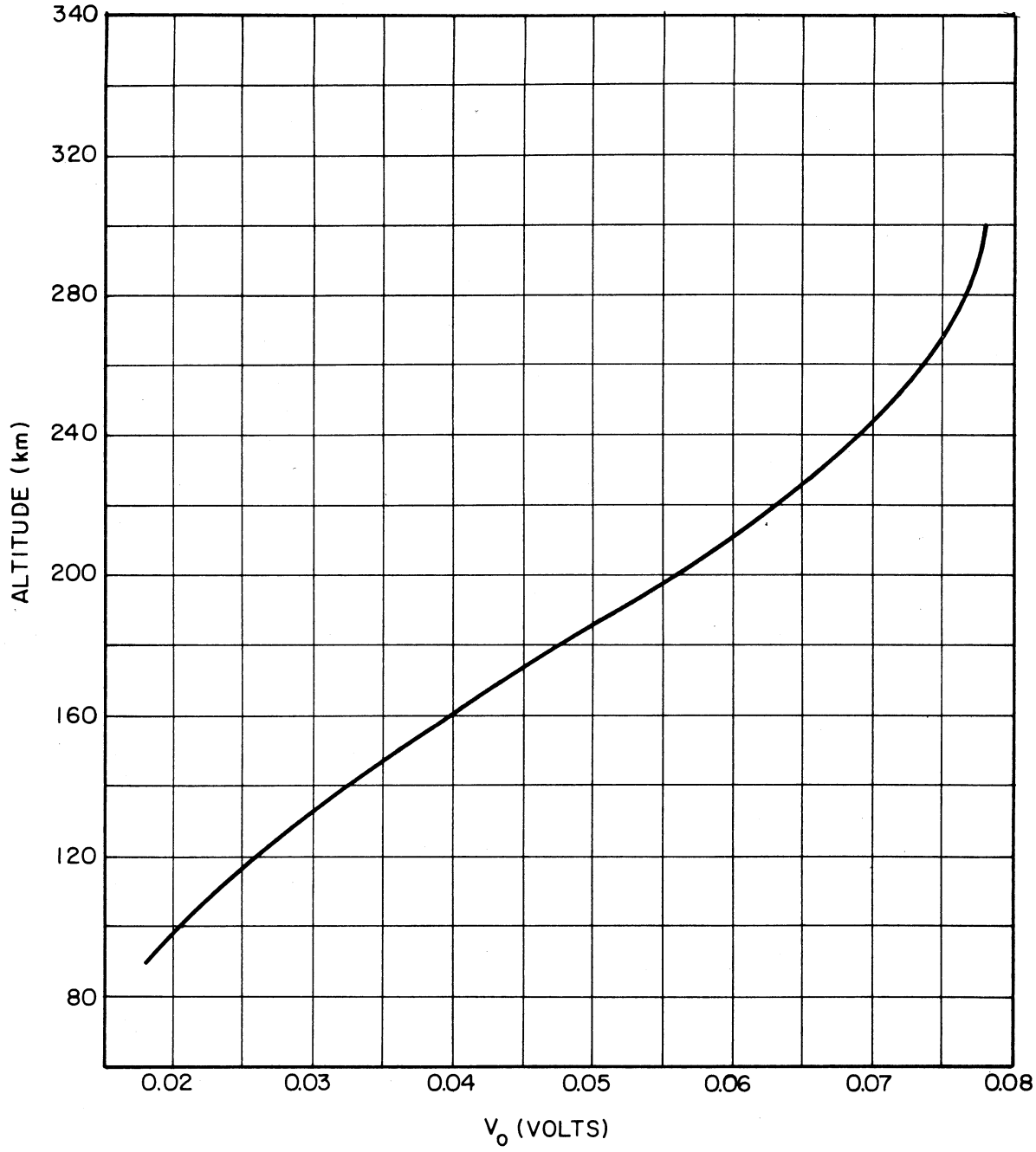

Fig. 39. Predicted voltage equivalent of temperature (V_o) from 80 to 320 km.

spherical electrode wall potential for NO ions and correction factors for the other ions is shown in Fig. 40.

The voltage equivalent of the temperature (V_o) and the random current density (J) are particularly useful in the case of an orbital-limited probe. In this case a characteristic curve of i_n vs. V/V_o for NO ion (Fig. 41) represents the characteristics for all altitudes where the NO ion predominates. Figure 42 presents, for comparison, the normalized characteristics for O_2, NO, and O ions.

In the case of an intermediate or sheath-area-limited solution, however, the transcendental relation of $(-\alpha^2)$ and the factor P which is a function of T/Nr^2 must be taken into account. Thus the volt-ampere characteristic must be calculated for each set of parameters. Characteristics have been calculated at 300, 160, and 120 km for these reasons: the lowest altitude at which all ions are assumed to be atomic oxygen is 300 km (Fig. 43); the approximate center of the E layer is at 160 km (Fig. 44); and the medial characteristics of the ionosphere measured by the Nike-Cajun instrumentation occur at approximately 120 km (Fig. 45).

The dashed curve in Fig. 45 illustrates the variation of the ion component of the current to the ion-collecting electrode as the probe difference voltage (δV) changes. This curve differs from the typical sheath-area-limited curve illustrated in Fig. 27, since the electrode potential does not change linearly with δV. Figures 44 and 45 illustrate a straight-line extension of the ion current. The purpose and justification of this representation of ion current follows in the chapter on data reduction.

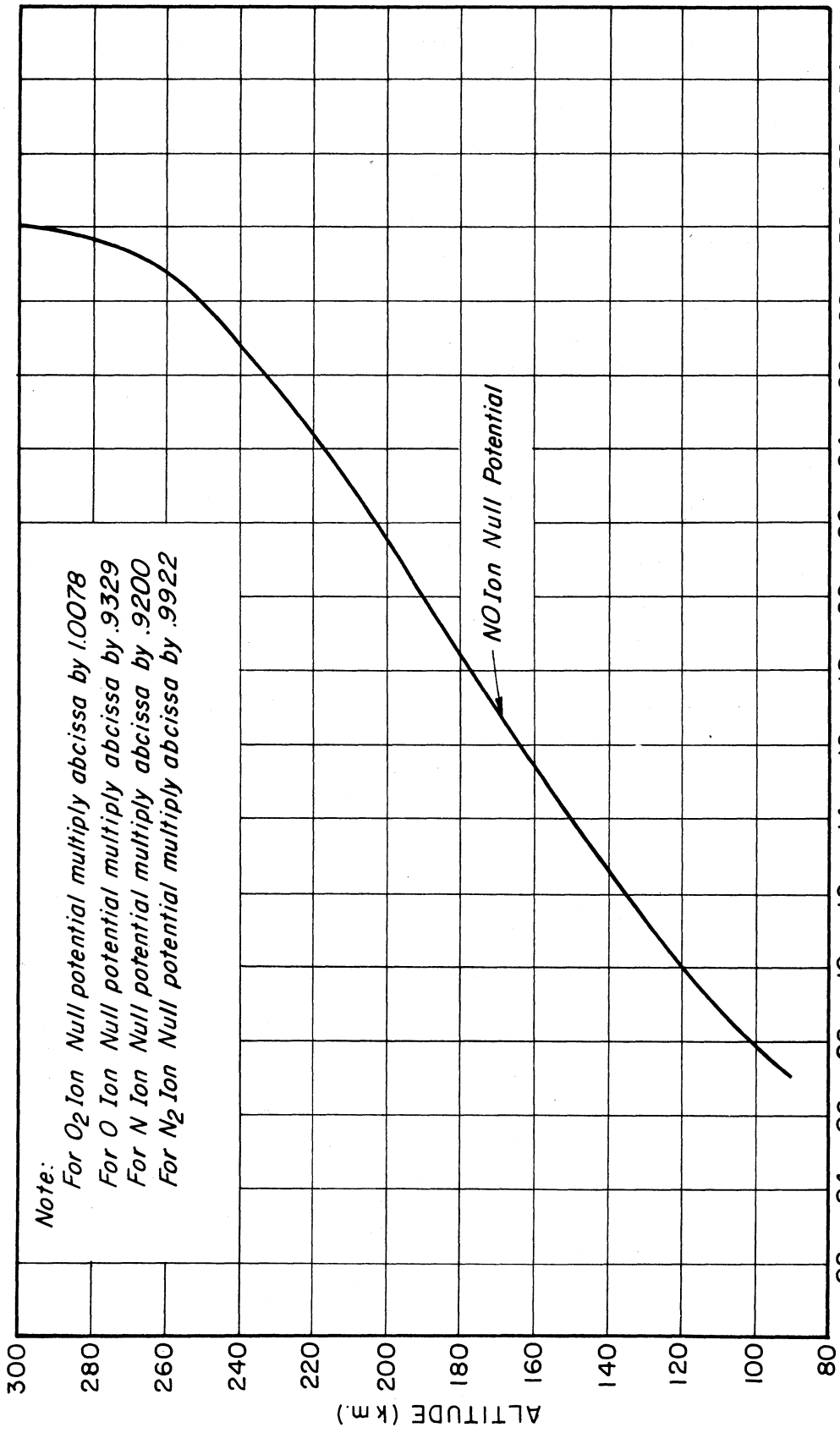

Fig. 40. Predicted spherical electrode null potential.

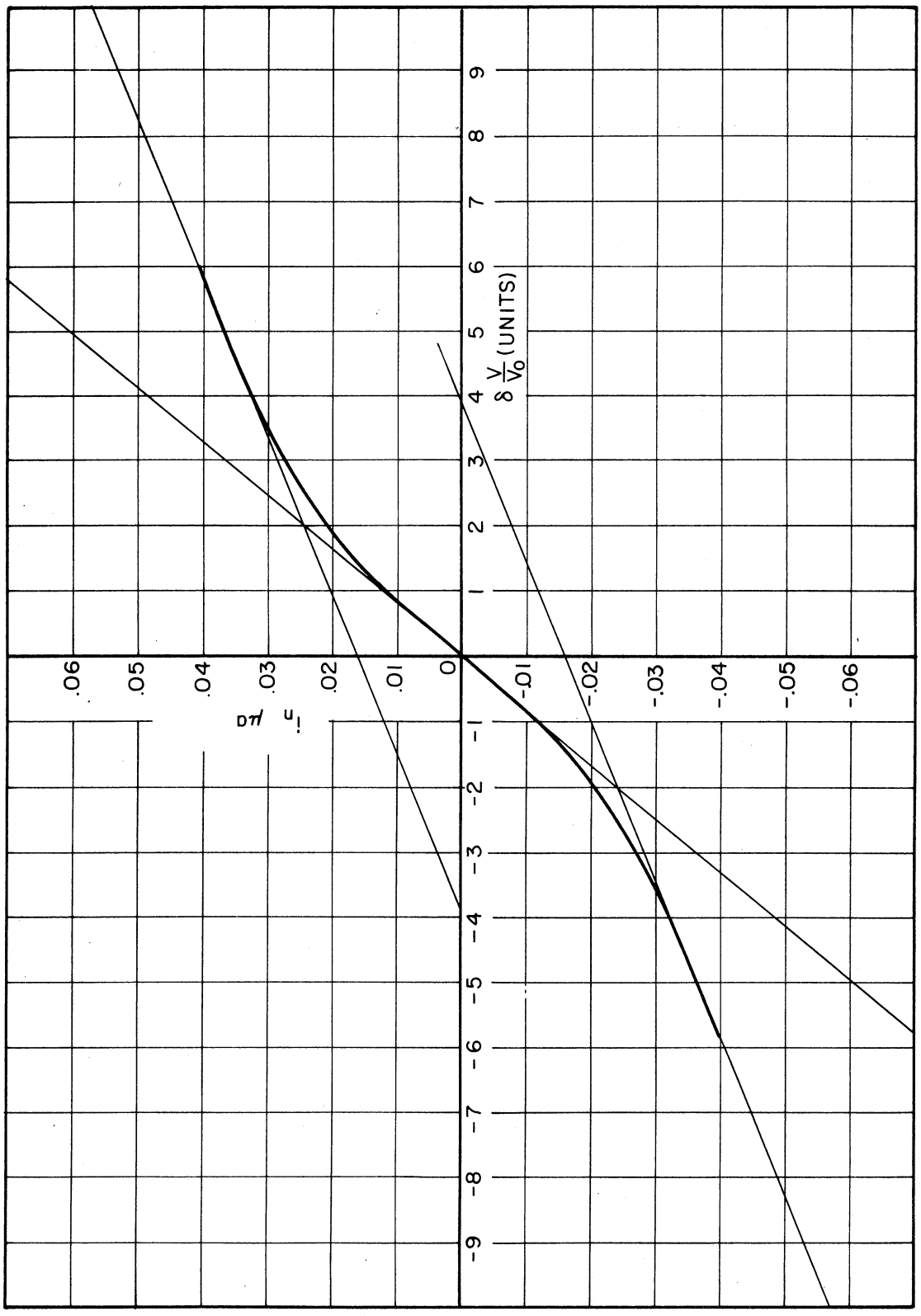

Fig. 41. Normalized orbital-motion-limited spherical electrode volt-ampere characteristic for NO ions.

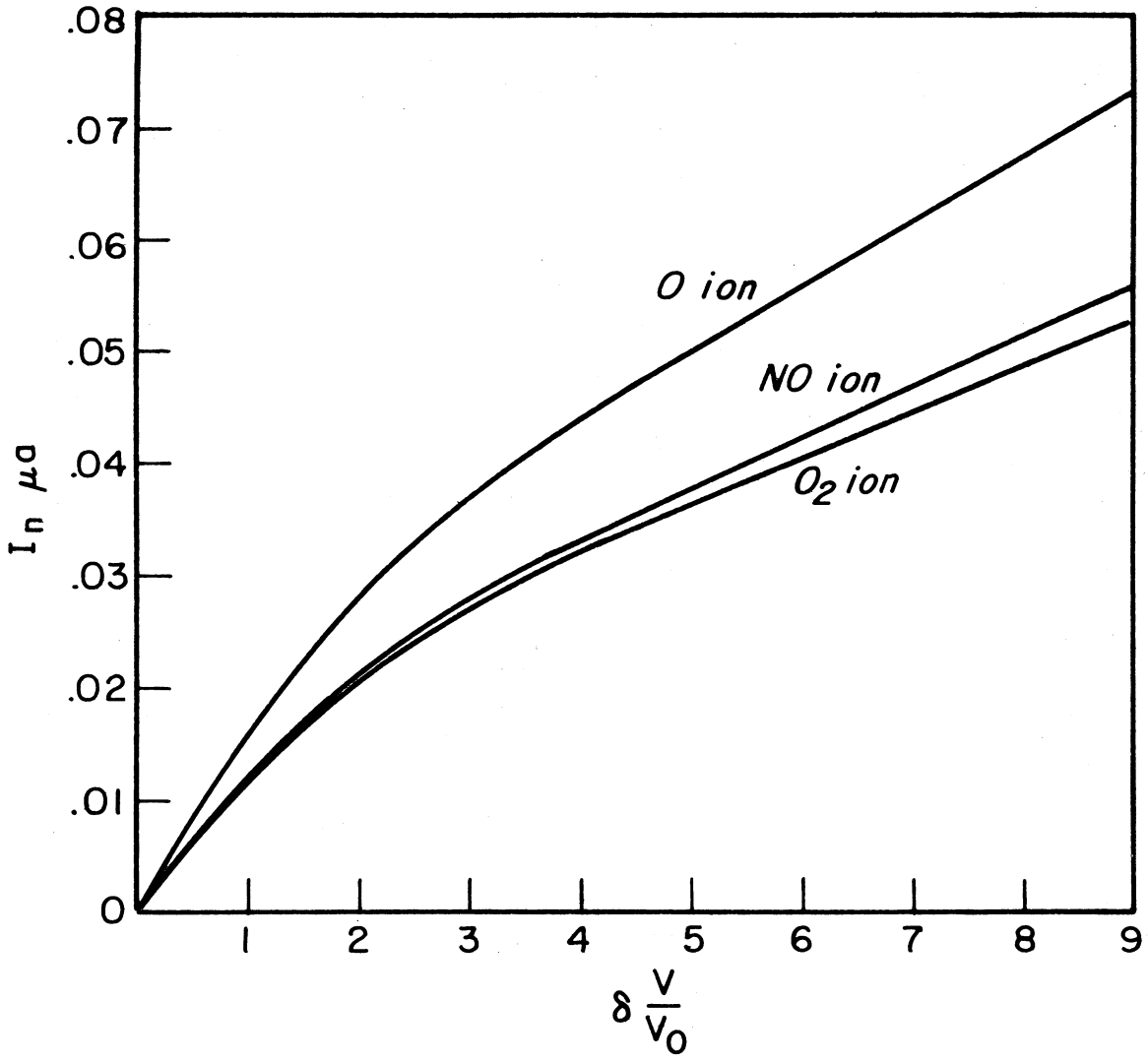

Fig. 42. Predicted spherical orbital-motion-limited electrode volt-ampere characteristics with the ion mass as a parameter.

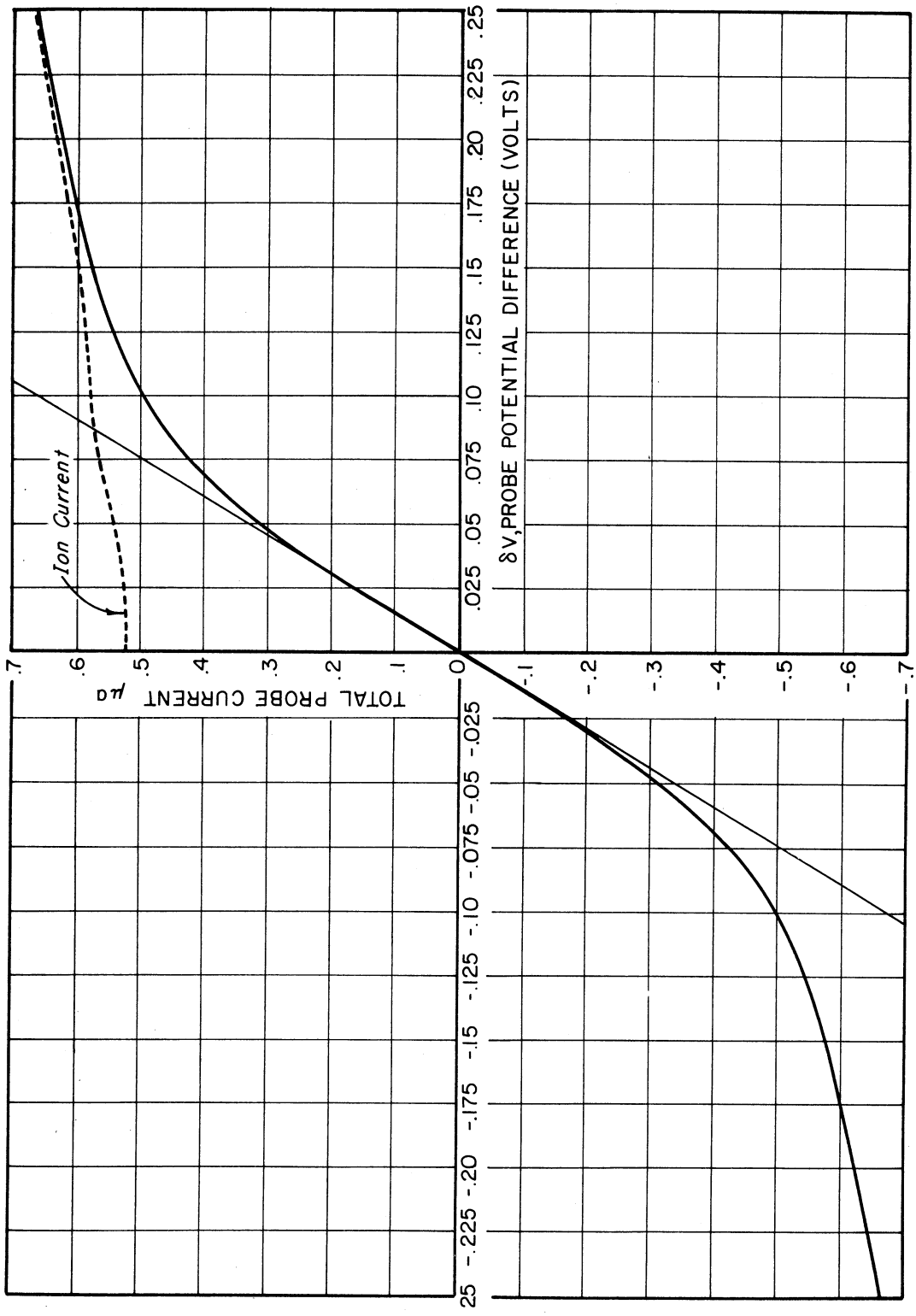

Fig. 43. Predicted bipolar probe volt-ampere characteristic at 300 km (hemispherical electrodes).

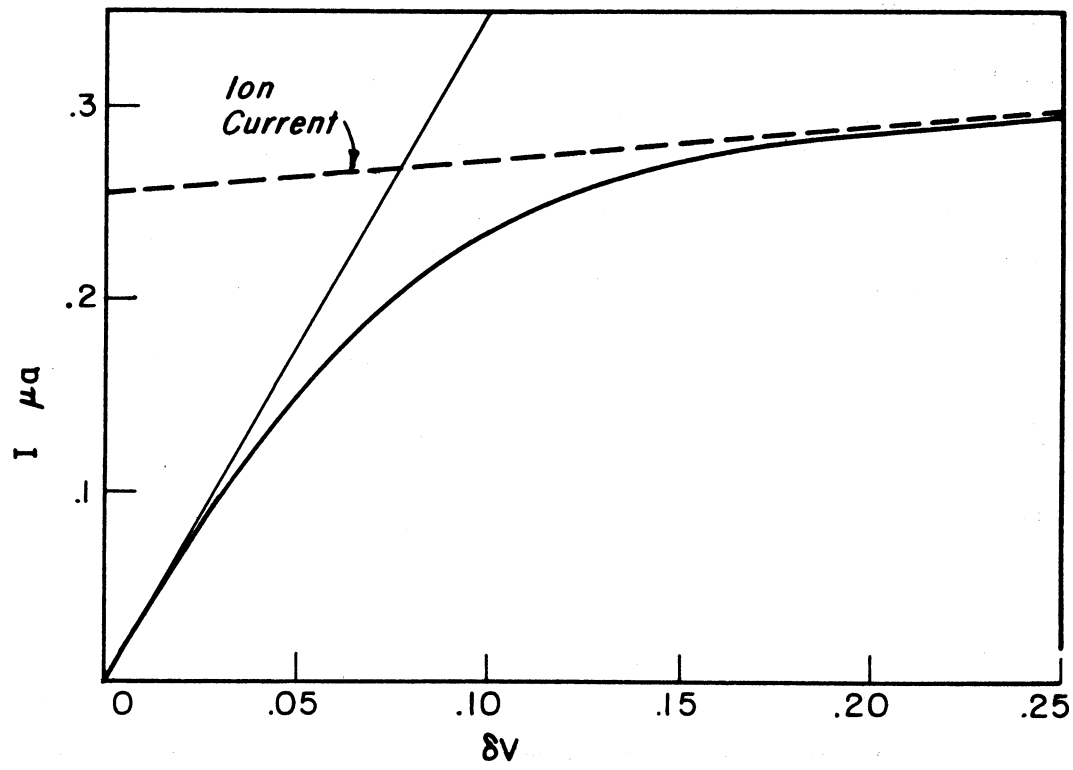

Fig. 44. Predicted bipolar probe volt-ampere characteristic at 160 km (hemispherical electrodes).

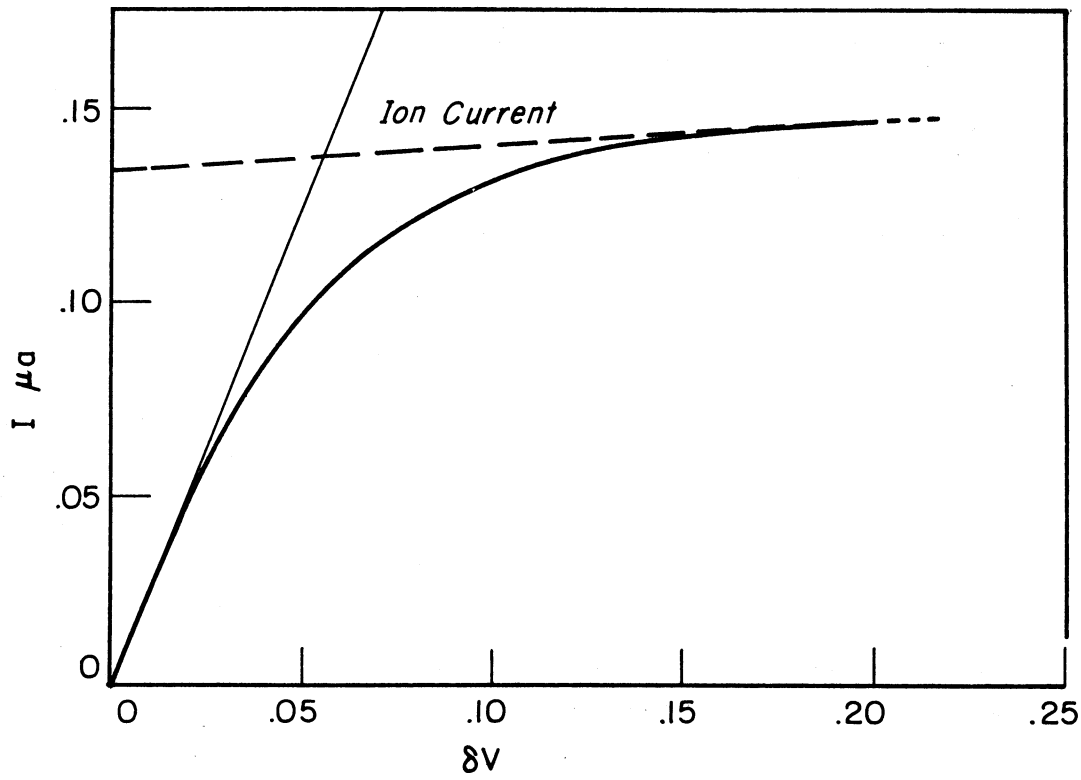

Fig. 45. Predicted bipolar probe volt-ampere characteristic at 120 km (hemispherical electrodes).

The Aerobee-300 rocket used for the second firing was capable of lifting the probe to an altitude of approximately 450 km. Thus it was necessary to calculate the probe volt-ampere characteristic at this altitude (Fig. 46). The ARCD model atmosphere provided the temperature (2400°K), an extension of the dotted line in Fig. 31. The ions were assumed to be atomic oxygen and the electron number density (2.5×10^{11}) was based on vertical-pulse soundings at Fort Churchill, Manitoba. The subsequent Fort Churchill vertical soundings have, in general, indicated higher number densities and a greater virtual height at all levels than the 80- to 320-km model chosen.

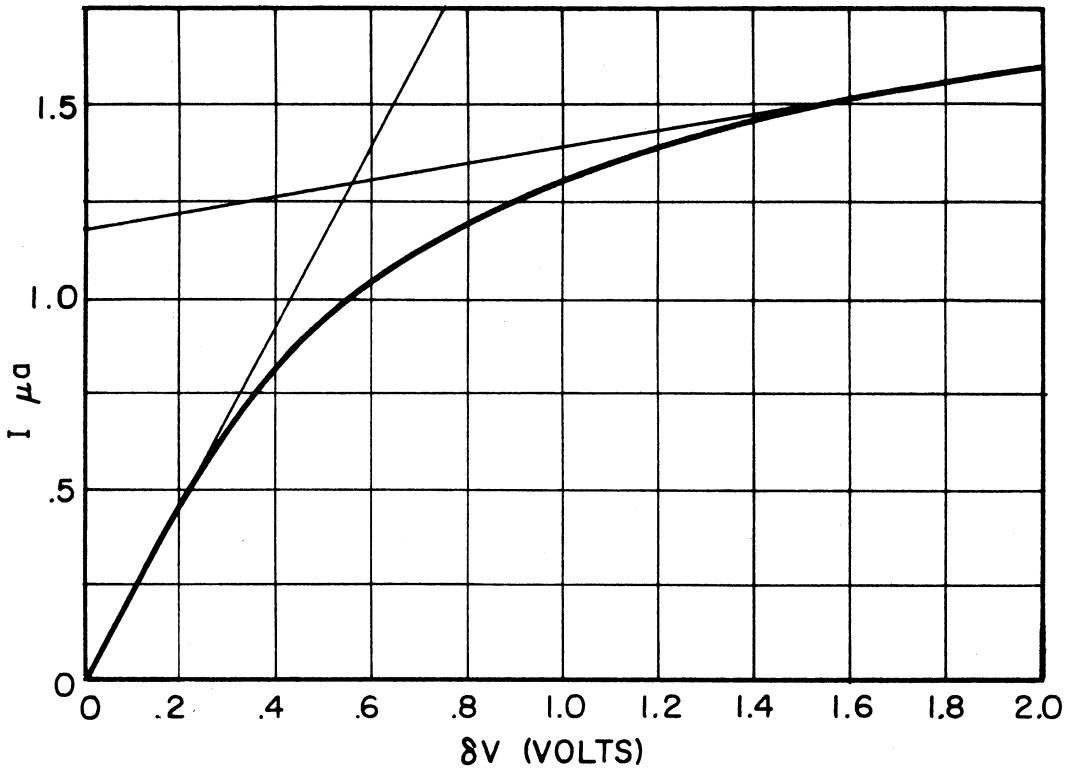

Fig. 46. Predicted bipolar probe volt-ampere characteristic at 450 km (hemispherical electrodes).

From the above calculations, current sensitivities of 0.75 and 3.0 μa were chosen. Sensitivity means here that a current change from zero to the value chosen results in the standard ± 7-1/2% deviation of the sub-carrier oscillator center frequency. The value of δV, however, cannot be chosen entirely from these calculations because of the biasing effect of the relative velocity between the probe and the plasma. This effect can result in voltages as high as 6 volts, corresponding to a velocity of 6300 fps, at the time of probe ejection from ABM 10.200* if the probe axis were parallel to the direction of motion. Thus δV sweeps of 2.55 and 8.5 volts (2 and 5 mercury cells under load) were chosen.

*ABM 10.200 is the Fort Churchill, IGY designation for the Aerobee-300 rocket used for the second probe launching. The Nike-Cajun rocket used for the first probe launching is designated ABM 6.207 by Fort Churchill (see page 74).

VII. THE INSTRUMENTATION

The implementation of the probe experiment required the proper functioning of two untried pieces of equipment, the ejection mechanism and the probe instrumentation. Thus two complete instrumentations were constructed for initial flight tests, the first to be used on a relatively inexpensive rocket to test the ejection mechanism and to make preliminary measurements of E-layer parameters, the second was to follow on a higher altitude rocket, if the ejection of the first probe was essentially successful. The first probe was successfully ejected at 80.5 km from ABM 6.207, a Nike-Cajun rocket which reached an altitude of 131 km; thus the second probe was flown on ABM 10.200, an Aerobee-300, on November 30, 1958. Ejection occurred at 88.5 km and telemetry signals were received until apparently the transmitter power supply failed at 186 km.

A Nike-Cajun is a two-stage, solid-propellant rocket. An Aerobee-300, or Spaerobee, is a boosted, two-stage rocket which is a combination of a liquid propellant first stage, an Aerobee-Hi, and a solid propellant second stage, a Sparrow. Both rockets were launched at Fort Churchill, Canada, as part of the International Geophysical Year Rocket Program.[23,24]

The instrumentation necessary to perform the ionospheric experiment through the determination of a volt-ampere characteristic includes a sawtooth-voltage generator, current detector, data-storage unit, and a data transmitter. Internal auxiliary instrumentation includes a timer, therm-

istor, and power supplies. External instrumentation includes the ejection mechanism, ejection timer and a DOVAP (DOppler Velocity And Position) transponder. Additional ABM 10.200 instrumentation included a magnetometer in the probe for aspect data, a DPN-19 radar beacon for tracking, and a DRW-3 receiver for destroying a dangerously off-course rocket. Other revisions in the second instrumentation were minor, generally concerned with better rf shielding within the probe.

A. MECHANICAL DESIGN

The probe was composed of four "spun" stainless-steel electrodes, two hemispheres and two "funnels." The "funnels" were assembled back-to-back on a Teflon insulating and supporting section. The hemispheres were separated from the funnel sections by rubber gaskets which also provided a gas seal. The hemispheres were positioned and fastened to the funnels by three Phenolite laminated plastic clips which were slipped over steel retaining pins after the gasket was compressed. To assure that the assembly was gas-tight, it was pressure-tested to twice atmospheric pressure differential. Figure 47 shows a partially disassembled probe showing the hemisphere, funnel, sealing gasket, retaining clips and the "O" ring seal on the Teflon center section. Flat-head stainless-steel screws which fasten the funnel to the Teflon are seen in the assembled portion. Figure 48 shows the detail of the pin-clip fastening system. The rubber gasket and Phenolite clip provide the d-c insulation necessary between the funnel and the hemisphere, as well as the mechanical strength to withstand the internal gas pressure and compressed gasket.

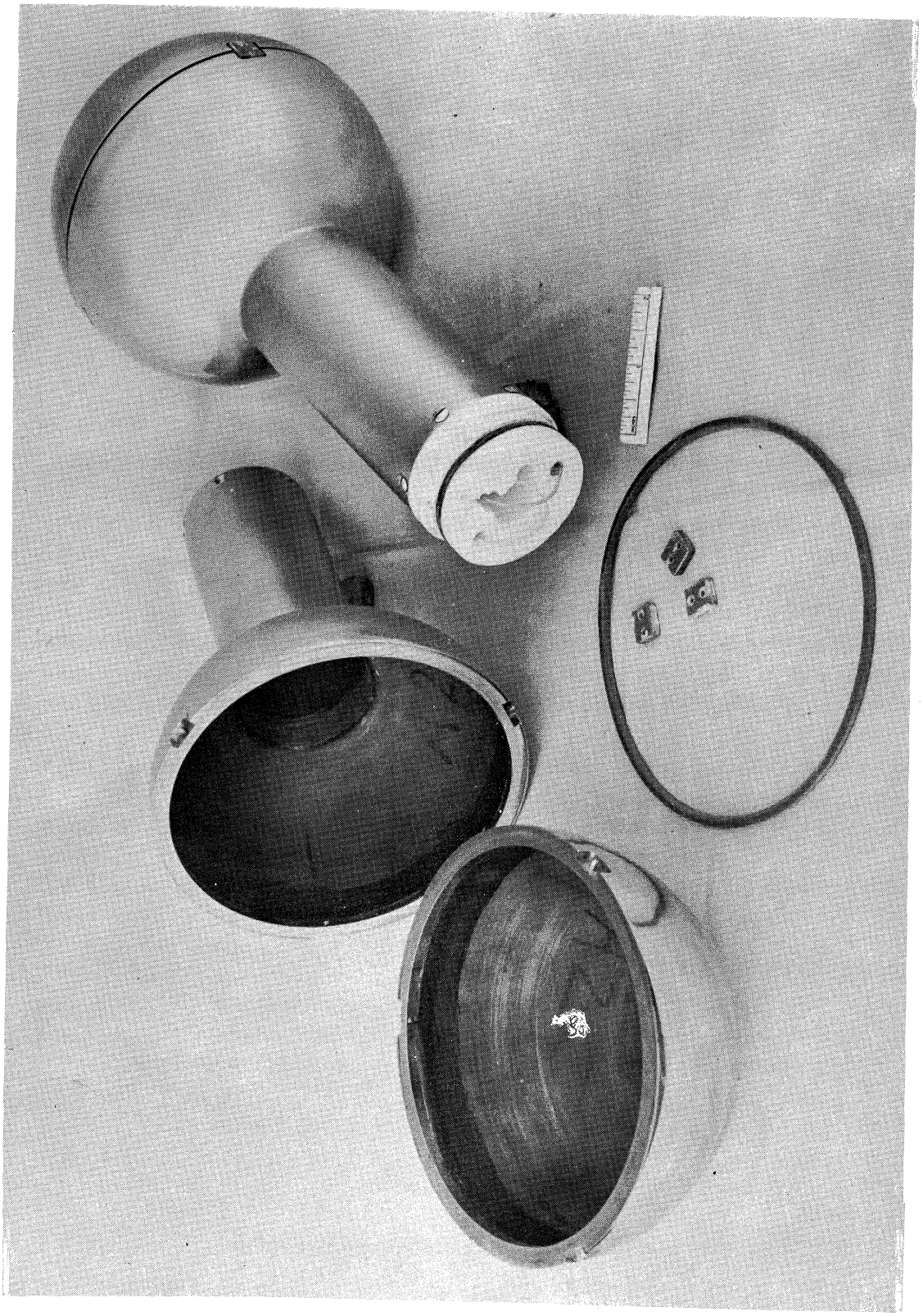

Fig. 47. Disassembled double-sphere probe shell.

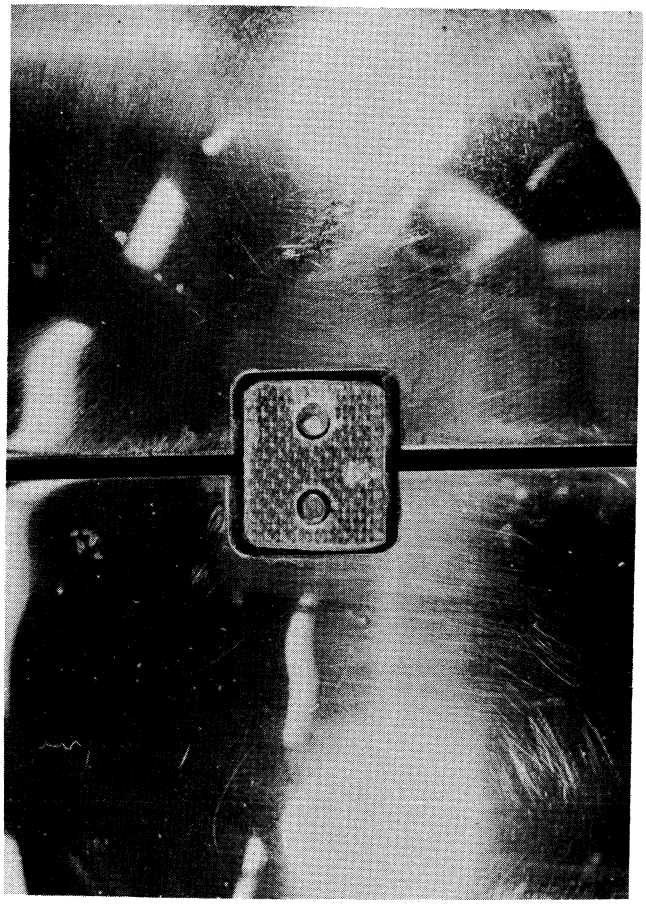

Fig. 48. Detail of the pin-clip fastening system.

Figure 49 shows the nose assembly which housed the probe and auxiliary instrumentation. Figure 50 shows the same assembly partially opened. The probe is supported by four "fingers" which also provide angular restraint of the probe during nose opening. Figure 51 shows the fingers and spring-loaded plunger which, when unlatched, releases the probe, ejecting it from the nose cone. The latch, which retains the plunger until the nose has opened approximately 60°, is seen to the right of the plunger. The cylindrical halves of the probe housing are hinged at the base with 1/2-in., close-tolerance dowel pins. The split nose cone is held together by a frangible-magnesium ring which just fills the undercut and completes the cone

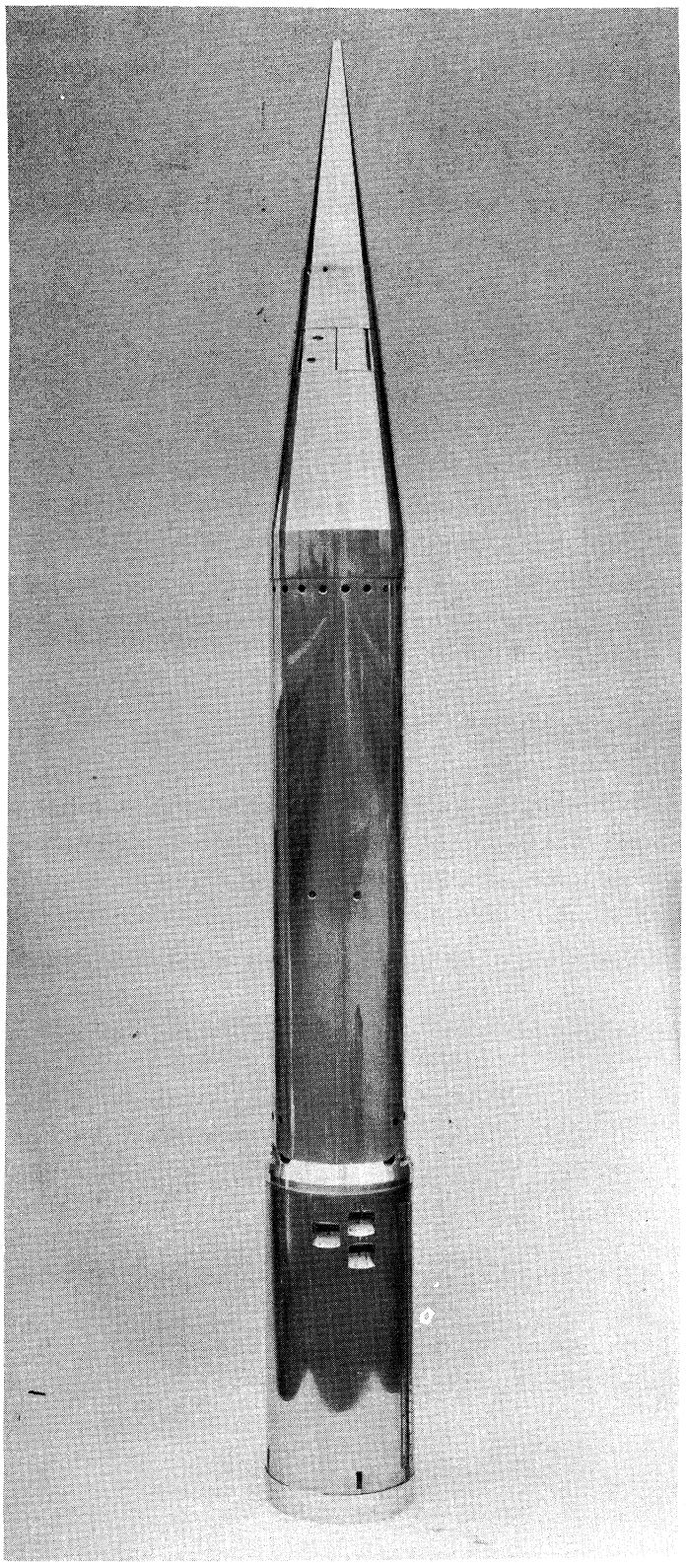

Fig. 49. Nose assembly in closed position.

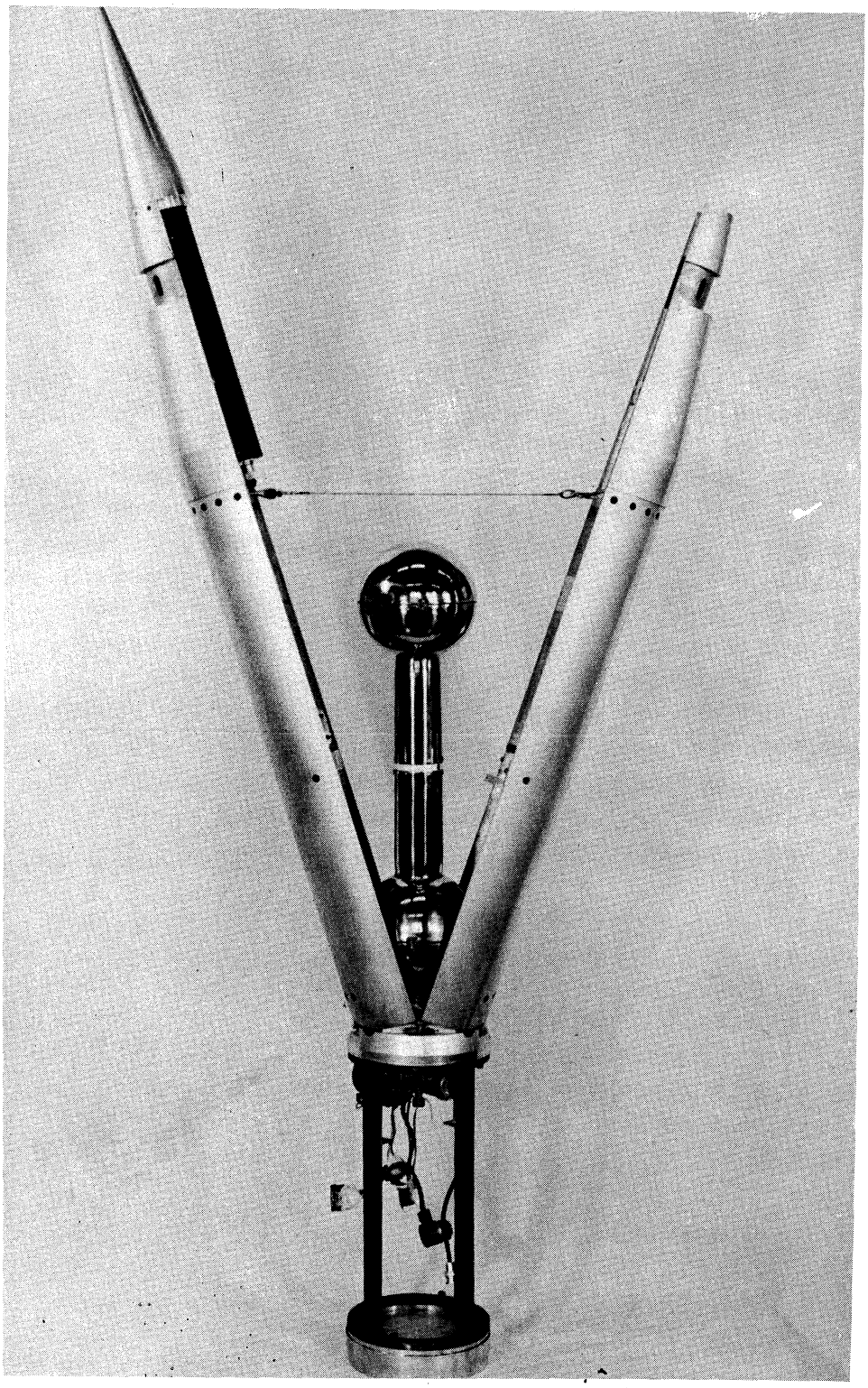

Fig. 50. Nose assembly in open position.

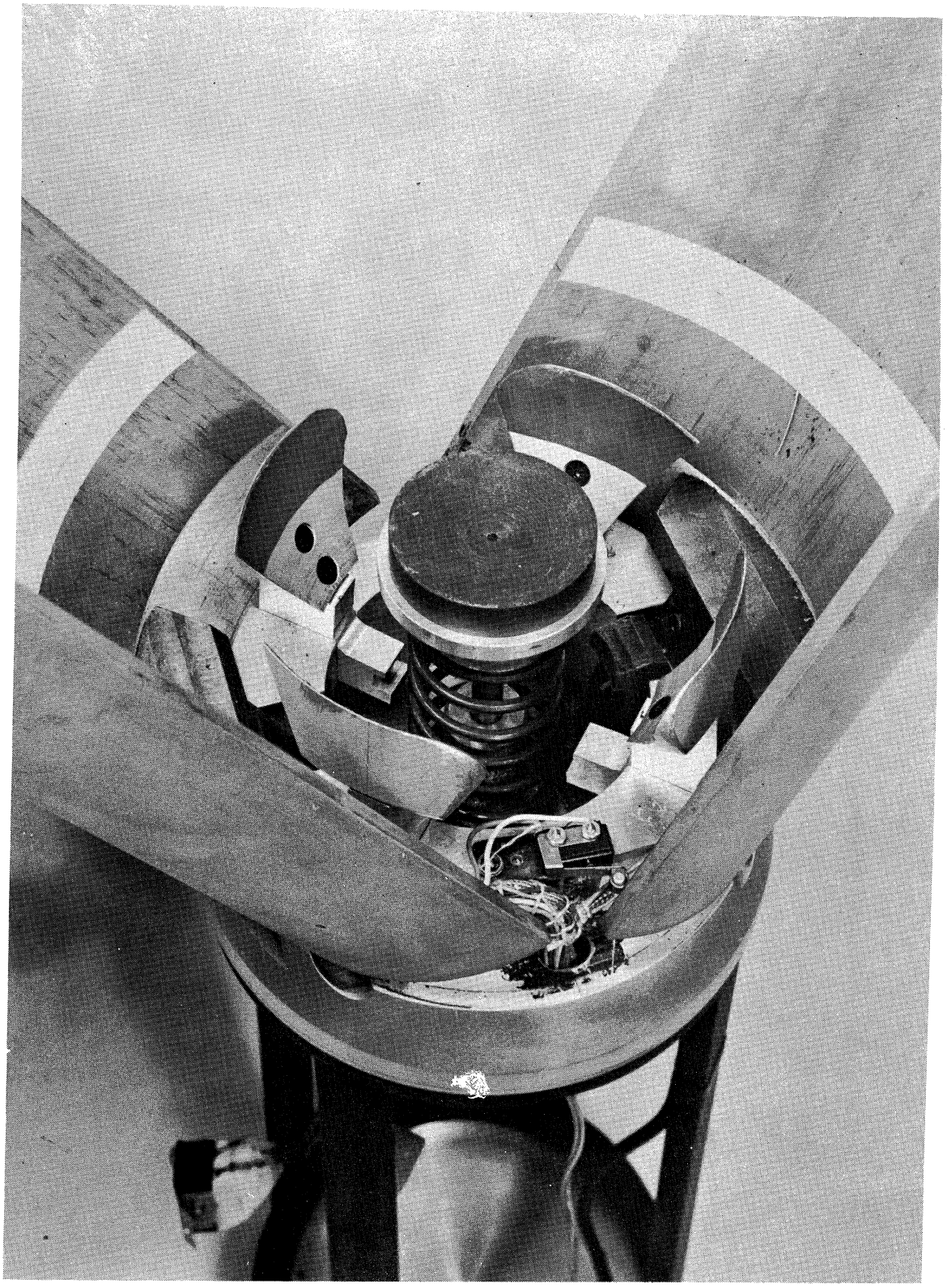

Fig. 51. Detail of probe support and ejection arrangement.

surface when in place. Shear strength along the split is provided by six 1/4-in. dowel pins (see Fig. 52). Opening was accomplished at the desired time by breaking the frangible ring with four electrically initiated primers. The controlling timer was set to explode the primers at an approximately 80-km altitude. Springs and centrifugal force due to the rocket roll caused the forward section to open, releasing the plunger which ejected the 14-lb probe at a velocity of approximately 10 fps. The nose section was held in the open position by centrifugal force.

B. CIRCUIT DETAILS

Figure 53 is a block diagram of the bipolar probe circuit. The desired electrode difference voltages (δV) were supplied by batteries and two precision potentiometers mounted on a common motor-driven shaft. Two equal, saw-tooth voltages were generated. One was applied between the two outer hemispheres and the other between the two inner funnels. The potentiometers were adjusted so that the voltage between the hemisphere and associated funnel was minimized. Actually the voltages differed by only a few millivolts throughout the voltage sweep.

As seen in the block diagram, current was measured only between the outer hemispheres which were considered to perform as a double-ideal-hemisphere geometry since practically all field distortion occurs in the vicinity of the cylindrical section of the funnel.

The current detector consisted of a semi-conductor ring modulator (Fig. 54), transistor modulator driver (Fig. 55), and a transistor amplifier and detector (Fig. 56). The ring modulator is a balanced diode-bridge

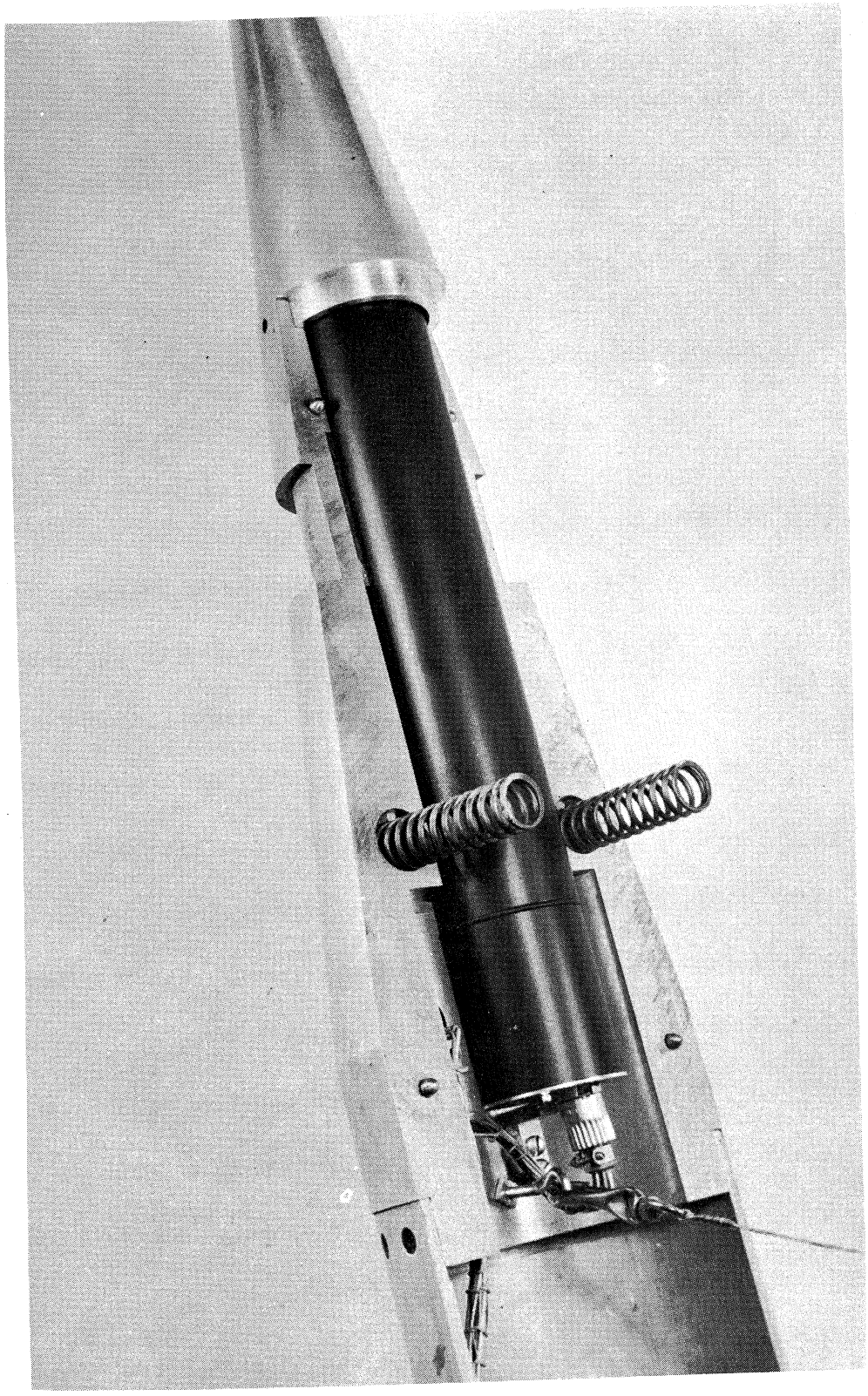

Fig. 52. Detail of nose section showing shear pins and opening springs.

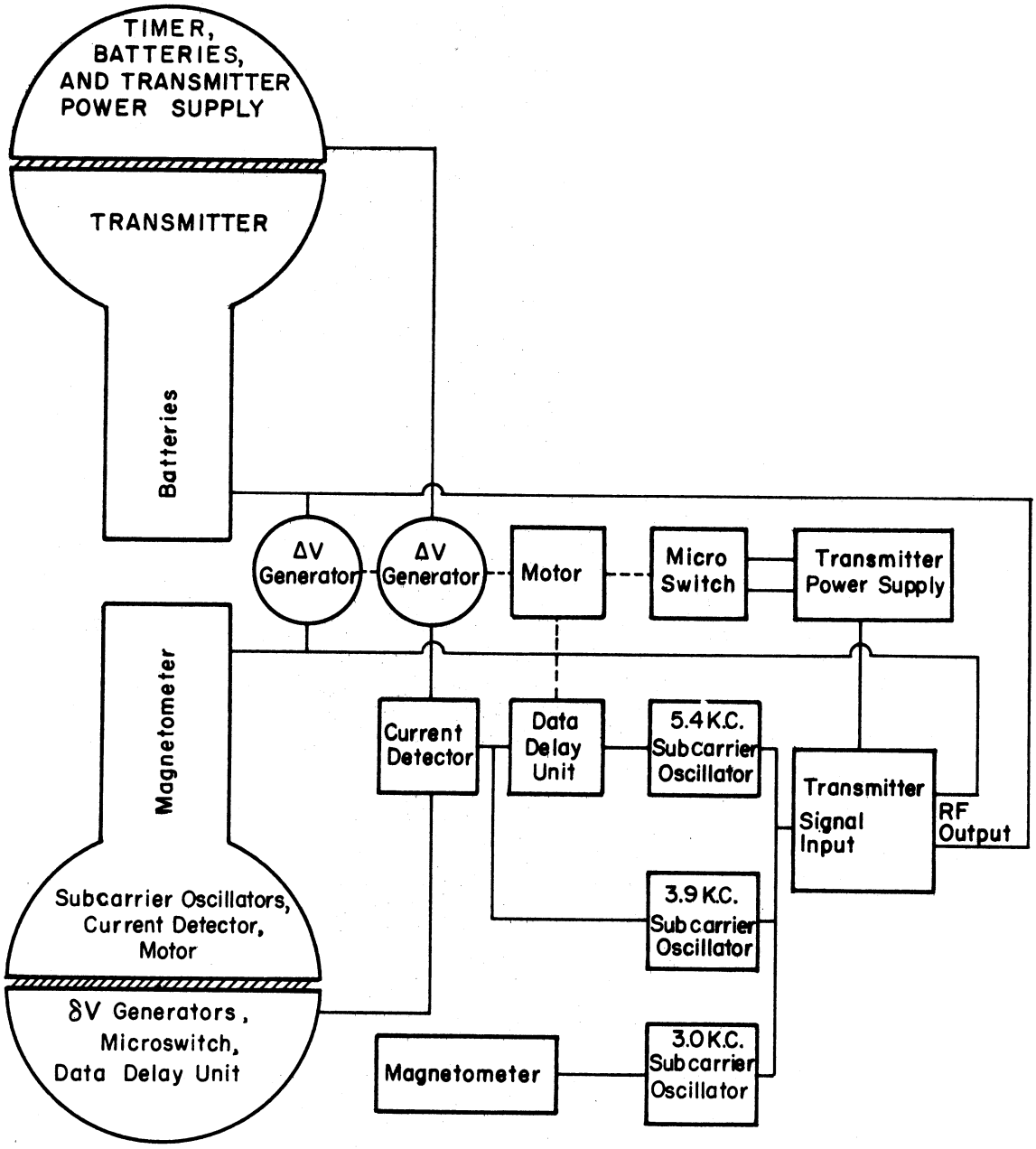

Fig. 53. Bipolar-probe instrumentation block diagram and component location.

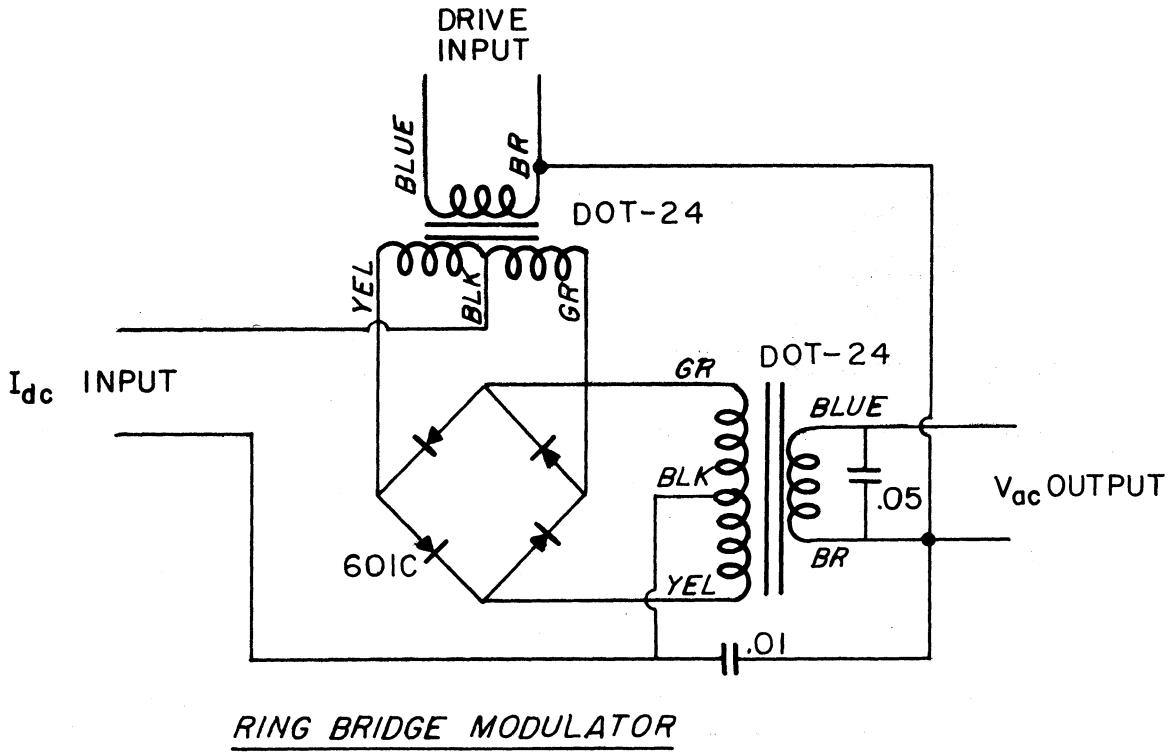

Fig. 54. Ring-bridge-modulator circuit.

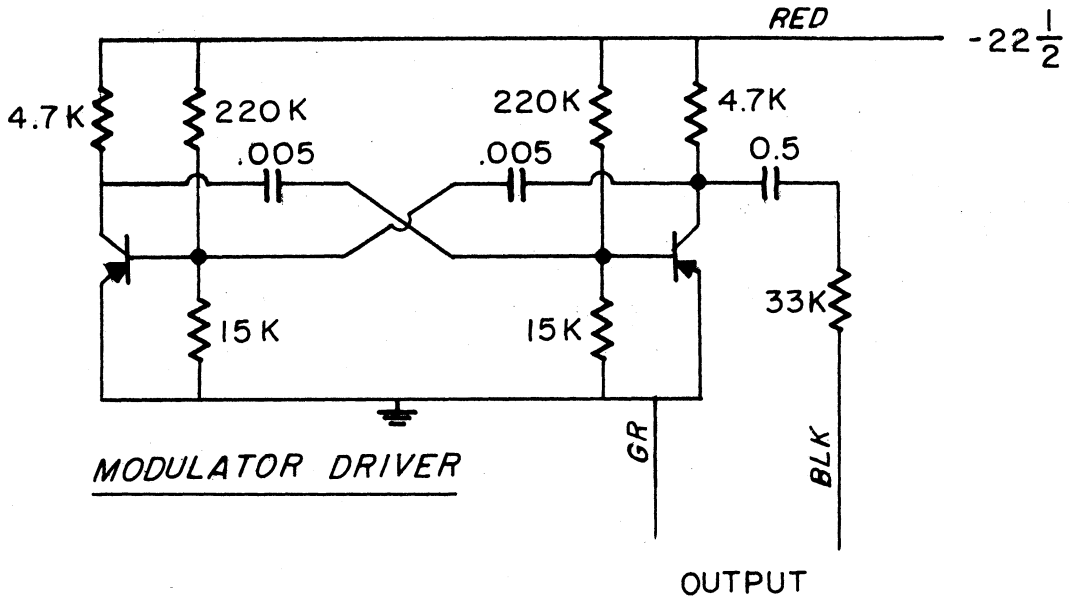

Fig. 55. Modulator-driver circuit.

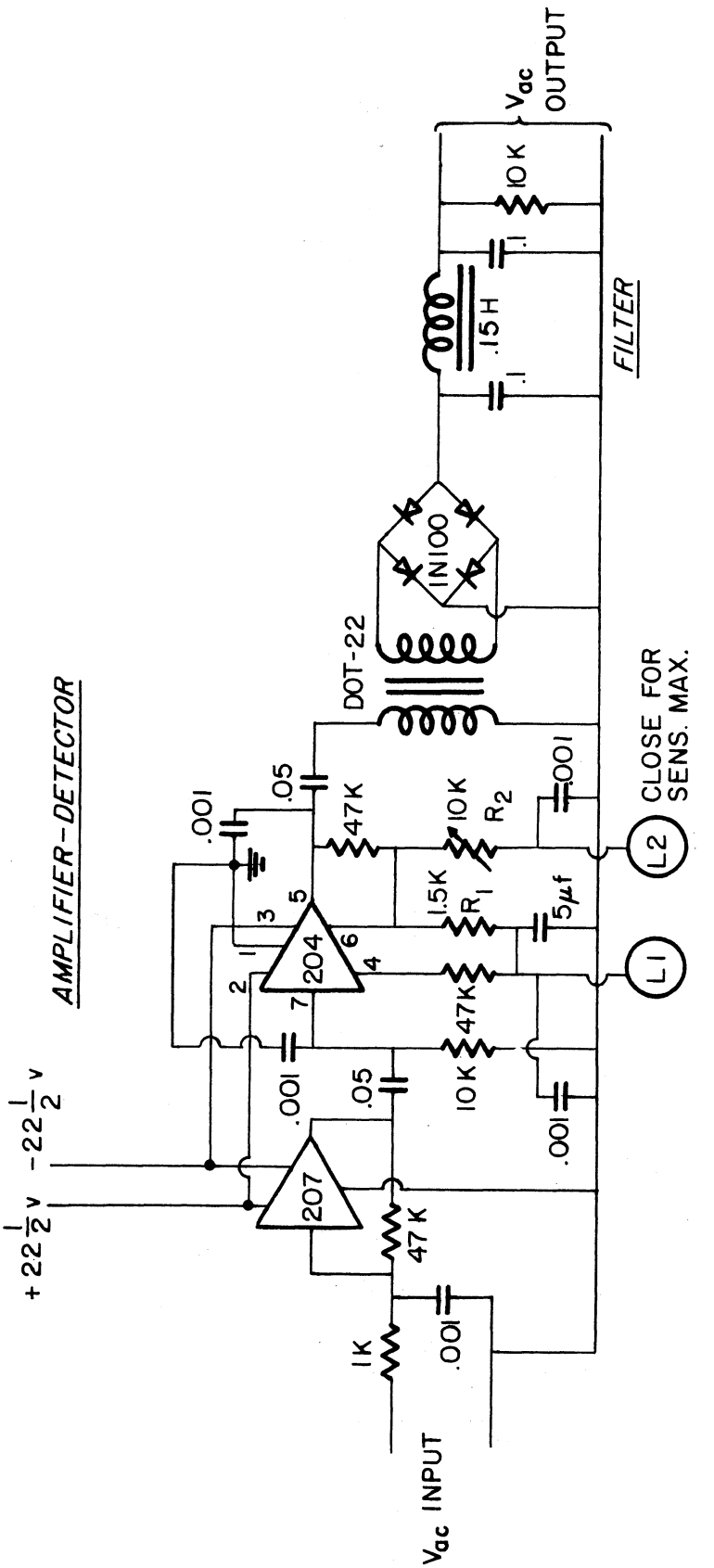

Fig. 56. Amplifier and demodulator circuit.

cuit which acts as a reversing switch of the d-c signal current, producing an a-c output at the frequency of the driver oscillator (4 kc). Thus the amplifier band-pass is centered on this frequency. The amplified signal is then rectified to provide the d-c bias for the subcarrier oscillators. The current detector utilized commercially available transistor amplifiers labeled 204 and 207 in Fig. 56.

The subcarrier oscillators (SCO) (Fig. 57) are transistorized multivibrators whose frequency is controlled by the emitter bias. The output of the current detector was applied directly to the 3.9-kc SCO and through a data-storage unit to the 5.4-kc SCO. The output of the magnetometer, used to help indicate "dumbbell" attitude, was applied to the 3.0-kc SCO.

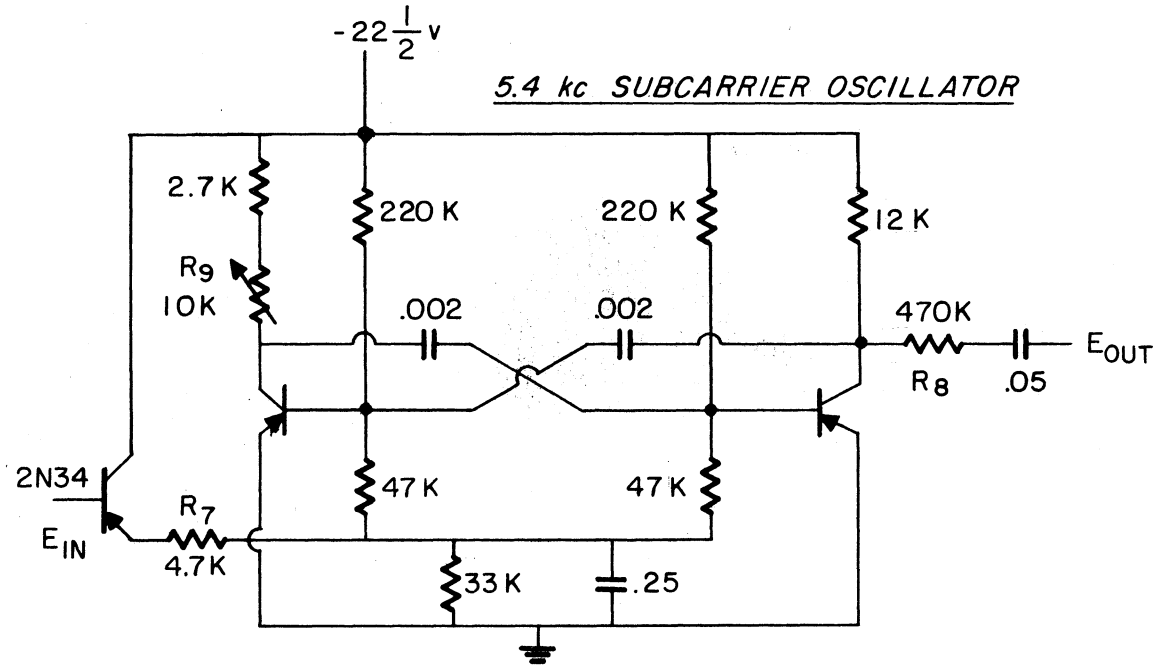

Fig. 57. Subcarrier oscillator circuit diagram.

The subcarrier oscillators provide a signal for modulation of the FM transmitter, which employs the "dumbbell" as a dipole antenna.

The 2-watt Bendix FM transmitter was powered by a transistor-oscillator power supply operating from a 24-volt battery pack; the transmitter filament power and the magnetometer were supplied from a separate 6-volt source.

A speed-regulated motor drove the δV potentiometers at approximately 6 rps. The motor also operated a microswitch which controlled the transmitter B+ and the input-output transfer relay of the data-storage unit. The transmitter was switched off and data were stored for approximately one out of four revolutions of the δV potentiometers. These data were then available for transmission via the 5.4-kc channel during the transmitter on-period, approximately three-fourths of the time. During the transmitter on-period, ionospheric data are transmitted directly via the 3.9-kc channel. This system permits comparison of data taken with and without presence of the rf field, within a 1/6-sec interval, which was considered a sufficiently short time.

Data storage employed a set of capacitors which were charged and then later sampled. In effect, it recorded 14 points of the VA characteristic curve. A tape-storage unit which recorded the SCO output proved unsatisfactory because of the stringent requirements of tape-speed regulation and constant amplitude necessary for adequate data recovery.

To display adequately the volt-ampere characteristic as the ionospheric parameters changed with altitude, and to allow for error in pre-

diction between the actual and assumed ionospheric parameters, the sensitivity of the current detector was altered periodically (two settings), as were the two values of battery voltage applied to the potentiometers. The necessary timing function was provided by a solenoid and relay-switching system energized by the previously mentioned microswitch. The timer also switched a resistor into the current-detection system for the purposes of calibration.

C. AUXILIARY EQUIPMENT

A DOVAP transponder was housed in the section just aft of the probe housing. On ABM 6.207 the ejection timer and power supplies were also housed in this section, and a radioactive ionization pressure gage was located in the nose (the black cylinder in Figs. 50 and 52). This was a completely independent experiment which measured the ambient density of the atmosphere to an altitude of 80-90 km.

On ABM 10.200 the ejection timer and power supply was moved forward to a position just above the probe. The angular position of two "wind vanes," placed on the tip to measure angle of attack, was monitored during the early powered portion of the flight to determine if the angle of attack was within allowable limits. If it was not, it was possible to prevent the ignition of the second stage by command signal from the ground through the use of a DRW-3 cut-down receiver. Destruction of the rocket also could be effected by a second command signal if the rocket was dangerously off course.

Figure 58 shows ABM 10.200 assembled for a horizontal pre-flight check. The small diameter section just aft of the probe instrumentation is the solid-propellant second stage with the DOVAP antennas in place. The flared skirt which mates the two stages provides stabilization of the second stage after separation. The forward section (15 in.) of the first stage housed the DRW-3 and the DPN-19. The remainder of the first stage is comprised of the fuel tanks, thrust chamber, and fins. The booster had not been installed at this time. Figure 59 shows the tower installation of the ABM 10.200 probe.

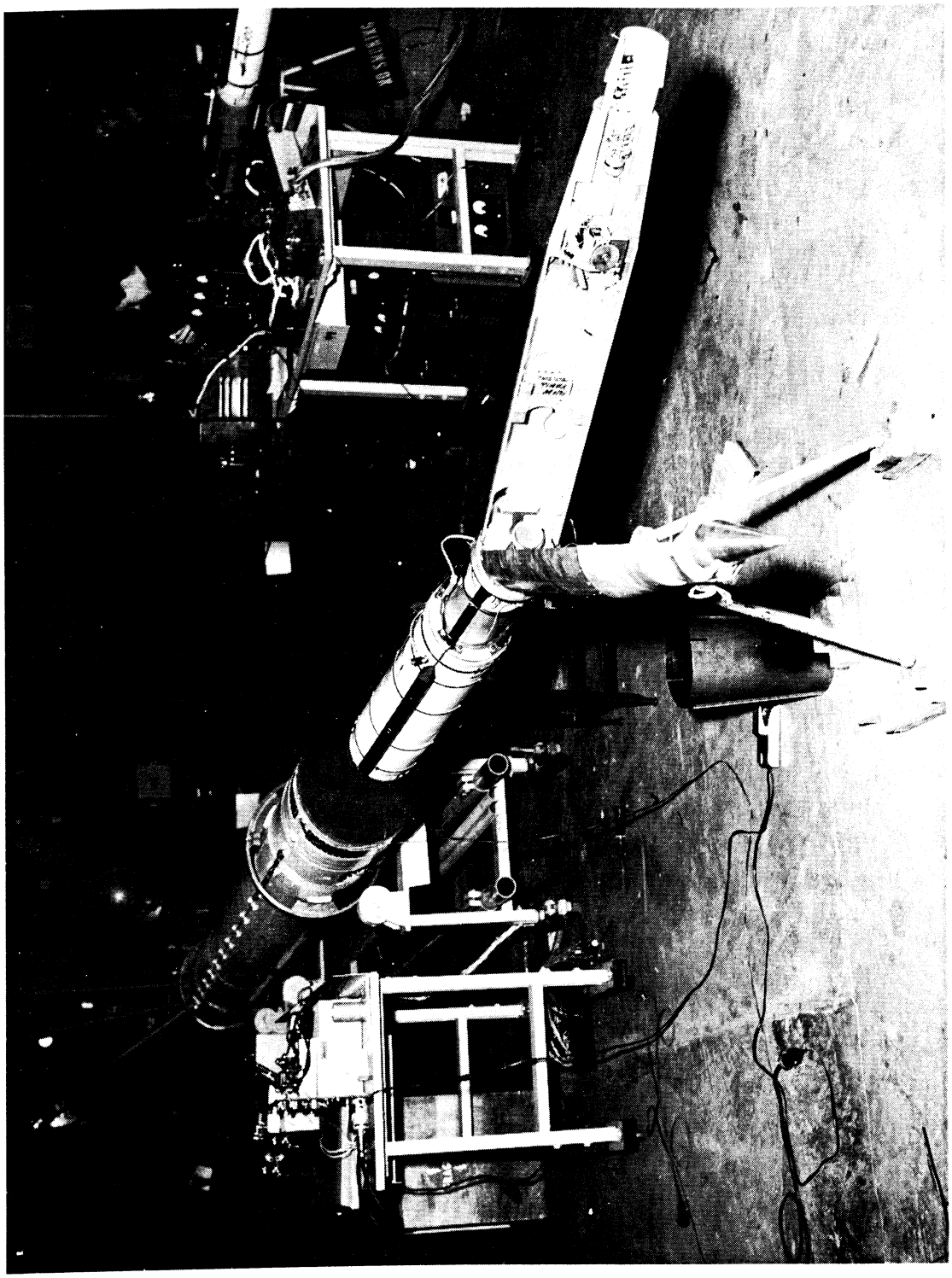

Fig. 58. ABM 10.200 rocket assembly.

Fig. 59. Tower installation of the probe.

VIII. DATA REDUCTION

ABM 10.200 was launched at 12:36:36 on November 30, 1958, a clear, cold day, at Fort Churchill. Figure 60 shows the rocket approximately 1 sec after launching. A telemetry signal was received following the ejection of the probe at 80 sec until 140 sec covering an altitude range of 88.5 to 186 km. From the data obtained, it was possible to determine that the volt-ampere characteristics were much as anticipated; however, the loss of the low current-sensitivity setting of the instrument due to rf interference complicated data reduction and resulted in relatively low data recovery. Both velocity and photoelectric-emission effects were apparent, but the relatively small number of samples, the near synchronism of the probe circuit sequencing and the motion of the probe (coincidental) permitted only a superficial study of these effects.

A. TRANSMITTED DATA

Figure 61 shows the real-time flight record from 111 to 127 sec, record time. Elapsed time from launching is obtained by subtracting 0.372 sec from the record time. The seven traces shown in Fig. 61 and the full-size section (Fig. 62) are, from top to bottom: range timing, reading reference, 3.9-kc channel (direct-probe data), 4.5-kc channel (delayed-probe data), 3.0-kc channel (magnetometer-probe attitude data), reading reference, and range timing. The timing traces provide 0.01 and 0.5 sec timing marks and a range time record consisting of a binary code group

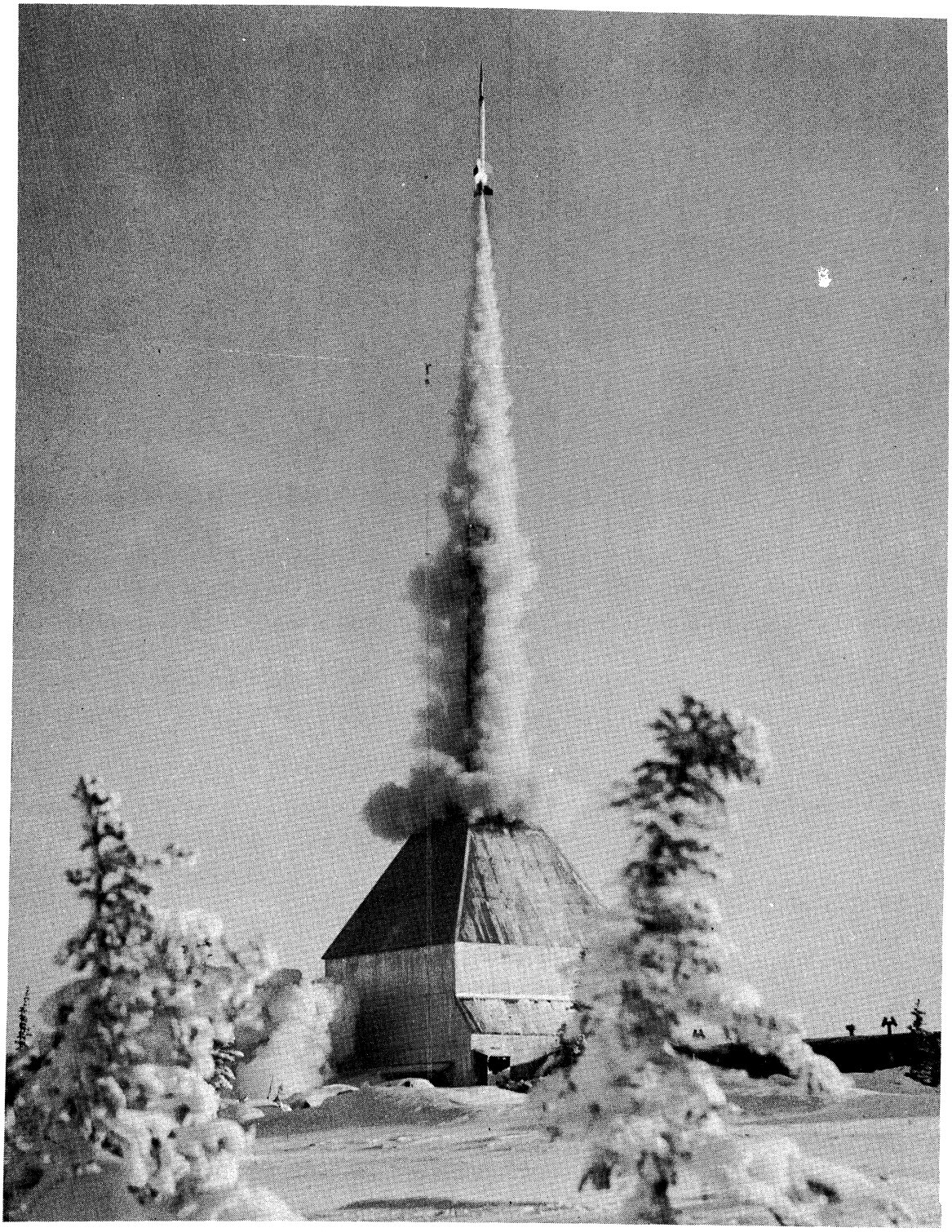

Fig. 60. Bipolar probe rocket, ABM 10.200, approximately 1 sec after launch.

Fig. 61. Real-time flight record from 111 to 127 sec.

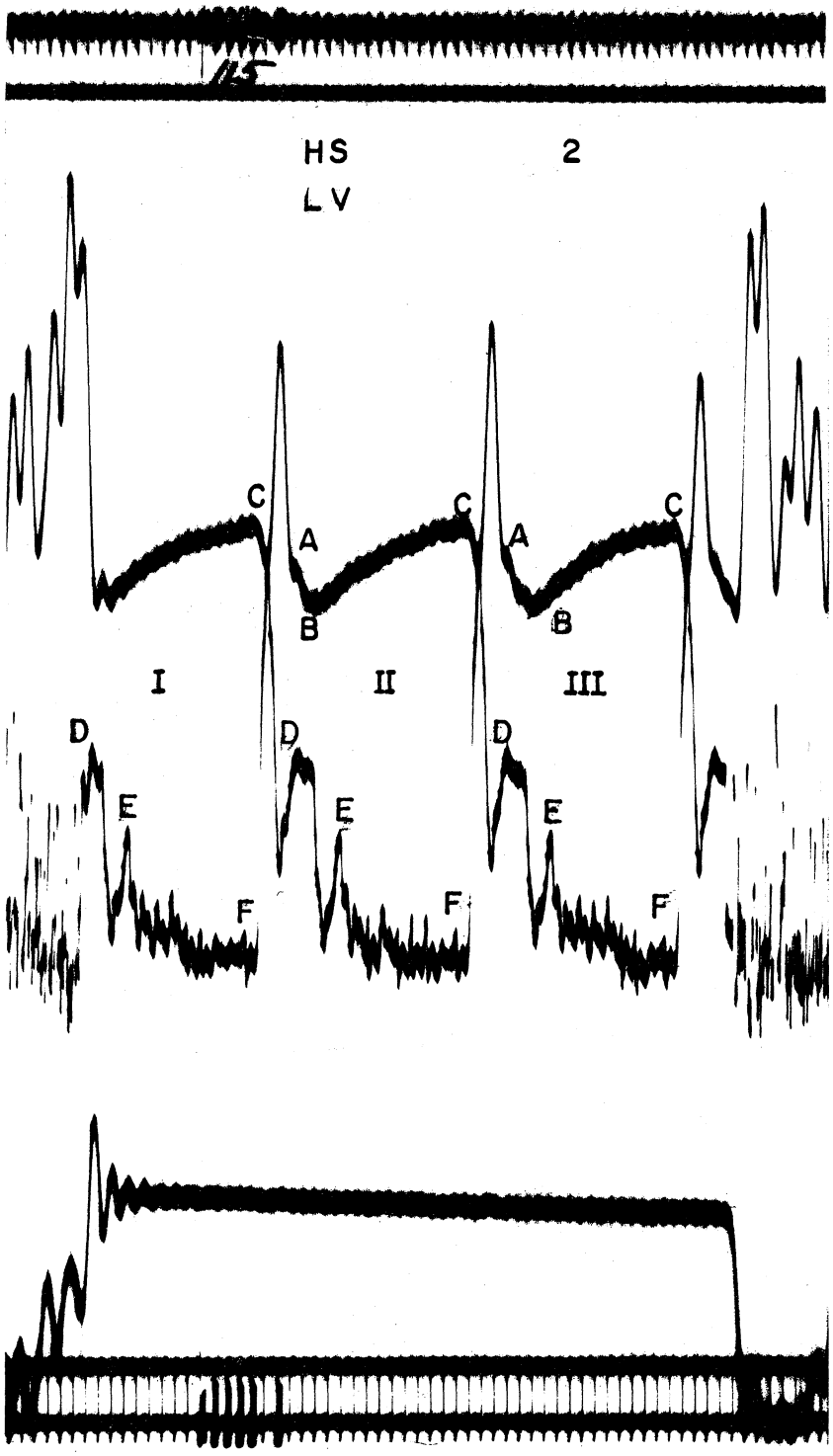

Timing

Data Reference

"3.9" Channel
Direct Data

"5.4" Channel
Delayed Data

"3.0" Channel
Attitute Data

Data Reference

Timing

Fig. 62. Raw data, high current-sensitivity low-voltage sequence at 115 sec.

every 5 sec. The coded time has been written beside the binary time code. It is seen that one volt-ampere characteristic was taken each 0.17 sec, the sweep voltage was changed every 0.68 sec, the current sensitivity was altered every 1.36 sec, and one complete series of readings was made in approximately 8.16 sec. The two portions of the record cover two complete timer cycles.

The inflight timer (function sequencing) alternated current sensitivities and probe sweep voltages, provided for calibration,and served as a commutator for sampling magnetometer output, magnetometer bias, and the internal temperature of the probe. The various positions of the timer, a rotary solenoid switch stepped by the motor-operated microswitch, are indicated by numbers 1 through 12. The low-voltage (LV) and high-voltage (HV) sweeps and low-sensitivity (LS) and high-sensitivity (HS) positions have been marked individually in Fig. 61; thus their position assignments are not listed. A calibration of the "3.9" channel and the "5.4" channels were provided in positions 10 and 11. The "3.0" channel was switched to a thermistor circuit which measured the internal surface temperature of the sphere containing the amplifier, in positions 10 and 11. The "3.0" channel in position 9 was used for measuring the magnetometer calibration bias.

Probe current data were stored and the transmitter switched off during the first 8V sweep following a change of timer position from positions 8 through 3. These stored data were read out and transmitted during the next three sweeps. The transmitter was not turned off in the other timer

positions while data were being stored, thus allowing a check of data with and without the transmitter functioning. The period that the transmitter was off can be determined readily by the corresponding abrupt break in the magnetometer data.

A study of the record indicates that the data taken during the high current-sensitivity sequences were approximately as expected. Temperature data were available during the high current-sensitivity low-voltage sequences. The high current-sensitivity high voltage sequences did not have adequate resolution to yield temperature data for the ionospheric parameters encountered while data were being received, but they did furnish a check on the calibration of the high-sensitivity setting of the current detector. The most serious loss of data occurred in the low current-sensitivity sequences; the signal in these sequences was overwhelmed by some low-frequency noise resulting from rf interference. The aspect data were well defined and indicate uniform motion having a period of approximately 8 sec.

B. DIRECTLY MEASURED DATA

Consider now the directly measured raw data (Fig. 63), which are the portion of the flight record at approximately 118 sec. The three portions of the curve marked I, II, and III are three successive samples of probe current for three successive sweeps of δV. Immediately below these are three repeated delayed-data readings stored during the last complete δV sweep during the transmitter off-period just preceding curve I. It is seen that these curves, direct and delayed, are approximately the same

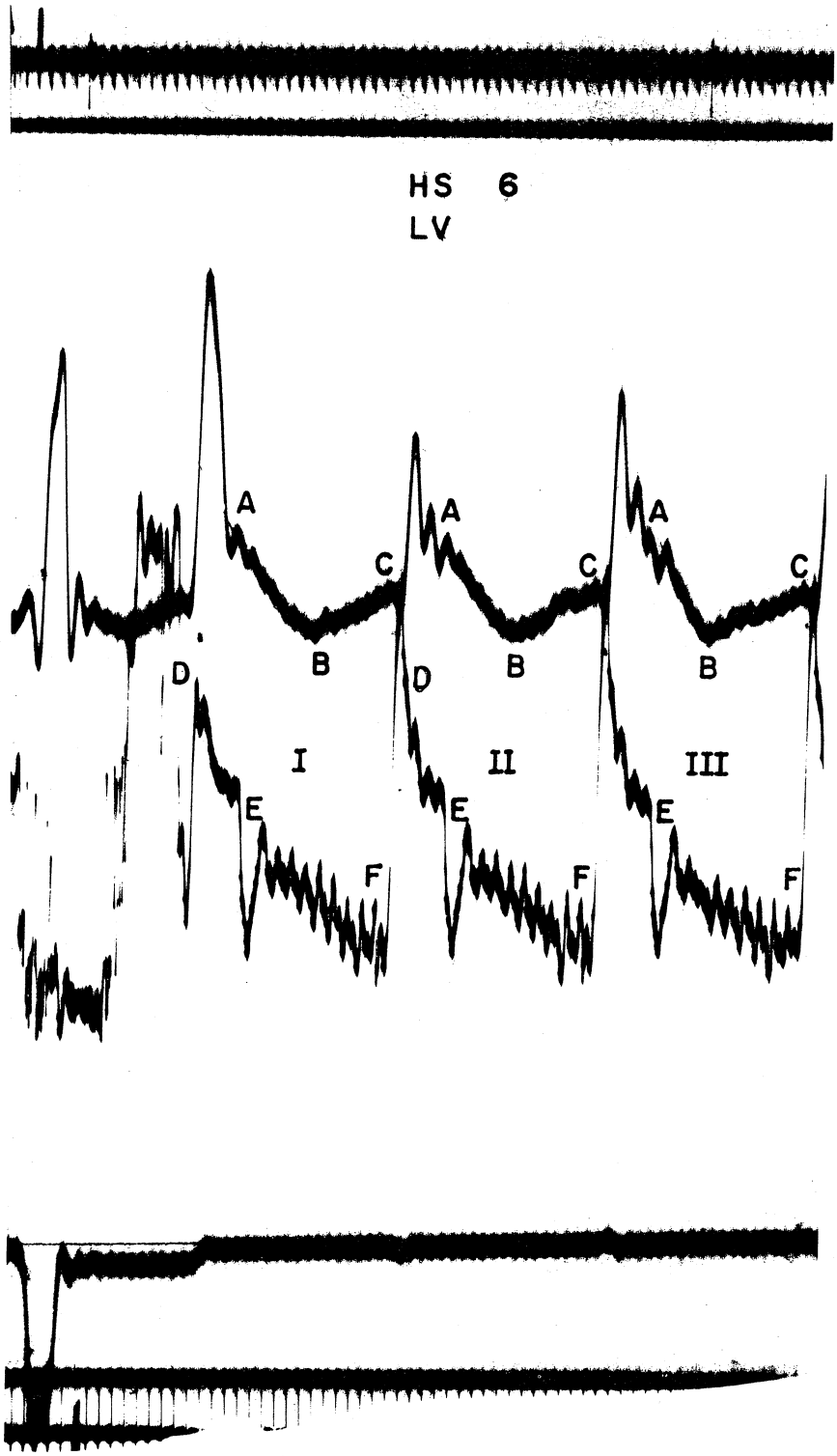

Timing

Data Reference

"3.9" Channel
Direct Data

"5.4" Channel
Delayed Data

"3.0" Channel
Attitude Data

Data Reference

Timing

Fig. 63. Raw data, high current-sensitivity low-voltage sequence at 118 sec.

except that the direct-data curve reverses slope at point B. Had this reversal not occurred, the trace would have appeared very much as anticipated (Fig. 44). The BC region of the data curve corresponds to the ion current saturated portion EF of the calculated curve.

The reversal of the direct-data channel was attributed to some instrumentation component since the delayed-data channel did not reverse with or without the transmitter operating, and the reversal was found to occur each time at the same current throughout the entire record, including calibrations made before launching. This was not a malfunction of the instrumentation, however, since the calibration was linear over the intended range 0.0 to 0.75 μa. The current which caused the reversal exceeded the normal range corresponding to a standard subcarrier oscillator (SCO) deviation of ± 7-1/2% of the center frequency. This portion of the curve must now be considered because data were not obtained during the low current-sensitivity sequence.

To have confidence in the 3.9-kc-channel data, it was necessary to determine the cause of the curve reversal. Since only this channel was affected, only those parts of the instrumentation used exclusively by the 3.9-kc channel were involved. These were the discriminator, its associated passive filters, and the recorder galvanometer in the ground station. A block diagram of one ground station is shown in Fig. 64. The 3.9-kc subcarrier oscillator was the only uncombined rocket-borne instrumentation in the "3.9" channel. Tests disclosed that the reversal was not caused by the ground equipment. Thus, by elimination, the 3.9 SCO was shown to

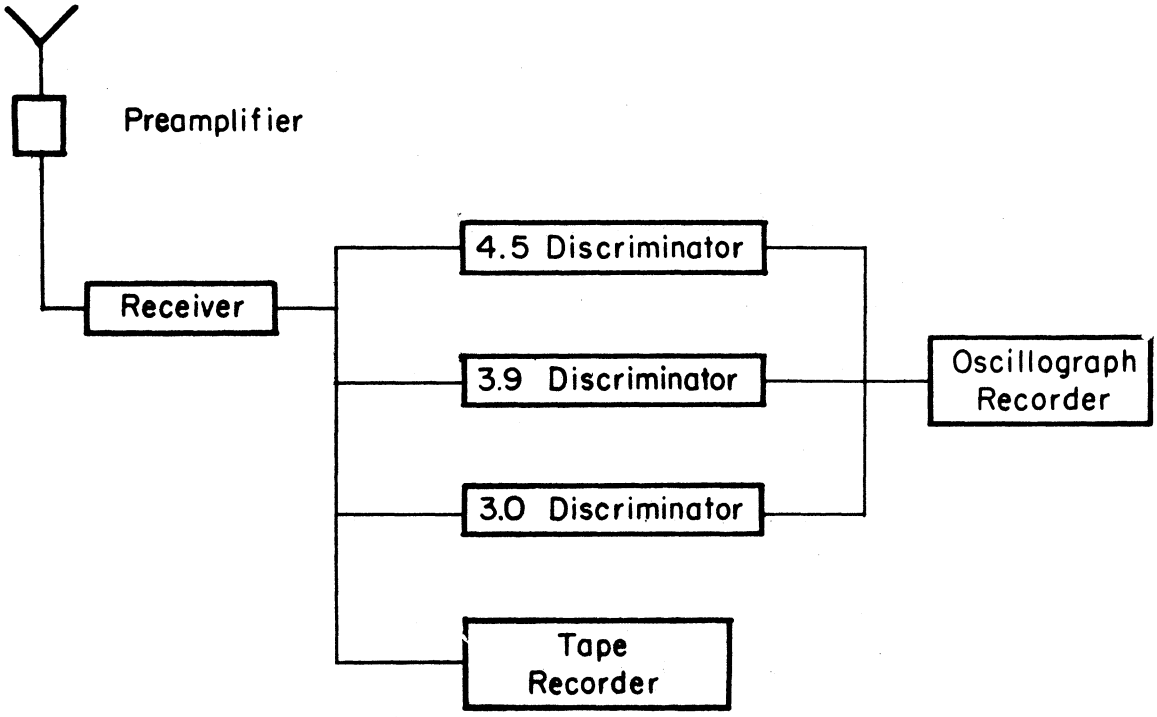

Fig. 64. Telemetering ground station block diagram.

be responsible for the reversal. This was verified when an overdriven spare SCO exhibited the same effect.

C. DIRECT-CHANNEL HIGH-SENSITIVITY CALIBRATION

Study of the flight record has disclosed that the high current-sensitivity data must be reduced to obtain ionospheric data. Thus, it is fortunate that the useful range of the ground and rocket-borne instrumentation was approximately twice that anticipated. However, the in-flight calibration of the instrumentation did not cover the entire range employed, and thus it was necessary to extend the calibration using pre-flight calibrations and bench calibrations of essentially equivalent component sections (current detector, amplifier, and subcarrier oscillator). Frequency-response tests of the ground-station discriminator disclosed

that it was linear over the range encountered; thus only the rocket-borne instrumentation was considered in extending the calibration.

The following calibrations were available: (1) a preflight systems calibration (Fig. 65) which provided a calibration of both the ground and rocket instrumentation; (2) bench calibration of frequency vs. drive voltage of the 3.9 SCO flown; and (3) a bench calibration of the current detector flown, input current vs. output voltage. The above calibrations extended well beyond the anticipated-current range but were not adequate for the high currents encountered. Thus it was necessary to test spare sections of the circuit to determine the most direct and accurate method of extending the system calibration.

Current and voltage scales could be associated with the calibration curve since a linear current variation was produced in the signal circuit as a result of inserting a calibration resistor (1.96×10^6 ohms) between the outer hemispheres, the information electrodes. The saw-tooth sweep voltage (0.0 to 2.55 volts) was linear. To use this preflight system calibration in conjunction with the second and third calibrations, it was necessary to provide a frequency-to-current correlation. This was obtained by replaying the magnetic tape recording of the receiver output (data which were stored on magnetic tape during the flight) and providing a frequency calibration of the 3.9 discriminator on the same paper record. In the following discussion, a reference to the preflight record assumes that the frequency correlation is included.

Further study of the flight record, especially the calibration posi-

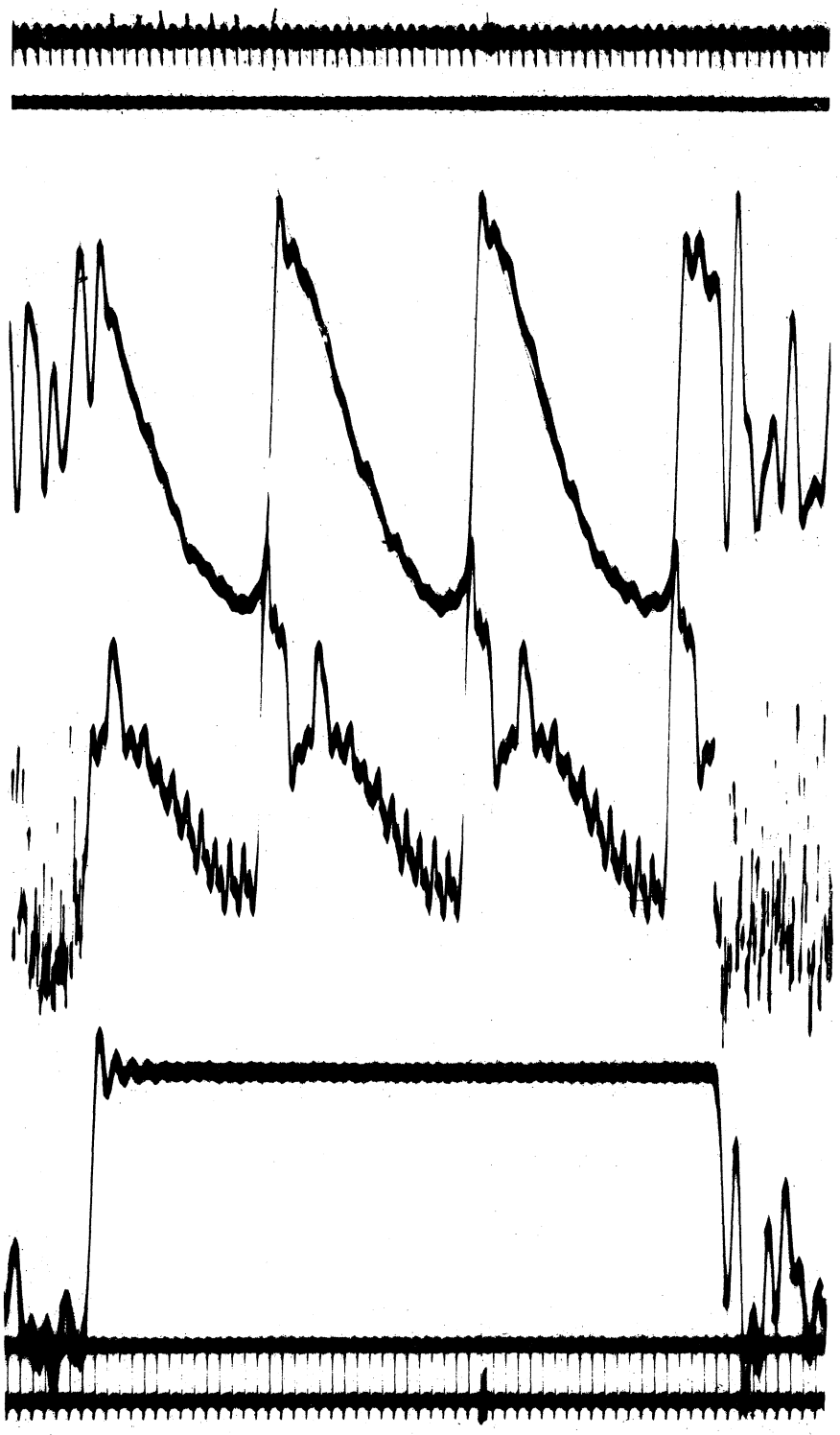

Fig. 65. High current-sensitivity low-voltage system calibration.

tions while the probe was in flight, disclosed that some instrument component was being saturated at high signal currents. Study of the individual spare components disclosed that the amplifier would saturate and that the point of the saturation would be determined primarily by the setting of an internal feed-back loop used to adjust the amplifier bias. The amplifier was found to be relatively insensitive to changes of supply voltage and temperature. Thus a family of curves of the spare amplifier was made with the bias adjustment as a parameter (Fig. 66). The proper curve was chosen by determining which of the family of curves in conjunction with the bench SCO calibration would correspond to the preflight calibration (Fig. 65).

Having determined the correct current detector calibration curve, it was then possible to extend the SCO bench calibration as far as the preflight calibration extended. This extension is shown in Fig. 67 by the three encircled points. The solid curve is the original bench calibration which was assumed to remain unchanged throughout the flight; the dashed curve is an extrapolation based on the study of several SCO calibrations, which indicated that the typical SCO characteristic was essentially symmetrical when driven beyond the reversal frequency.

The extended and extrapolated SCO calibrations and the previously selected current detector calibration were then combined to yield the system calibration used for data reduction. While this may seem a rather circuitous plan to obtain a calibration, it has the advantage of clearly separating the two main effects determining the shape of the composite curve,

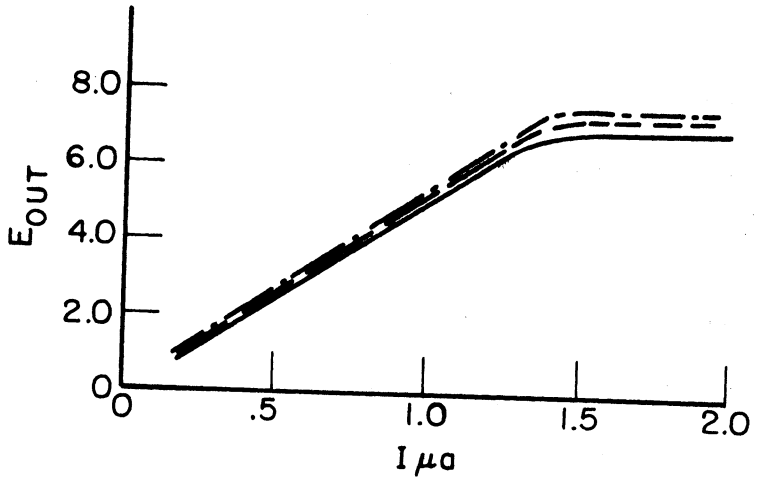

Fig. 66. Current detector calibration.

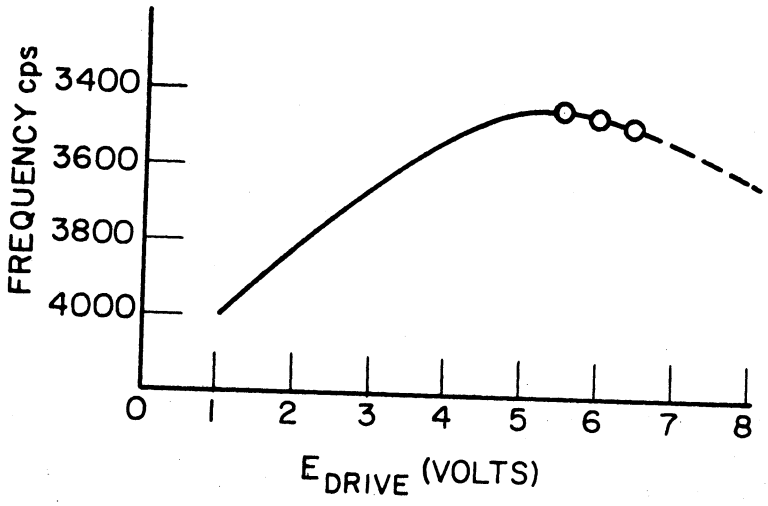

Fig. 67. Subcarrier oscillator calibration.

namely, the saturation of the amplifier and the frequency reversal of the SCO. The accuracy of the final calibration chosen (Fig. 68) was demonstrated by the reduction of the high-voltage high-sensitivity data in which case the raw data reduced to two intersecting straight lines. This was the expected result since the resolution of the instrument would not be great enough to indicate the rounding at the intersections for the ionospheric conditions encountered. In addition, the calibration has produced no detectable systematic error in the reduced data.

D. EXPERIMENTAL PROBE VOLT-AMPERE CHARACTERISTICS

Raw data, such as the upper trace in Fig. 62, were converted to probe volt-ampere characteristics by measuring the distance from the curve to the upper reference at 15 equally spaced points. To provide a consistent spacing of the measurements and to aid in indexing the 15 measurements per voltage sweep, a ruled grid was used to determine the reading positions. This grid was indexed so that the first reading was made at the highest value of the sweep voltage, since this position was well defined by an abrupt change in current immediately afterward (point C in Fig. 62) as the sweep voltage dropped to zero. The current corresponding to the distance measured was then read from the calibration curve determined in the preceding section. A particular value of sweep voltage could be associated with each point since the voltage sweep was linear and the reading grid was indexed. However, the potential difference between electrodes was less than the generated voltage due to a voltage drop in the input

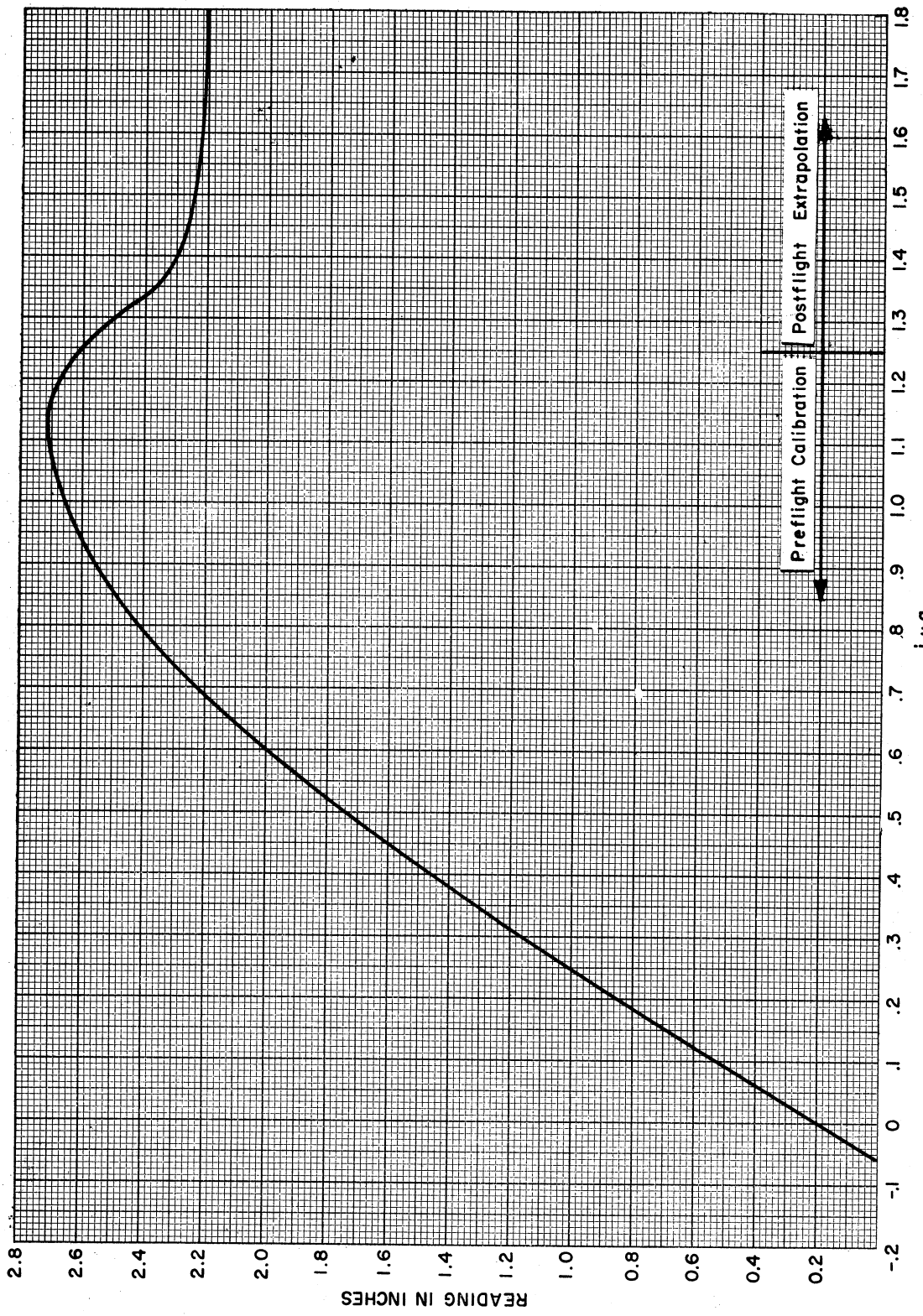

Fig. 68. System calibration of high current-sensitivity sequence.

impedance of the current detector (40,000 ohms). The characteristic corrected for this and the uncorrected points (circled) are seen in Figs. 69 and 70, respectively. The straight lines also seen in Figs. 69 and 70 are the plot of $\log_e i_e$ vs. δV which will be discussed in the following paragraph. This curve clearly indicates the region yielding temperature data, and additional measurements were made to improve the accuracy of determining the temperature.

E. ELECTRON TEMPERATURE DATA REDUCTION

The electron temperature was obtained by the methods previously outlined. The ion-saturated section of the volt-ampere characteristic was extended as a straight line and the difference between it and the signal current was interpreted as the electron current. The current so determined will be less than the true current. The electron temperature was determined from the electron current so obtained by plotting the $\log_e$ of the electron current vs. voltage. Since δV decreases more rapidly than the ion electrode potential, the true ion current is greater than indicated. The error is less than 5%. Predicted ion current is shown in Fig. 43.

$$i_e = AJ_e \exp - (V/V_o) \quad , \tag{38}$$

thus

$$\frac{1}{V_o} = \frac{-d \log_e I_e}{dv} \quad , \tag{39}$$

where

$$T_e = \frac{e V_o}{k} \tag{40}$$

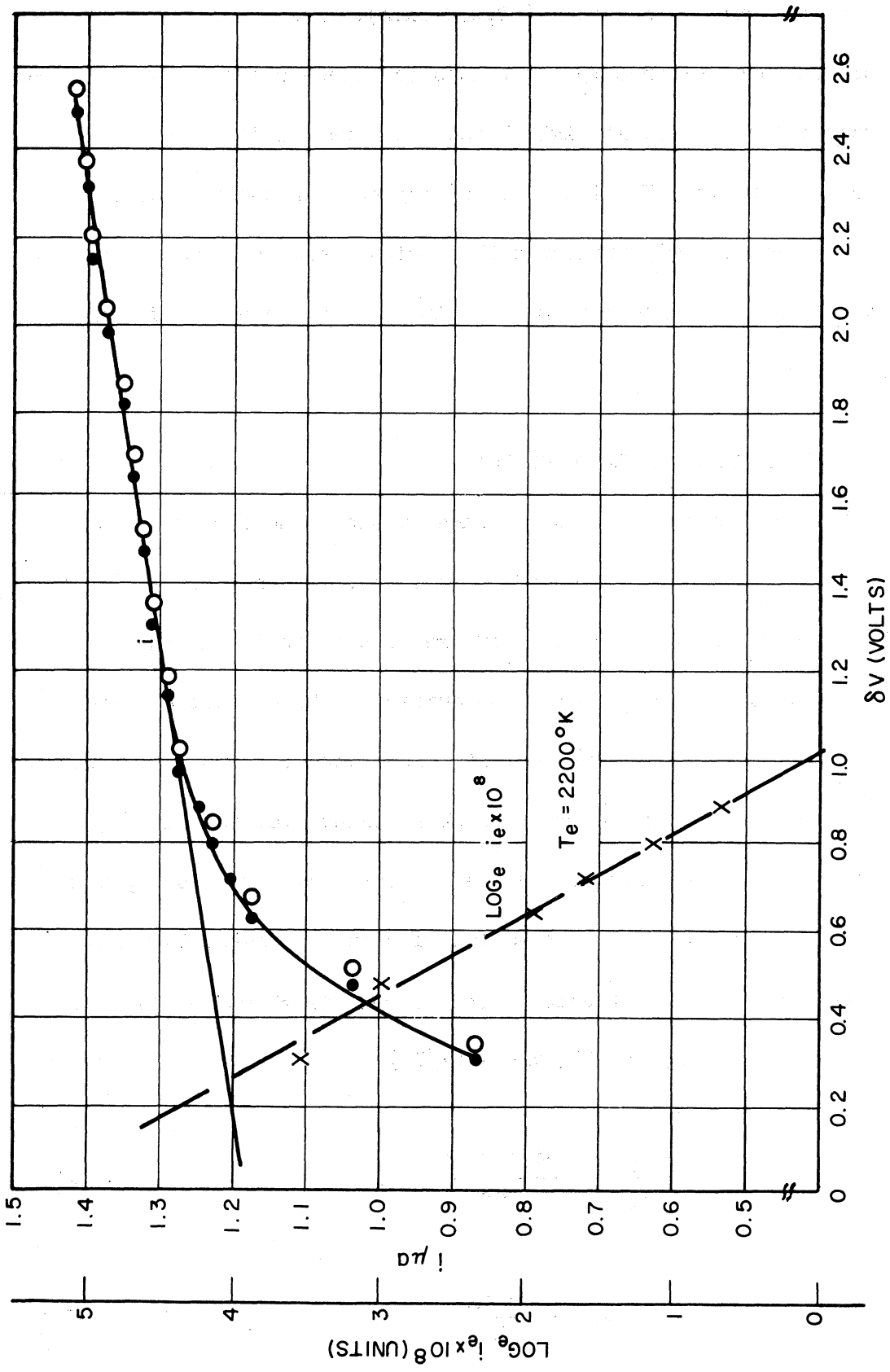

Fig. 69. Probe volt-ampere characteristic and $\log_e i_e$ at 149 km.

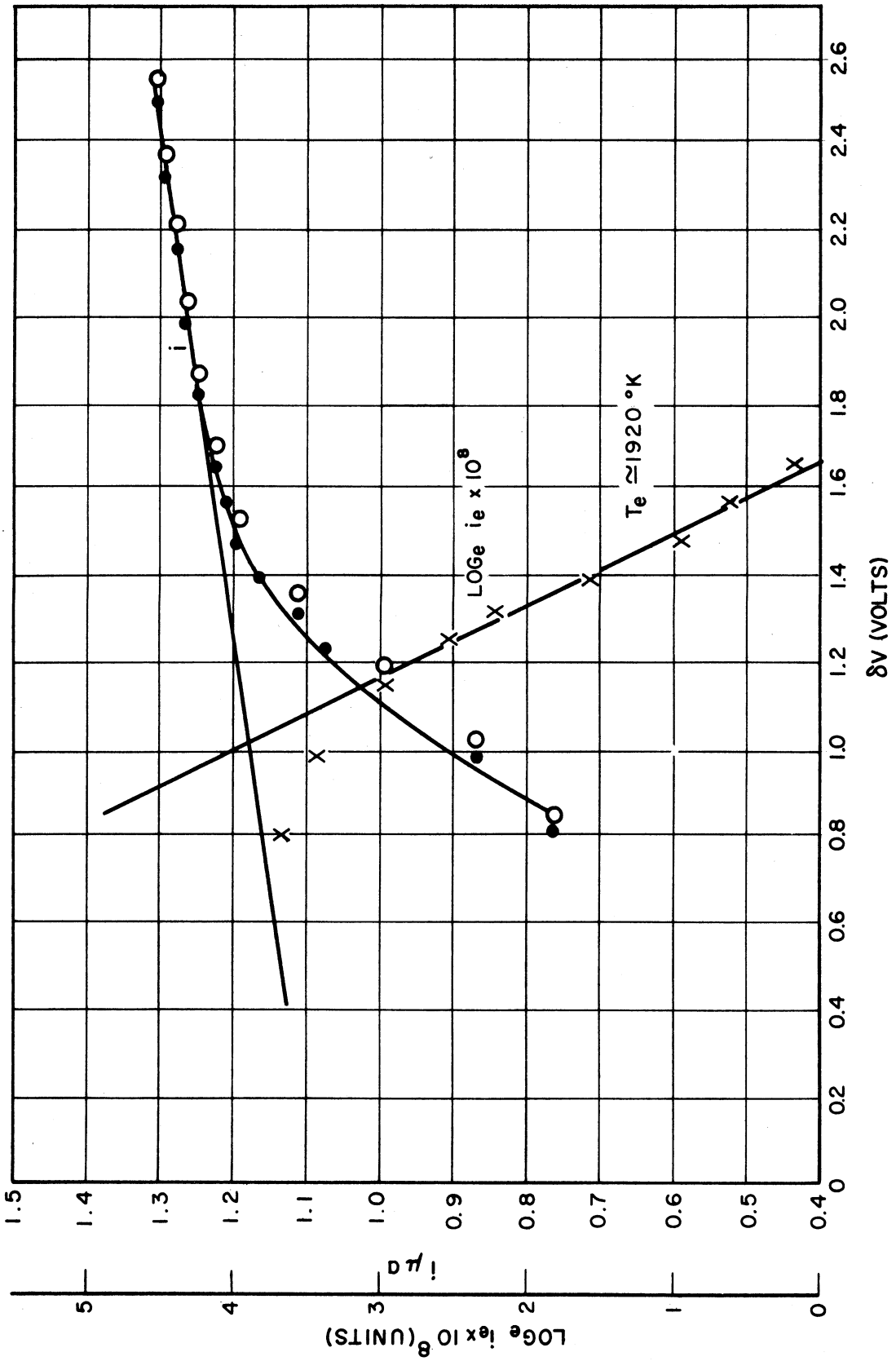

Fig. 70. Probe volt-ampere characteristic and $\log_e i_e$ at 153 km.

The above relations are based on the assumption of a Maxwellian electron-energy distribution. The experimental data indicate that this assumption is reasonable to a first approximation since the graph of $\log_e i_e$ is a reasonably straight line. The departure from the straight line at the higher values of electron current is a result of the signal current no longer being dominated by current to the positive-ion current electrode. The higher electron current corresponds to low values of δV where both electrodes are approaching null potential and the resultant bipolar characteristic is approaching a straight line. The CD portion of the theoretical volt-ampere characteristic is discussed in Section IVB and illustrated in Fig. 43.

In addition to the systematic error mentioned above, the determination of the electron current is subject to random errors at low values of electron current since it is the difference between two relative large quantities. In reducing the data of this flight, another random reading error occurred in the current range between 1.08 and 1.17 μa due to the indeterminate nature of the calibration as the subcarrier oscillator reversed frequency shift. Both types of errors are seen in Figs. 69 and 70. The systematic error is best seen in Fig. 70 but the random errors are relatively small in this figure. The plot of $\log_e i_e$ in Figs. 69 and 70 represents temperatures of 2200°K and 1900°K, respectively.

F. ACCURACY OF DATA REDUCTION

Since the system, including the rocket-borne and the ground equipment, was self-calibrating over 85% of the useful current range, the question of

accuracy of this part becomes a question of the ability to ready repetitive data. Such a test was provided by the 5 calibrations made just before launch. These were recorded in a relatively short period of time and thus could be assumed to represent identical data. Repeated readings of the five preflight calibration curves indicated a reading accuracy of 0.02 in. standard deviation from the average readings. The indistinct trace edge (Fig. 63) was the greatest source of error.

A similar indication of the accuracy of reducing the raw data to current may be determined by reading the same data curve several times and determining the standard deviation. For the sake of objectivity, the data at 115 sec (Fig. 62) were reproduced photographically and 9 readings of the same curve were made. The standard deviation from the average volt-ampere characteristic determined was 0.04 μa or 2.9% of the maximum current. However, this accuracy figure does not apply to the electron current since it is the difference between two relatively large numbers. The random error remains the same and represents a much greater percentage error. Therefore, to establish some measure of accuracy of the reduced temperature data, five readings of each of the three raw-data curves in the low-voltage high-sensitivity sequence at 115 sec were read and reduced independently. The standard deviation from the average of the reading was found to be 250°K, or approximately 13%. Since in general the temperature changes between adjacent characteristics were small in comparison with the various reading errors, all temperature data of a sequence

(three characteristics) were averaged, and the standard deviation from the average was computed.

G. ELECTRON TEMPERATURES

The electron temperatures measured are listed in Table II and plotted vs. altitude in Fig. 71. Since the temperatures are averages of several readings, the standard deviation (reading error), the total number of readings, and the number of included volt-ampere characteristics are listed. The standard deviation is also illustrated by a bar in Fig. 71. A low signal current, which indicates the probe has not yet entered the E-layer, does not permit temperature data reduction below 111 km and a high signal current above 177 km results in the loss of temperature data due to the saturation of the current detector, which has been discussed previously.

TABLE II

MEASURED ELECTRON TEMPERATURES

Altitude, km	Temperature, °K	No. of Readings	No. of Curves	Standard Deviation, °K
112	1580	5	3	237
116	1880	3	1	89
136	1814	6	2	304
140	1840	6	2	161
149	2050	10	2	260
153	1984	12	3	278
165	2247	6	3	250
173	1375	2	1	194
177	1368	9	3	194

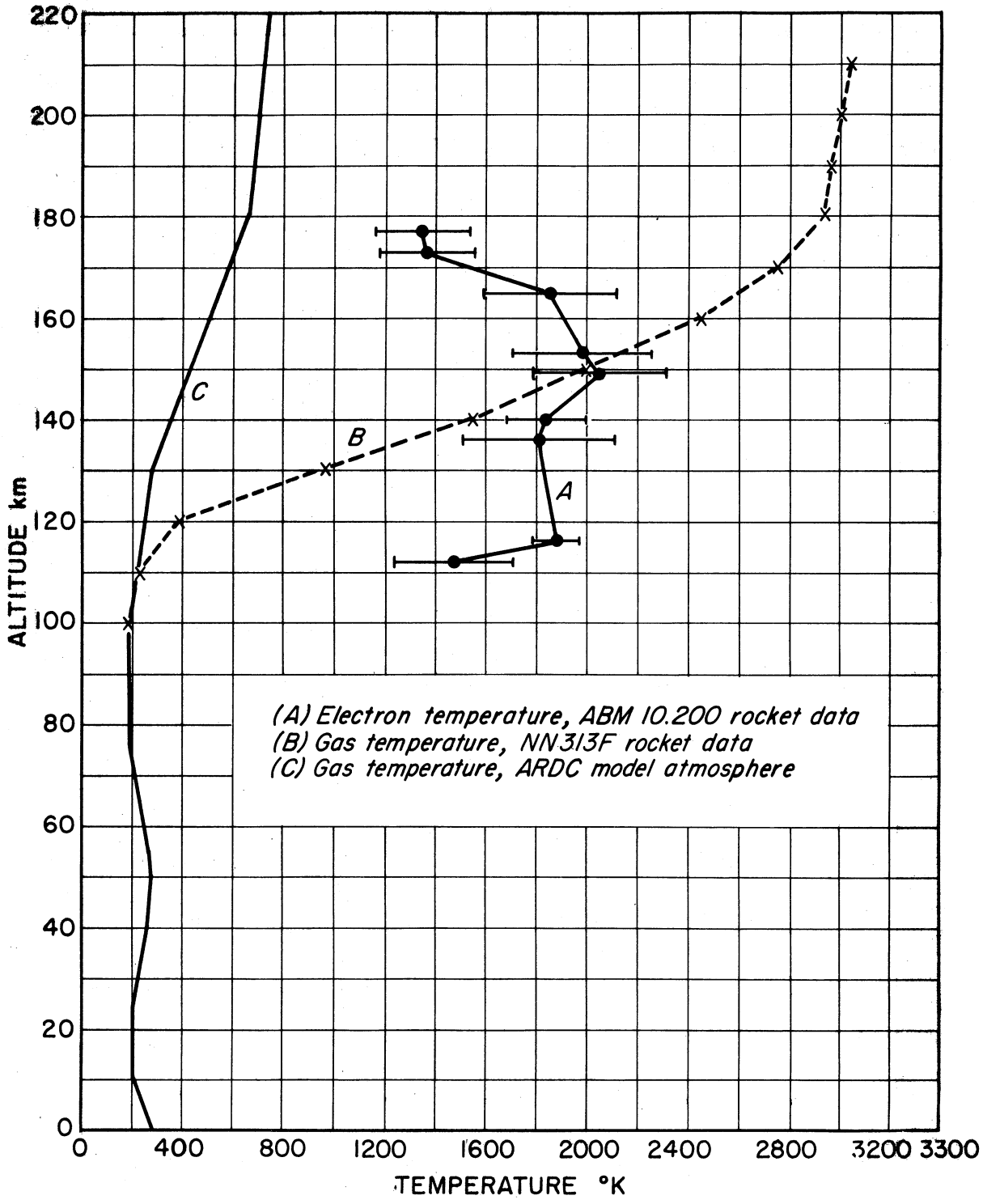

Fig. 71. Experimental and estimated temperatures.

An interesting correlation may be drawn between the curve of electron temperature vs. altitude shown in Fig. 71 and the ionograms in Fig. 72. An ionogram is a record of vertical pulse signal reflected from the ionosphere. It indicates the virtual height and relative electron number density of the various layers of the ionosphere. The IGY Manual (Vol. IV)[25] gives a complete description of the type of equipment used and the interpretation of the data obtained. The ionograms of Fig. 70 were made at the Fort Churchill ionosphere station. The records shown were taken a few minutes before and a few minutes after the rocket data were recorded. The station was approximately 29 km from the launcher and approximately 67 km horizontal distance from the rocket during the time the rocket was in the E-region. The rapid increase in temperature occurring between 112 and 116 km corresponds very well with the virtual height (approximately 120 km) of the E-layer as shown by the ionograms. The virtual height is always several kilometers higher than the actual height of the layer being measured due to the partial penetration of the rf sounding wave. The E-layer is indicated on the ionograms by the dark area between the 2- and 3-mc markers. The indicated decrease in temperature occurs at approximately the highest indication of an E-layer.

The kinetic gas temperature experimentally determined by Horowitz and LaGow[26] through measurements of pressure and pressure change on the side of a rolling rocket, IGY NN3.13 Aerobee-Hi, flown at 4:00 p.m. on July 29, 1957, at Fort Churchill, is also shown in Fig. 71 The gas temteratures were calculated from scale heights determined from the pressure

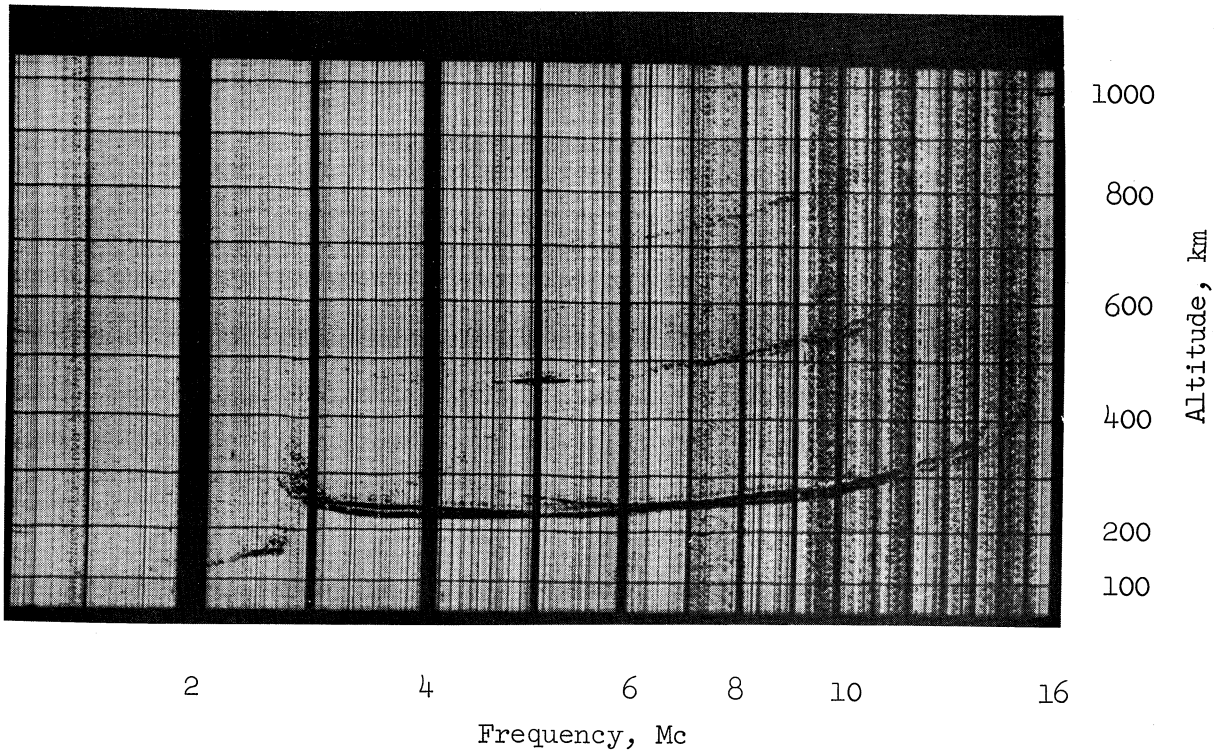

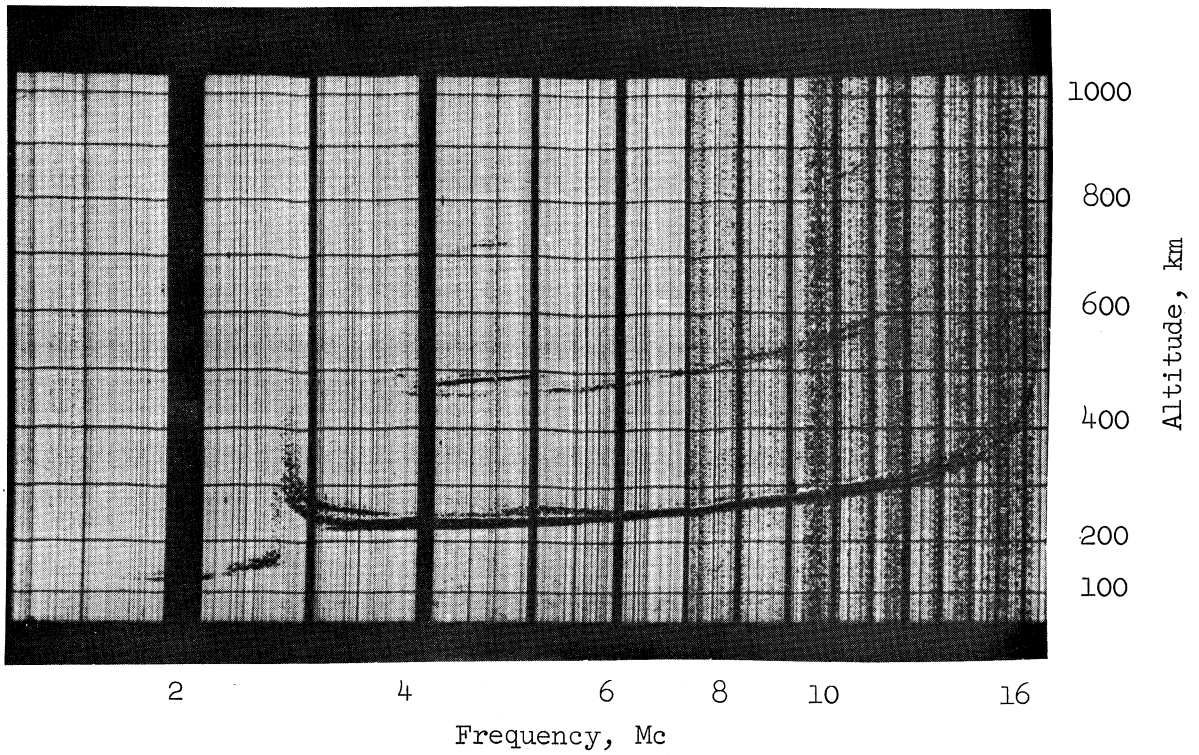

Fig. 72. Preflight (top) and postflight (bottom) ionograms.

measurements. A constant gram-molecular weight of air (28.9) was assumed to an altitude of 210 km. The data of Horowitz and LaGow also indicate higher temperatures and higher temperature gradients at this altitude than those predicted by the ARDC model which is plotted in Fig. 71 for comparison. Close correlation of the experimental data is not possible, of course, since the character of the ionosphere would be expected to differ between summer and winter. The presence of an F_1-layer in the summer might account for the higher temperature measured by Horowitz and LaGow at the higher altitudes. No F_1-layer was present during the flight of the bipolar probe experiment, nor is one usually present in the winter at the higher latitudes. If temperature equilibrium does not exist, the electron temperature would be higher than that of the gas. The opposite is not being suggested by comparing the experimental data. The decrease in electron temperature at 165 km is perhaps the most interesting aspect of the probe data. The generally accepted models of the ionosphere show a monotonically increasing temperature. However, such simple models have had to be revised in the lower regions of the upper atmosphere, and this may be the first indication of the more complex nature of the ionosphere.

H. FRACTION OF TOTAL AVAILABLE ELECTRONS COLLECTED

The electrons collected by an equal-area bipolar probe constitute only a small percentage of the total electrons. Thus the electron temperatures measured by the present experiment are representative of the total electron population only if a simple Maxwellian distribution exists. If the energy distribution is more complex, the present experiment has determined the temperature of the higher-energy family of electrons. However, to a first approximation at least, a Maxwellian distri-

bution of these high-energy family is indicated, since the $\log_e i_e$ was a reasonably straight line.

It is of interest now to determine the percent of the electrons sampled by the present probe. The electron current, when the probe is at wall potential, is

$$i_e = AJ_e \exp - \frac{V_w}{V_o} \quad . \tag{41}$$

The positive-ion current, neglecting the sheath thickness, is

$$i_p = AJ_p \quad . \tag{42}$$

Since the positive ion and electron current are equal at the wall potential, Eqs. (41) and (42) may be equated, from which the following is obtained, using Eq. (25) to express J_p and J_e.

$$V_w = - V_o \log_e \frac{N_p}{N_e} \sqrt{\frac{T_p m_e}{T_e m_p}} \tag{43}$$

The ratio of random electron-current density at the electrode to the random electron-current density in the undisturbed plasma is

$$\frac{J_o}{J_r} = \exp - \frac{V_w}{V_o} \quad . \tag{44}$$

Substituting Eq. (43) in Eq. (44)

$$\frac{J_o}{J_r} = \frac{N_p}{N_e} \sqrt{\frac{T_p m_e}{T_e m_p}} \quad . \tag{45}$$

If $N_p = N_e$ and $T_p = T_e$, Eq. (45) reduces to

$$\frac{J_o}{J_r} = \sqrt{\frac{m_e}{m_p}} \tag{46}$$

which has the value of .00427 for NO positive ions. Thus the current density at the electrode surface is 0.427% of the random current density in the undisturbed plasma. It is a familiar fact of kinetic theory[14] that the energy distribution of the electrons reaching the electrode and of the larger number of electrons entering the sheath is the same. Thus 0.427 is also the percentage of the total electrons available for collection that are collected. Thus the ratio of current is also the ratio of number density. Approximately half this number are collected in the region determining the electron temperature since the positive ion-collecting electrode is nearly twice as negative as the wall potential (see Fig. 43). Less than twice this number are collected by the electron-collecting electrode. The increased ion-collection area due to the sheath thickness will not increase the percentages by a factor of more than 1.3.

I. DELAYED DATA

A temperature of 1800°K was obtained via the delayed data channel at an altitude of 116 km. This compares favorably with the 1880°K obtained via the direct channel. Insufficient data were received at other altitudes to permit temperatures to be determined, but segments of the characteristic curves could be compared. The conclusion drawn from these segment comparisons and the temperature agreement was that the rf did not disturb the instrument ot a degree detectable with the present equipment, if at all.

Unlike the useful range of the direct-data channel, the useful range of the delayed-data channel was limited by a cathode follower which provided an impedance match between the data storage capacitors and the "5.4"

SCO. This circuit was cut off by currents higher than 1.25 μa, thus resulting in the loss of ion-current data at higher altitudes. In addition to this restriction, the low-voltage portions of the volt-ampere characteristics (Section DE in Fig. 63) were not "stored" due to the transfer time of the storage control relay. The motor speed, which was higher than anticipated, increased this loss.

J. NUMBER DENSITY

The positive-ion number density of the plasma may be estimated from the volt-ampere characteristics since the ion mean free path is long (relative to the sheath). Thus the environment is not disturbed by the collection of ions of remote origin. Two methods were used. The first method[5] assumes that the ion and electron temperatures are equal, while the second method assumes that the ion and electron densities are equal and the current to an electrode is relatively independent of the ion temperature. The latter has been demonstrated by Bohm.[19] The number densities obtained by both methods are approximately the same, indicating that the assumptions are reasonable in both methods.

The first method permits the measured temperatures to be used in the current-voltage relation in the positive-ion sheath:

$$I_{np} = \frac{P}{(-\alpha^2)} (V/V_o)^{3/2} \quad . \tag{30}$$

The normalized ion current (I_{np}) to a sheath-area-limited electrode is also

$$I_{np} = (a/r)^2 \quad . \tag{33}$$

Equating Eqs. (30) and (33) and taking the $\log_e$ yield,

$$\log_e I_{np} = 2 \log_e (a/r) = \log_e P + 3/2 \log_e (V/V_o) - \log (-\alpha)^2 , \quad (47)$$

Differentation results in

$$d \log_e I_{np} = 2 d \left[\log_e (a/r)\right] = 1.5 d \left[\log_e (V/V_o)\right] - d \left[\log_e (-\alpha^2)\right], \quad (48)$$

from which

$$\frac{d\left[\log_e(-\alpha^2)\right]}{d\left[\log_e(a/r)\right]} = \frac{d\left[\log (a/r)^2\right]}{d\left[\log (V/V_o)\right]} = 3 \frac{idv}{V_{di}} - 2 . \quad (49)$$

Then the positive-ion density may be calculated from the current, the voltage, and the slope of the volt-ampere characteristic at a single point in the ion-current saturated portion. A plot of the left member of Eq. (49) as a function of (a/r) provides the means for determining the normalized ion current (Eq. 33) from the experimental data. The ion number density may be calculated by using the expressions for the random ion-current density

$$J_p = N_p e \sqrt{\frac{kT}{2\pi m_p}} . \quad (25)$$

The left-hand side of Eq. (49) is presented in Fig. 73 as a function of (a/r) for low values of (a/r). The left term has been presented for higher values of (a/r) by Hok.[5]

A second method of calculating ion number density from an experimental volt-ampere characteristic is presented by J. E. Allen, R. L. F. Boyd, and P. Reynolds[27] in the paper describing the potential distribution about a spherical electrode. They assumethe electron density is given by Boltzmann's equation.

$$n_e = N_e \exp - (V/V_o) . \quad (50)$$

The ion density is expressed as

$$n_p = i_p \left[4\pi r^2 e^{(2eV/m_p)}\right]^{-1} \quad (51)$$

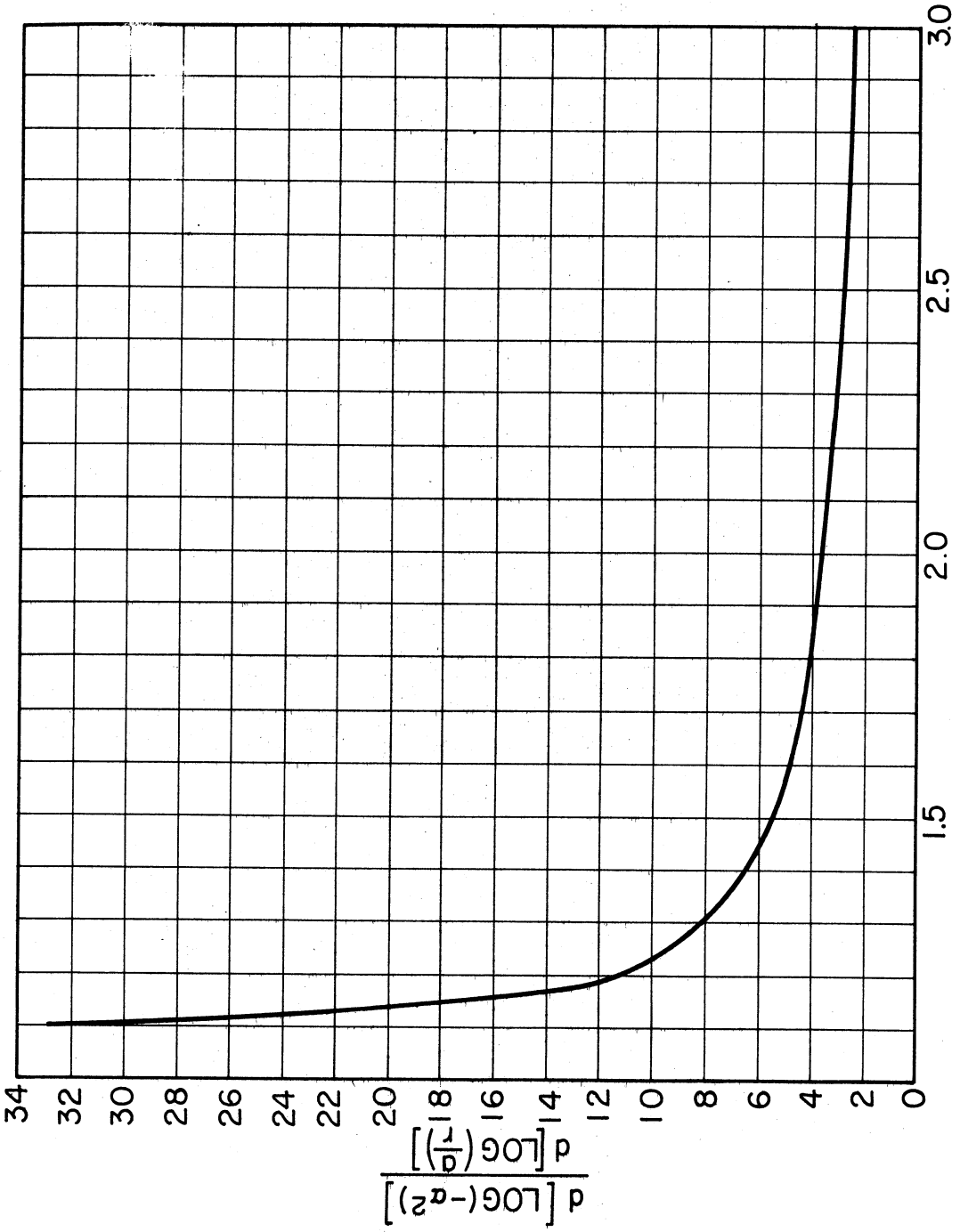

Fig. 73. Spherical probe. $d[\log(-\alpha^2)]/d[\log(a/r)]$ vs. (a/r).

for values of r such that $|V| \gg V_o$. The term $(2e\ V/m)^{1/2}$ is the ion velocity when the ions have reached energies that are large compared with their initial energies.

The above values of number densities were then substituted in Poisson's equation

$$\frac{1}{r}\frac{d}{dr}\left(r^2\frac{dV}{dr}\right) = -4\,(n_p - n_e)e \tag{52}$$

and machine solutions obtained. However, a simple solution

$$N_p = \frac{i_p}{0.61\ e\left(\frac{kT}{m_p}\right)^{1/2} A} \tag{53}$$

is obtained if $N_p = N_e$ and the sheath thickness is ignored. The voltage between the sheath and plasma is assumed to be $1/2\ (k\ T_e/e)$ which was shown to be the maximum potential difference the plasma can sustain.

The ion density calculated by the second method is shown in Fig. 74 as curve C. Since Eq. (53) does not consider the increase in current due to the sheath, the lowest value of current in the ion-current saturated region was read. Even so, the number density would be expected to be too high by a factor of approximately 20%. The ion density as calculated by the first method is shown in Fig. 74 as curve D.

A comparison of the experimental curves and the theoretical curves suggests that the experimental curves are shifted by some constant value of current and voltage which remains relatively constant throughout a reading sequence. This is verified by comparing Fig. 69 with Fig. 70. The two sets of data were taken at a difference in altitude of only 4 km and the two

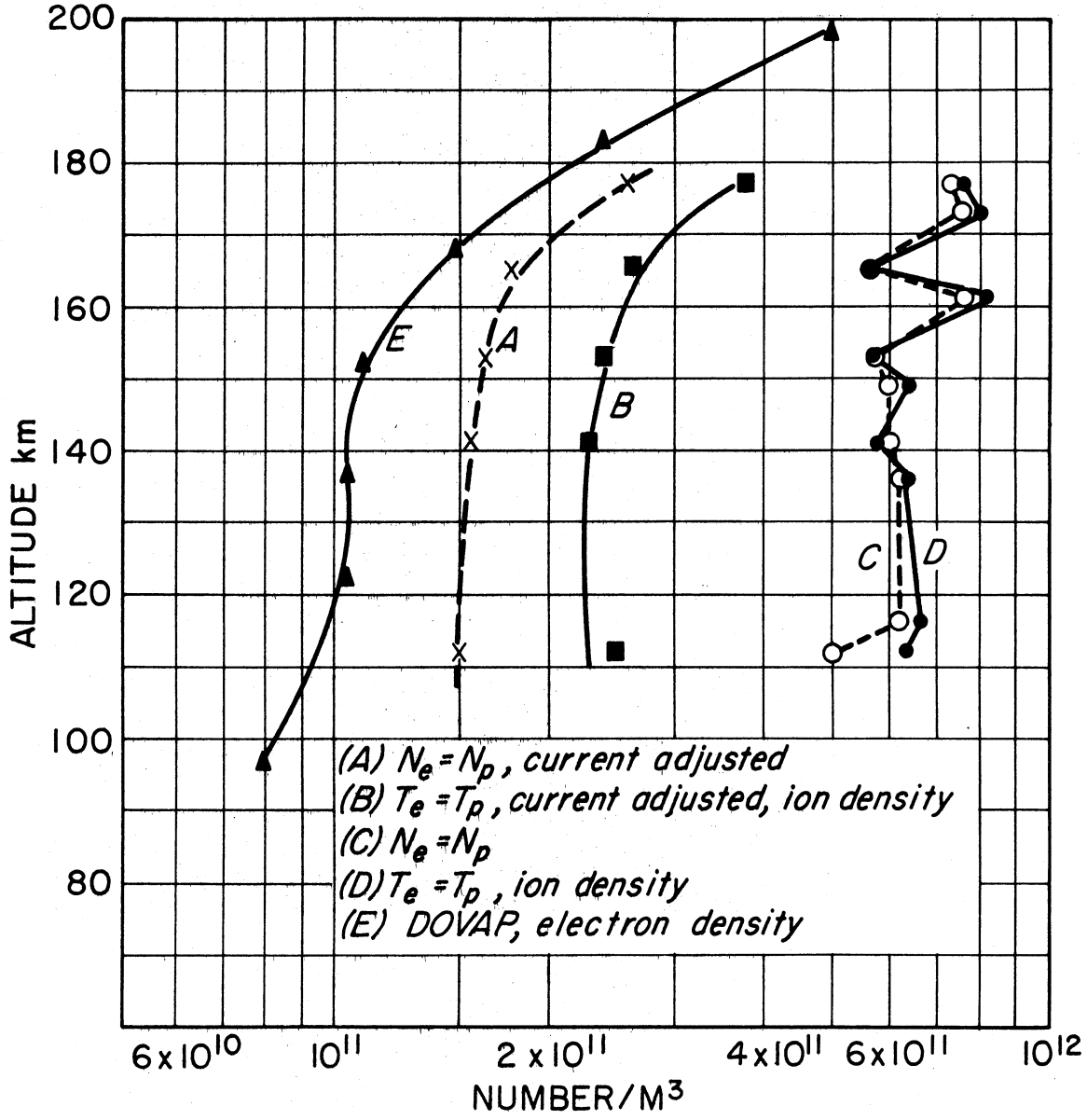

Fig. 74. Ion number density from ABM 10.200 data.

curves are nearly identical except that the second is shifted approximately 0.7 volt. This voltage shift is seen consistently throughout the record, the higher voltage always occurring with the same probe attitude. It is presumed at present that the high currents are due to photoemission and their motion dependence is undetected due to the small number of data samples.

It had been hoped that a study of the magnetometer data coupled with a study of the change of the volt-ampere characteristic with position would define the motion errors permitting corrections to be made. However, coincidental near synchronism of the sequencing timer and the motion of the probe resulted in the probe being in the same relative position each time the data were taken, making only qualitative evaluation of the motion error possible.

An approximate correction of the assumed high current has been made by empirically determining that the signal current is approximately 1.25 times the value of electron current at the point the bipolar signal current becomes straight (segment CD Fig. 21). As mentioned, previously, this point is indicated by the departure of the $\log_e$ plot of the electron current from a straight line. When such a correction was applied to the experimental characteristics, it was found a nearly constant correction was required. Thus, the density was recalculated by both methods for the lower currents. The adjusted current densities are also shown in Fig. 74 as curves A and B.

Since the probe is moving at a relatively high velocity with respect to the plasma, the accuracy of the density given cannot be determined precisely. It is within an order of magnitude and is probably no better than

20%, since it is based on the temperature data. Curve B is considered to more nearly represent the positive-ion density, since it was not necessary to assume equality of electrons and positive ion in its derivation. The difference between the positive-ion density of curve B and the as yet unpublished electron density curve E (DOVAP data), as determined by Mr. Warren Berning of the Ballistics Research Laboratory, may be due to the presence of negative ions. A similar finding of presumably a greater number of ions than electrons was reported by Hok[5] in the case of the earlier probe instrumentation. The ionograms of Fig. 72 indicate an electron density of 9×10^{10} el/m^3, which agrees with the DOVAP data.

K. ABM 6.207 DATA

The data-reduction techniques discussed in detail in the preceding sections pertain to ABM 10.200 data but they are applicable to ABM 6.207 data with only slight modifications. ABM 6.207 is the Fort Churchill IGY designation of the first rocket which carried the "dumbbell" probe instrumentation. This flight, launched on October 20, 1958, preceded the ABM 10.200 flight by approximately one month.

The external configuration of the probe was the same on both flights and the internal instrumentation was basically the same. The significant changes made in the ABM 10.200 instrument were: (1) improved internal rf shielding, (2) improved circuit layout, (3) the inclusion of a magnetometer, and (4) the synchronism of the data storage with the sweep voltage. The internal shielding for rf interference noise and crosstalk improved the stability of the instrument considerably in ABM 10.200. An improved cir-

cuit layout permitted the better shielding as well as providing space for the magnetometer. The magnetometer provided aspect data so that the effects of the relative velocity between the probe and plasma could be studied. The sweep voltage and the sampling rate of the capacitor storage unit was purposely not synchronized in the first instrumentation (ABM 6.207). It was intended that the presence or absence of rf interference would be demonstrated by comparing a section of the delayed or stored volt-ampere characteristic with a directly transmitted characteristic rather than by comparing reduced data. This permitted all available segments (12) of the storage commutator to be devoted to a section of the volt-ampere characteristic. The portion of the total curve which would be stored would change for each voltage sweep if unit were not synchronized. Thus, the desired section, the knee of the curve, would be seen progressing through the stored data. However, after seeing the quality of the ABM 6.207 stored data, it was decided to synchronize the ABM 10.200 delayed data unit. The entire V-A characteristic was recorded and could be regarded as backup for the direct channel if the rf interference could be ignored.

The electron temperatures measured by ABM 6.207 are plotted in Fig. 75. It is seen by comparing Fig. 75 with Fig. 71 that the electron temperatures obtained by both ABM 6.207 and ABM 10.200 were in general agreement. The comparison is of interest since the ABM 6.207 data were obtained via a delayed data channel (data recorded while not transmitting) whereas the ABM 10.200 data were obtained via a direct channel (data re-

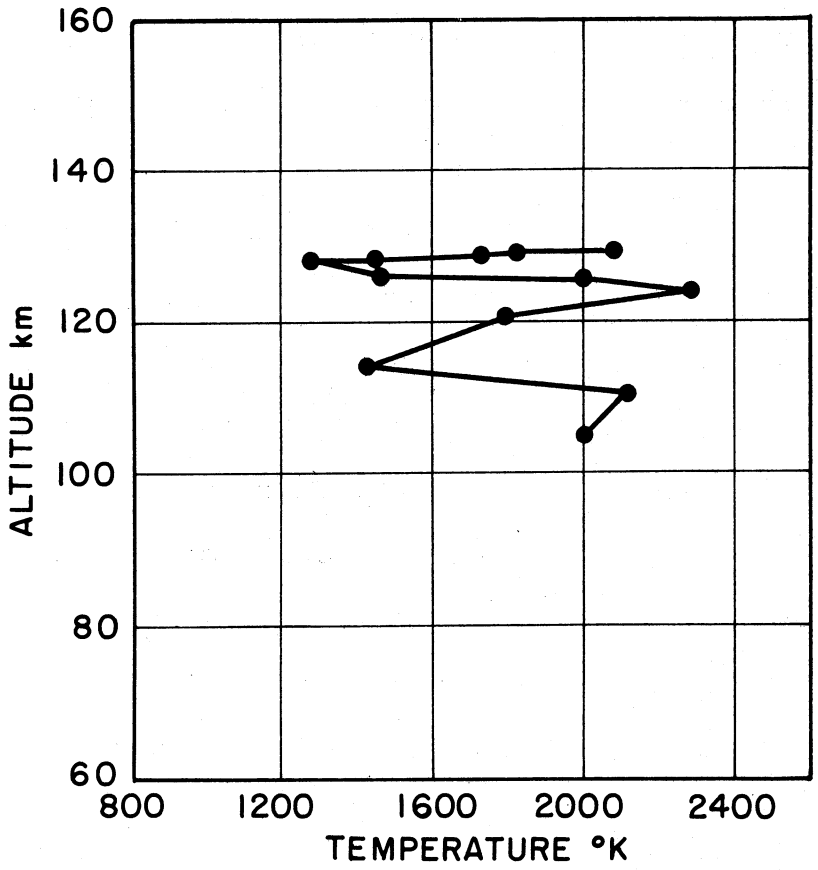

Fig. 75. ABM 6.207 electron temperatures (delayed data).

corded while transmitting), further verifying the conclusion drawn previously from comparing both direct and delayed ABM 10.200 data that telemetering did not seriously disturb the plasma. A close comparison is not possible since the two vehicles were launched at different times. However, both rockets were launched during the afternoon of a cold clear day at Fort Churchill, Canada, and at a time when the Fort Churchill ionosphere station reported a quiescent ionosphere.

Since the direct channel of ABM 6.207 failed just after ejection, it was not possible to compare the delayed data obtained with direct data obtained at the same time. The failure was abrupt suggesting the opening of a circuit, perhaps by wire breakage. Oddly enough, the failure occurred after ejection was completed, at a time when the instrumentation was in free fall. It also occurred in the simpler path of the instrumentation.

The reduction of ABM 6.207 data differed from that of ABM 10.200 data in that a smooth curve was drawn through the raw data points first. Readings were made from this smoothed curve at equal time intervals as indicated by range timing marks on the record. The smoothing of the raw data was advantageous since only points of the volt-ampere characteristic curve were recorded by the delay unit. Unfortunately, these points were not spaced equally in time due to irregularities in the drive belt. The smoothing was done by hand since it required considerable personal judgment gained from previous experience in reducing ABM 10.200 data and is the reason that the ABM 10.200 data were reduced first.

It is difficult to determine a significant evaluation of the accuracy of the ABM 6.207 data. The overall standard deviation was found to be 317°K; however, the smoothing of the raw data would tend to reduce the deviation, and while this is representative for most points, others may be in error by a factor greater than this.

IX. CONCLUSIONS

It is felt that the experience gained from the successful flight of ABM 10.200 and ABM 6.207 will be of great value in the design of future electrical probes. Although technical difficulties prevented the attainment of some of the objectives of the experiment, as described in the preceding pages, four major goals were achieved:

(1) The measurement of electron temperature in altitude range from 105 km to 177 km.

(2) The measurement of the ion number density from 112 km to 177 km.

(3) Evidence concerning the relationship between the presence of rf (227.5 Mc) and the ionospheric data obtained.

(4) The successful ejection of the instrumentation in working order from a rocket moving at high velocity.

In addition, a correlation between the rocket velocity and the voltage shift of the volt-ampere characteristic was observed. It was demonstrated that a high rocket velocity does not appreciably affect the measurement of the electron temperature. It is believed that a current due to photoemission was observed, but this could not be confirmed because of the limited data.

The theoretical treatment was verified by the experimental results. Although this probe design was considered a preliminary exploratory design,

it is now felt that it may be profitably used in the study of the ionosphere. Two instrumentations, in addition to those discussed in this report, have been flown.

It is also planned that additional "dumbbell" instrumentations will be flown in the future. A third "dumbbell" instrumentation was flown on June 30, 1959, at Wallops Island, Virginia. However, the performance of the launching vehicle was poor and the probe did not reach the E-layer of the ionosphere. As a result, no interpretation has been made of the measured D-layer currents. The theory as presented earlier is not applicable in this short mean-free-path region. In addition, a different design consisting of a spherical reference electrode and four cylindrical orbital-motion-limited electrodes placed at the points of an inscribed tetrahedron was launched at Wallops, on July 1, 1959. This probe configuration was designed to be unaffected by the relative velocity between the instrument and the plasma and to sample a larger percentage of the electrons available for collection. Thus it will determine the electron energy distribution more fully. The data obtained by this launching has not been reduced at this time. A relatively high interfering current which varied in synchronism with the sweep voltage but of an unknown origin makes the reduction of these data difficult. This design had a larger area ratio and thus samples a greater percentage of the total electrons available for collection. This permits the electron energy distribution to be determined more completely.

The errors introduced in the transition from the unipolar to ambi-

polar diffusion regions have not been considered in this report. The error in number density introduced by ignoring the ambipolar diffusion region was calculated for ABM 10.200 data and in each case investigated was found to be less than the experimental error. Similar procedures have been outlined in the report by Hok[5] et al. It is felt that such errors are not large compared with present instrumental errors. As the study of the ionosphere continues, independent experimental determination of ambipolar diffusion coefficient, mean free path, volume recombination, and average ion mass will be a prerequisite for more accurate data reduction.

The results reported here represent only a small fraction of the potential of this versatile experiment.

X. REFERENCES

1. Seddon, J. C., Pickar, A. D., and Jackson, J. E., "Continuous Electron Density Measurements up to 200 Km," J. Geophys. Res., 59, No. 4 (December, 1954).

2. Seddon, J. C., "Electron Densities in the Ionosphere," J. Geophys. Res., 59, No. 4 (December, 1954).

3. Seddon, J. C., and Jackson, J. E., "Absence of Bifurcation in the E-Layer," Phys. Rev., 97, 1182-1183 (February 15, 1955).

4. Jackson, J. E., "A New Method for Obtaining Electron-Density Profiles from P^1-f Records," J. Geophys. Res., 61, No. 1 (March, 1956).

5. Hok, G., et al., Dynamic Probe Measurements in the Ionosphere, Univ. of Mich. Eng. Res. Inst. Report, Ann Arbor, August, 1951. Reprinted as Univ. of Mich. Res. Inst. Report 2521-5-S, AFCRC TN-58-616.

6. Hok, G., Spencer, N. W., and Dow, W. G., "Dynamic Probe Measurements in the Ionosphere," J. Geophys. Res., 58, No. 2 (June, 1953).

7. Reifman, A., and Dow, W. G., "Theory and Application of the Variable Voltage Probe for Exploration of the Ionosphere," Phys. Rev., 75, 1311A (1949).

8. Reifman, A., and Dow, W. G., "Dynamic Probe Measurements in the Ionosphere," Phys. Rev., 76, 987 (1949).

9. Langmuir, I., and Mott-Smith, H., Jr., "Studies of Electric Discharges in Gases at Low Pressures," Gen. Electrical Rev.; "Part I," 27, No. 7 (July, 1924); "Part II," No. 8 (August, 1924); "Part III," 27, No. 9 (September, 1924).

10. Tonks, L., and Langmuir, I., "Theory of the Arc Plasma," Phys. Rev., 34, 876 (1929).

11. Boyd, R.L.F., "The Collection of Positive Ions by a Probe in an Electrical Discharge," Proc. Roy. Soc. A, 201, 329 (1950).

12. Johnson, E. O., and Malter, L., "A Floating Double Probe Method for Measurements in Gas Discharges," Phys. Rev., 80, 58-68 (October, 1950).

13. Koyiuna, S., and Takayana, K., J. Phys. Soc. Japan, 4, 349 (1949).

14. Dow, W. G., Fundamentals of Engineering Electronics, 2nd ed., New York, John Wiley and Sons, 1952.

15. Dow, W. G., Fundamentals of Physical Electronics, in preparation.

16. Hok, G., Sicinski, G. S., and Spencer, N. W., "Temperature and Electron-Density Measurements in the Ionosphere by a Langmuir Probe," Scientific Uses of Earth Satellites (Ed. J. A. Van Allen), The University of Michigan Press, Ann Arbor, 1956.

17. Krassovsky, V. I., "Exploration of the Upper Atmosphere with the Help of the Third Soviet Sputnik," presented at the International Astronautical Federation Congress in Amsterdam, August, 1958.

18. Sloane, R. H., and Emeleus, K. G., "An Effect of Positive Space Charge in Collector Analysis of Discharges," Phys. Rev., 44, No. 5 (September, 1933).

19. Bohm, D., Burhop, E.H.S., and Massey, H.S.W., "Minimum Tonic Kinetic Energy for a Stable Sheath," The Characteristics of Electrical Discharges in Magnetic Fields (eds. Guthrie, A., and Wakerling, R. K. , (New York, McGraw-Hill Book Co., 1949), Ch. 3.

20. Kallmann, H. K., White, W. B., and Newell, H. E., Jr., "Physical Properties of the Atmosphere from 90 to 300 Kilometers," J. Geophys. Rev., 61, No. 3 (September, 1956).

21. Minzner, R. H., and Ripley, W. S., "The ARDC Model Atmosphere 1956," Air Force Surveys in Geophysics, No. 86, Geophysics Research Directorate, Air Force Cambridge Research Center, TN-56-204, ASTIA Document 110 233. (ARDC is the Air Research and Development Command.)

22. Johnson, C. Y., Meadows, E. B., and Holmes, J. C., "Ion Composition of the Arctic Ionosphere," J. Geophys. Res., 63, 443 (June, 1958).

23. Spencer, N. W., "Forty-Seven Research Rockets at Fort Churchill," a paper presented at the American Rocket Society Semi-Annual Meeting, Los Angeles, Calif. (June 9-12, 1958).

24. Berkner, L. V. (ed.), Rockets and Satellites (Vol. VI of Annals of the International Geophysical Year), New York, Pergamon Press, 1958.

25. Beynon, W.J.G., and Brown, G. M., (eds.), The Ionosphere (Vol. IV of Annals of the International Geophysical Year), New York, Pergamon, 1958.

26. Horowitz, R., and LaGow, H., "Auroral-Zone Atmosphere-Structure Measurements," J. Geophys. Res., 68, 757 (1958).

27. Allen, J. E., Boyd, R.L.F., and Reynolds, P., "The Collection of Positive Ions by a Probe Immersed in a Plasma," Proc. Phys. Soc., B-70, 297 (1957).

APPENDIX

Estimated Photoelectric Emission

It has been estimated in reference to the chosen probe (Section VII) that the emission from a stainless steel surface exposed to the solar radiation in the E layer of the ionosphere is approximately 5×10^{-3} amp/m^2. This estimate is based in part on unpublished data obtained in the rocket investigation of extreme ultraviolet (100-1500Å), a region of the spectrum in which the quantum efficiency of radiation (fraction of incident photons that produce emission) is relatively high. This current density could result in signal currents as great as 1.2×10^{-6} depending on the probe attitude. Thus the estimated current density is of the same order of magnitude as the 0.6×10^{-6} amperes presumed to be caused by photoemission (VIII J).

A similar current density 2.38×10^{-3} amp/m^2 is obtained by representing the sun as a 6000°K black body above 1700Å and a 4500°K black body below 1700Å. The absorption of the shorter wavelengths in the upper ionosphere is recognized by the reduction of apparent black body temperature. This latter estimate does not consider changes in quantum efficiencies nor does it consider high-intensity radiation such as Lyman α at 1215.7Å. However, their spectrum is so narrow that they do not appreciably increase the total current. In addition, this estimate does not consider changes in quantum efficiencies and thus would be considered too low rather than too high.

---

*By personal communication with Dr. Hans E. Hinteregger, Chief of the Physical Measurements Unit at the Geophysical Research Directorate, AFCRC, which is gratefully acknowledged.